UC Berkeley
UC Berkeley Electronic Theses and Dissertations

Title

Electrospun Bilayer PLLA Scaffolds for Fibrous Tissue Engineering: From Microstructure to Cell Response

Permalink

https://escholarship.org/uc/item/9hb6j116

ISBN

9798173788276

Author

Echeverria Molina, Maria Ines

Publication Date

2026-08-10

Peer reviewed|Thesis/dissertation

eScholarship.org Powered by the California Digital Library
University of California

Electrospun Bilayer PLLA Scaffolds for Fibrous Tissue Engineering: From Microstructure to Cell Response

by

Maria Ines Echeverria Molina

A dissertation submitted in partial satisfaction of the
requirements for the degree of
Doctor of Philosophy
in
Engineering - Mechanical Engineering
in the
Graduate Division
of the
University of California, Berkeley

Committee in charge:
Professor Kyriakos Komvopoulos, Chair
Professor Lisa Pruitt
Professor Kevin E. Healy

Summer 2026

Electrospun Bilayer PLLA Scaffolds for Fibrous Tissue Engineering: From Microstructure to Cell Response

Copyright 2026

by

Maria Ines Echeverria Molina

Abstract

Electrospun Bilayer PLLA Scaffolds for Fibrous Tissue Engineering: From Microstructure to Cell Response

by

Maria Ines Echeverria Molina

Doctor of Philosophy in Engineering - Mechanical Engineering

University of California, Berkeley

Professor Kyriakos Komvopoulos, Chair

Millions of surgical procedures are performed each year to repair or replace damaged tissues, yet the regeneration of fully functional tissue remains a significant clinical challenge. Tissue engineering seeks to address this need through the integration of cells with biodegradable scaffolds that provide structural and biochemical cues during tissue formation. In these systems, scaffold features such as architecture, mechanics, degradation, and chemistry influence cell attachment, organization, migration, and phenotype. However, these parameters are highly interconnected and depend on the local biological and biomaterial environments, making cellular behavior difficult to predict from isolated design variables.

This work investigates how scaffold architecture, culture time, and mechanical stimulation regulate the behavior of cells seeded onto electrospun bilayer poly-L-lactic acid (PLLA) scaffolds composed of aligned-fiber and random-fiber regions. Electrostatic finite element modeling was first used to analyze fiber deposition and guide the fabrication of bilayer constructs with controlled structural heterogeneity. The degradation behavior of the scaffolds was then characterized over extended periods to evaluate the evolution of scaffold morphology, molecular weight, crystallinity, and thermomechanical properties. The effects of scaffold architecture and culture time on fibroblast morphology were investigated through quantitative analyses of cellular and nuclear shape descriptors. Finally, the combined effects of fiber organization and uniaxial mechanical loading were evaluated, revealing a coupled regulation of cell morphology in response to scaffold structure and mechanical cues.

The sequential studies of this dissertation establish a framework for designing fibrous scaffolds to regulate cell shape, a parameter linked to functional tissue organization. Specifically, scaffold architecture and mechanical stimulation are shown to regulate cell shape through distinct but interacting mechanisms underlying anisotropic and structurally heterogeneous tissue development. Beyond bilayer PLLA systems, the electrospinning methodologies developed in this work were extended to alternative biomaterial platforms, highlighting the generalizability of the established fabrication, characterization and testing framework.

To my babies, Elena and Mateo, whose presence fills my life with greater purpose and joy.

To my husband, Jairo, for his unwavering support and boundless love.

To my parents, Ines and Felipe, for their endless love and encouragement.

To my sisters, Daniela and Betty, for a lifetime of laughter and for always being there.

Contents

Dedication **i**

Contents **ii**

List of Figures **iv**

Acknowledgments **ix**

1 Introduction **1**
1.1 Clinical Motivation 1
1.2 Background 1
1.3 Contributions and Outline 4

2 Design Challenges in Polymeric Scaffolds for Tissue Engineering **7**
2.1 Introduction 7
2.2 Scaffold Main Characteristics 9
2.3 Immunomodulation 27
2.4 Outlook and Future Perspectives 30

3 An Electrostatic Finite Element Analysis of the Electrospinning Process of Bilayer Constructs Using a Parallel-Plate Collector **34**
3.1 Introduction 34
3.2 Simulation Methodology 35
3.3 Results and Discussion 36
3.4 Conclusions 39

4 In Vitro Degradation of Fibrous Bilayer Poly-L-Lactic Acid Scaffolds **41**
4.1 Introduction 41
4.2 Materials and Methods 43
4.3 Results and Discussion 46
4.4 Conclusions 53

5 Influence of Scaffold Topography and Culture Duration on Fibroblast Morphology in Tissue Engineering **54**
5.1 Introduction 54
5.2 Materials and Methods 56
5.3 Results and Discussion 58
5.4 Supplementary Data 66

6 Scaffold Fiber Architecture and Uniaxial Stretch Differentially Regulate Cell and Nuclear Morphology in Human Dermal Fibroblasts **68**
6.1 Introduction 68
6.2 Materials and Methods 71
6.3 Results 74
6.4 Discussion 81
6.5 Conclusions 85

7 Conclusions and Future Directions **87**
7.1 Conclusions 87
7.2 Future Directions 88

Bibliography **90**

List of Figures

2.1 Design characteristics of biomaterial scaffolds 11
2.2 Click chemistry and PDA functionalization strategies 15
2.3 Structure and morphology scaffold parameters 19
2.4 Parameters affecting scaffold degradation rate 21
2.5 Parameters affecting scaffold mechanical properties 27
2.6 Overview of innate immune response 29
2.7 Synergy of scaffold design parameters for tissue engineering 31

3.1 (a) Finite element mesh of the needle holder (left) and mandrel assembly with a 60 µm-thick polymer layer between the plates (right). The models are not to scale. (b) SEM images of fiber morphologies representative of all the polymer regions between the plates of a bilayer construct consisting of (i) aligned and (ii) randomly oriented fibers. (c) Electric field intensity in the vicinities of (i) the left plate and (ii) the needle tip for a 60 µm-thick polymer layer, and (iii) between the plates and in the vicinities of the left plate and (iv) the needle tip for a 100 µm-thick polymer layer. These plots were obtained at a plane dissecting the model along the needle axis and the mandrel axis. (d) Electric field intensity versus distance from the needle tip for a 60 µm-thick polymer layer. The distance from the needle tip is measured in the y-direction. The inset shows a cross-sectional view of the mandrel and the (x, y) coordinate system with its origin at the center of the needle tip. 37
3.2 Electric field intensity versus distance measured in the y-direction (specified in the insets) and polymer layer thickness (shown in the legend) along (a) the wall surface of the left plate and (b) the axisymmetric axis of the electrospinning system and the needle axis. The insets show cross-sectional views of the mandrel and the (x, y) coordinate system used in each plot. The origin of the coordinate system is 100 µm below the top of the plates and in (a) it is 5 µm to the right from the inner wall surface of the left plate, whereas in (b) it is in the middle of the distance between the plates. 38

3.3 Electric field in the symmetry plane of the electrospinning setup defined by the mandrel axis and the needle axis for a polymer layer thickness (a) 0 (air), (b) 60 µm, and (c) 100 µm. The vector scaling factor, geometry scale, and color legend of the electric field intensity in (b) and (c) are the same. Only the left plate is shown in each panel. The color of the vectors in (a) is not representative of their magnitudes; it only shows the directionality of the electric field. 39

4.1 (a) Representative SEM images of as-fabricated PLLA scaffold surfaces with aligned fibers (AFL, top) and random fibers (RFL, bottom). (b) Cross-sectional SEM images of a scaffold showing the AFL (top) and RFL (bottom). The inset shows a closer view of the AFL. (c) Representative distributions of fiber alignment (2D FFT plot) on AFL and RFL scaffold surfaces. 47
4.2 Representative SEM images and fiber diameter histograms (insets) of RFL (left column) and AFL (right column) surfaces of (a) and (b) as-fabricated and (c)–(f) degraded PLLA scaffolds. All the magnification scale bars are equal to 30 µm. . 48
4.3 Fiber diameter statistics of the AFL and RFL of as-fabricated and degraded PLLA scaffolds. The error bars indicate one standard deviation above and below the corresponding mean value. Lines with end dots represent statistically significant differences between groups ($p < 0.05$). 49
4.4 Variation of (a) mass loss, (b) weight-average molecular weight, and (c) crystallinity with degradation time of PLLA scaffolds. The error bars indicate one standard deviation above and below the corresponding mean value. 51
4.5 (a) DSC thermogram of PLLA with a dominant peak assigned to the melting temperature (173 °C) of the material and (b) melting temperature T_m and glass transition temperature T_g of PLLA determined from DSC thermograms versus degradation time. 52
4.6 (a) Average stress–strain curves for a strain rate equal to $0.017\,s^{-1}$, (b) ultimate tensile strength σ_U, (c) yield strength σ_Y, and (d) elastic modulus E of as-deposited and degraded electrospun PLLA scaffolds. For all the data presented, the tensile load was applied in the direction of the aligned fibers. Lines with end dots represent statistically significant differences between groups ($p < 0.05$). The error bars indicate one standard deviation above and below the corresponding mean value. 52

5.1 Representative scanning electron microscopy (SEM) images of the fibrous layers in the bilayer scaffolds: (a) aligned fiber layer (AFL) and (b) randomly oriented fiber layer (RFL). 59

5.2 Representative fluorescent images of PWK-F cells stained for F-actin filaments (green, AlexaFluor 488 phalloidin) and nuclei (blue, Hoechst 33342) attached to AFL (first-row images) and RFL (second-row images) scaffold surfaces obtained after 1, 3, 6, and 9 days of cell culture (20× magnification). Subparts (a) and (b) show composite images of overlaid SEM (grayscale) and fluorescent (actin/nucleus) images. The SEM images within the upper right circles show corresponding fiber morphologies. Scale bars: 200 µm (fluorescence images), 5 µm (SEM inserts). 60
5.3 Effects of scaffold topography and culture duration on nuclear shape descriptors of PWK-F cells on AFL and RFL scaffold surfaces: (a) roundness, (b) eccentricity, and (c) aspect ratio. The horizontal solid and dashed lines inside each box symbol represent the median and mean values, respectively, of the particular dataset, while the horizontal solid lines above the box symbols indicate statistically significant differences for $p < 0.05$. The red + symbols represent boxplot outliers. 62
5.4 Effects of scaffold topography and culture duration on cell shape descriptors of PWK-F cells on AFL and RFL scaffold surfaces: (a) roundness, (b) eccentricity, (c) aspect ratio, and (d) area ratio. The horizontal solid and dashed lines inside each box symbol represent the median and mean values, respectively, of the particular dataset, while the horizontal solid lines above the box symbols indicate statistically significant differences for $p < 0.05$. The red + symbols represent boxplot outliers. 64
5.5 Effects of scaffold topography, cell culture duration, and imaging magnification on nuclear shape descriptors of cells seeded on AFL and RFL scaffold surfaces: (a) roundness, (b) eccentricity, and (c) aspect ratio. The horizontal solid and dashed lines inside each box symbol represent the median and mean values, respectively, of the particular dataset, while the horizontal solid lines above the box symbols indicate statistically significant differences for $p < 0.05$. The red + symbols represent boxplot outliers. 66
5.6 Effects of scaffold topography, cell culture duration, and imaging magnification on shape descriptors of cells seeded on AFL and RFL scaffold surfaces: (a) roundness, (b) eccentricity, (c) aspect ratio, and (d) area ratio. The horizontal solid and dashed lines inside each box symbol represent the median and mean values, respectively, of the particular dataset, while the horizontal solid lines above the box symbols indicate statistically significant differences for $p < 0.05$. The red + symbols represent boxplot outliers. 67

6.1 Custom uniaxial stretching device showing an electrospun scaffold maintained under elongation within a 35-mm-diameter cell culture dish. 72

6.2 Scaffold topography and fiber alignment analysis. Representative SEM micrographs of RFL scaffold surfaces (a, c, e) and AFL scaffold surfaces (g, i, and k) together with the corresponding two-dimensional FFT-derived fiber orientation distributions for elongation (b, h) 0 %, (d, j) 10 %, and (f, l) 20 %. Uniaxial stretching was applied in the vertical direction of the SEM images. The RFL scaffolds exhibited progressive fiber realignment with increasing elongation, whereas the AFL scaffolds maintained their pre-existing alignment throughout the deformation range examined. Scale bars = 5 µm. 75
6.3 Effects of scaffold topography and 10 % uniaxial elongation on the nuclear shape descriptors of HDFa cells cultured on AFL and RFL scaffold surfaces, quantified in terms of (a) roundness, (b) eccentricity, and (c) aspect ratio. The solid and dashed horizontal lines within each box symbol denote the median and mean values, respectively. Horizontal lines above the boxplots indicate statistically significant differences ($p < 0.05$). Red "+" symbols represent outliers identified by the boxplot analysis. 76
6.4 Effects of scaffold topography and 10 % uniaxial elongation on the cell shape descriptors of HDFa cells cultured on AFL and RFL scaffold surfaces, quantified in terms of (a) roundness, (b) eccentricity, (c) aspect ratio, and (d) area ratio. The solid and dashed horizontal lines within each box symbol denote the median and mean values, respectively. Horizontal lines above the boxplots indicate statistically significant differences ($p < 0.05$). Red "+" symbols represent outliers identified by the boxplot analysis. 79
6.5 Representative fluorescence micrographs of HDFa cells stained for F-actin filaments (green; Alexa Fluor 488 phalloidin) and nuclei (blue; Hoechst 33342) cultured on AFL (left column) and RFL (right column) scaffold surfaces. Cells were cultured on unstretched scaffolds for (a, b) 3 days and (c, d) 5 days. Panels (e) and (f) show cells cultured for 3 days followed by an additional 2 days under 10 % uniaxial elongation (i.e., 5 days of total culture duration). The direction of uniaxial stretching is horizontal in the fluorescence images and corresponds to the aligned fiber direction in the AFL scaffolds. Scale bars = 300 µm. 80

6.6 Schematic illustration of the influence of scaffold topography and mechanical stretching on cellular and nuclear morphology. The left panel depicts the effect of topographical cues (contact guidance), whereby AFL scaffolds promote elongated cell and nuclear morphologies, whereas RFL scaffolds support more spread cellular morphologies and nuclei with greater roundness after 5 days of culture. The right panel illustrates the combined effects of topographical cues and mechanical stimulation (mechanotransduction). Application of uniaxial tensile strain induces directional organization even on initially random fiber networks, resulting in modestly increased cellular and nuclear elongation along the stretch direction. This combined action of aligned fiber topography and mechanical loading produces the most pronounced response, characterized by highly elongated and aligned cells and nuclei exhibiting the highest aspect ratio and lowest roundness among all experimental conditions. 85

Acknowledgments

I want to express my deepest gratitude to my advisor, Professor Kyriakos Komvopoulos, whose vast and profound knowledge has been instrumental in shaping my research. From our countless discussions to the thoughtful back-and-forth exchanges, his incisive questions and steady commitment to rigorous scientific inquiry continually challenged me to grow. I am especially grateful for the freedom he gave me to pursue my own ideas; it was his trust and guidance that allowed this work to take shape.

His encouragement, confidence in my abilities, and unwavering support were foundational throughout my doctoral journey. Beyond academia, his understanding during personal and family moments over the years meant more than words can express. It has been a privilege to have had not only an advisor but also a mentor and an ally, someone who offered me wisdom and kindness. I deeply admire and honor his many years of teaching and research across diverse fields. His dedication to science and education has been truly inspiring, and I am profoundly grateful for the opportunity to learn from him.

I also would like to thank my qualifying exam committee members, Professors Lisa Pruitt, Kevin E. Healy, and Robert O. Ritchie, for their time, thoughtful feedback, and valuable suggestions on my dissertation proposal. Their insights helped shape the direction of my research and strengthened its foundation. Likewise, I extend my gratitude to my dissertation committee, Professors Lisa Pruitt and Kevin E. Healy, for their time, comments, and constructive critiques throughout this process. Thank you for helping me shape my growth as a researcher and scholar. Your guidance has been invaluable in bringing this dissertation to completion.

Thank you to Professor Hayden Taylor for his support, for welcoming me into his group during our collaboration, for the invaluable discussions, and for providing research funding that supported me during key moments of my doctoral journey.

Furthermore, I am deeply grateful to my friends and colleagues in Professor Komvopoulos's lab, whose support and camaraderie have shaped my daily research life. I am equally thankful to members of Professor Healy's lab and to many others across campus, for their generosity and collaborative spirit. Whether through in-depth scientific discussions, listening to my evolving ideas, or helping me navigate the challenges of research, your support, friendship, and advice have been invaluable. Thank you for the countless conversations, encouragement, and sense of community that have made this journey all the more rewarding.

To the people who manage the collaborative labs, Paul Lum (BNC), Danielle Jorgens (EML), and Mary West (CTAF) — thank you for your insight and invaluable help with my experiments. Your expertise and willingness to assist made a significant impact on my work, and I truly appreciate your time and support.

I am also deeply grateful to the generous individuals who have funded fellowships in support of research and the advancement of knowledge. Their generosity has allowed scholars like me to pursue knowledge and innovation. A special thank you to Meltem Erol, who, through the College of Engineering, offered me invaluable support and encouragement and

provided funding when it was needed most. Your confidence in me and my work made a world of difference.

Most importantly, I am profoundly grateful to my husband for his unconditional love and support. His encouragement, patience, and unwavering belief in me have been my greatest source of strength. Through every challenge, he stood by my side, never giving up, always lifting me up, and constantly reminding me of what I am capable of. I could not have asked for a better partner, not only on this journey but throughout our life together as a family. I am forever thankful for his love, resilience, and companionship. To my babies, thank you for teaching me patience, resilience, and the beauty of finding wonder in everyday things. You have revealed the strength I didn't know I had and inspired me to finish this chapter of my life with determination and excitement for what comes next. I also want to thank my sisters for their camaraderie, for being a constant source of encouragement, laughter, and support, no matter the distance. And to my mom and dad, for their love, their unwavering support, the sacrifices they made to raise my sisters and me, and for always keeping us in their prayers.

Chapter 1

Introduction

1.1 Clinical Motivation

The human body is an intricate biological machine, composed of multiple interdependent systems that operate together to sustain life, generate movement, and respond to constantly changing physical demands. Distributed throughout these systems are the fibrous connective tissues, which range from densely aligned structures such as tendons, ligaments, and aponeuroses to the more multidirectional arrangements found in the dermis, fascia, and joint capsules. Though functionally distinct, these tissues share a common design strategy. They consist of hierarchically organized collagen fibers arranged according to the mechanical demands placed upon them. These matrices are populated by fibroblasts that continuously sense, maintain, and remodel the surrounding microenvironment (Mienaltowski et al. 2021). This structural organization spanning from the nanoscale fibril to the macroscale tissue gives fibrous connective tissues their mechanical function. In load-bearing tissues such as tendons and ligaments, however, this architecture is notoriously difficult to restore once damaged due to their inherent limited vascularity, low cellularity, and slow matrix turnover. These limitations constrain the regenerative response, leading to an injury site that typically resolves through disorganized scar formation rather than recovery of the native hierarchical structure (Leong et al. 2020).

1.2 Background

Fibrous connective tissue injuries are a widespread clinical challenge. In particular, tendon and ligament injuries represent one of the most common categories of musculoskeletal trauma, affecting athletes, aging populations, and workers exposed to repetitive mechanical loads alike. When conservative management, including physical therapy and rehabilitation, fails to restore function, surgical intervention to repair the injury site becomes necessary. Current repair strategies include primary suture repair, autografts, allografts, and synthetic grafts. While autografts remain the clinical gold standard due to their biocompatibility and

biological activity, they are limited by donor-site morbidity, restricted tissue availability, extended operative time inherent to harvesting from a second surgical site, and long-term donor-site complications. Allografts, though more readily available, carry risks of immune rejection, disease transmission, and high rates of recurrent rupture due to donor-recipient mismatch. Primary suture repair is the simplest approach, but it fails in a subset of patients, particularly those with chronic or large-volume defects, often leaving them with reduced mobility and even fewer treatment options. Synthetic grafts offer an alternative but have historically been limited by poor durability, wear debris, and inadequate integration with host tissue (Lim et al. 2019).

Producing fully functional tissue requires more than filling a defect. It requires recreating the organized biological microenvironment of the native tissue, including its structural organization, cellular alignment, and mechanical cues, while eliciting an appropriate immune response. Current clinical strategies are ill-equipped to meet this combined demand. Tissue engineering has emerged as a promising approach to address this unmet need, offering the possibility of designing biomaterial scaffolds that guide the regeneration of organized, functional tissue rather than solely occupying a defect. Central to this approach is the scaffold, which is a temporary, three-dimensional physical structure that guides the growth of new living tissue. The scaffold can be engineered to recapitulate key aspects of the native extracellular matrix (ECM), thereby directing cell adhesion, morphology, proliferation, differentiation, and ultimately tissue formation (Echeverria Molina, Malollari, Komvopoulos 2021).

One of the most versatile and widely adopted fabrication methods for fibrous scaffolds for tissue engineering is electrospinning. In the electrospinning process, a polymeric solution is pushed through a needle under a high-voltage electric field, the liquid deforms into a cone shape and ejects a stable, continuous jet that later stretches and forms fibers with diameters ranging from tens of nanometers to several micrometers (Wang et al. 2025; Shaban et al. 2026). Thus, a scale that closely mimics the collagen fibers of the native ECM. The resulting nonwoven fiber mats exhibit high porosity, large surface area, and, critically, tunable fiber diameter and alignment. For instance, by modifying the collector geometry, aligned or randomly oriented fiber architecture can be produced, directly governing the contact guidance cues presented to seeded cells (Jenkins, Little 2019; Chi et al. 2022; Shaban et al. 2026).

A broad range of polymeric materials has been explored for electrospun scaffold fabrication. Among synthetic biodegradable polymers, poly(L-lactic acid) (PLLA) is one of the most widely used and well-characterized materials. PLLA is a bio-based, biodegradable aliphatic polyester derived from renewable resources, valued for its notable mechanical properties, biocompatibility, and controlled degradation via hydrolysis into lactic acid, carbon dioxide, and water. The primary degradation product is lactic acid. Lactic acid has been shown to regulate macrophage metabolism and limit excessive inflammatory responses, suggesting that PLLA resorption may confer beneficial immunomodulatory effects in the tissue engineering context (Shi et al. 2024). PLA and its copolymers are used in a broad range of FDA-approved biomedical applications, including implantable medical devices, drug delivery

systems, and surgical sutures (Yang et al. 2024), reflecting a long-standing track record of safety and clinical translatability.

For an electrospun scaffold to successfully guide fibrous tissue regeneration, it must satisfy several interconnected design requirements. In no particular order, and starting with its biochemistry, the affinity of cells for a scaffold depends on both surface and bulk chemical cues. Surface hydrophilicity, charge density, and chemical specificity govern initial cell attachment, whereas bulk chemical characteristics influence cell signaling and infiltration. Acting together, these regulate cell growth, migration, differentiation, and ECM synthesis, and are central to achieving biocompatibility. This is followed by the scaffold microarchitecture, including fiber diameter, alignment, porosity, and layer organization, which must present appropriate contact guidance cues that promote cell elongation and directed migration along the axis of tissue loading. Another important requirement is the scaffold mechanical properties. The scaffold must be sufficiently stiff to provide structural support during regeneration, but not so stiff that it stress-shields the cells from the mechanical cues that drive tissue development (Yamamoto et al. 1993). Furthermore, the scaffold degradation profile must be tuned such that scaffold resorption proceeds in concert with new tissue formation, maintaining mechanical integrity throughout the critical healing window. Finally, the scaffold must support an appropriate immunological response, facilitating tissue integration without triggering chronic inflammation or fibrosis. These requirements are examined in detail in Chapter 2 (Echeverria Molina, Malollari, Komvopoulos 2021).

A particularly challenging design consideration in fibrous tissue engineering is the need to replicate the structural heterogeneity of native tissues. Many fibrous tissues, including the tendon-bone interface, the dermis, and the periodontal ligament, do not exhibit uniform fiber organization throughout their volume. Instead, they feature gradual transitions between regions of distinct fiber orientation, which are essential for distributing mechanical loads across structural boundaries and preventing stress concentrations at tissue interfaces (Chi et al. 2022; Feng et al. 2026). Replicating this organizational complexity in a synthetic scaffold represents a significant fabrication challenge and has motivated the development of bilayer and gradient scaffold designs that spatially vary fiber architecture across the scaffold depth.

Moreover, cell morphology, specifically the shape, elongation, and orientation of cells and their nuclei, is an active and meaningful indicator of tissue state, cellular function, and regenerative potential (Janmey, Miller 2011; Haftbaradaran Esfahani, Knöll 2020). On aligned fibrous substrates, fibroblasts adopt elongated morphologies oriented parallel to the fiber axis, whereas randomly oriented fibers produce more spherical or polygonal shapes (Jenkins, Little 2019; Echeverria Molina, Malollari, Komvopoulos 2021). This configuration is closely linked to the deposition of organized, dense extracellular matrix resembling that of native tendon, whereas rounded cell morphologies on randomly oriented substrates yield looser, disorganized matrix (Chi et al. 2022). Disruption of this organization, as occurs when injured tendon and ligament heal through disorganized scar formation rather than restoration of the native hierarchical architecture, is associated with impaired mechanical function (Leong et al. 2020; Korcari, Buckley, Loiselle 2022).

Quantifying cell morphology through shape descriptors such as roundness, eccentric-

ity, and aspect ratio provides a biologically informative readout of scaffold–cell interactions (Echeverria Molina, Komvopoulos 2025). Shape descriptors therefore offer a non-destructive and scalable measure of cellular response to topographical and mechanical cues, and are the primary metric used throughout this work.

In addition to topographical guidance, connective tissues are subjected to dynamic mechanical loading *in vivo* (Wang 2006). Cells sense and respond to these cues through mechanotransduction, the process by which external mechanical signals are converted into intracellular biochemical responses that regulate cytoskeletal organization, gene expression, and ECM remodeling (Wang, Thampatty 2006; Sun, Guo, Fässler 2016). Understanding how scaffold microarchitecture and mechanical loading interact to regulate cell morphology is therefore essential for designing scaffolds capable of recapitulating the organized cellular microenvironment of native fibrous tissue.

1.3 Contributions and Outline

This dissertation provides a comprehensive investigation of a bilayer electrospun PLLA scaffold, spanning the design and computational modeling of its fabrication process, its full material characterization, and ultimately its biological evaluation through the morphological response of dermal fibroblasts under temporal, topographical, and mechanical cues. Using a simple, unmodified, fully characterized material system without biochemical additives or surface modifications, this work provides mechanistic insight into scaffold-cell interactions that are often obscured in more complex, multi-component systems.

The contributions presented in this dissertation can be summarized as follows.

Chapter 2 provides a comprehensive review of the design challenges of polymeric scaffolds for tissue engineering. It examines key scaffold design parameters, including biochemical composition, microarchitecture, mechanical properties, biodegradability, and immunomodulation, and places them in the broader context of fibrous connective tissue regeneration. The chapter is based on the paper "Design Challenges in Polymeric Scaffolds for Tissue Engineering" by Maria I. Echeverria Molina, Katerina G. Malollari, and Kyriakos Komvopoulos, published in *Frontiers in Bioengineering and Biotechnology* (Echeverria Molina, Malollari, Komvopoulos 2021).

Chapter 3 presents an electrostatic finite element analysis (FEA) of the parallel-plate electrospinning configuration used to fabricate the bilayer membrane. The analysis reveals how the intensity and directionality of the electric field govern the deposition of aligned versus randomly oriented fibers. In addition, it shows that polymer accumulating between the collector plates exerts a local effect on the electric field itself. Beyond this specific collector geometry, this chapter establishes a computational methodology to evaluate alternative collector configurations and design electrospinning setups to produce fibrous membranes with tailored microstructures. This chapter is based on the paper "An Electrostatic Finite Element Analysis of the Electrospinning Process of Bilayer Constructs Using a Parallel-Plate

Collector" by Maria I. Echeverria Molina and Kyriakos Komvopoulos, published in *Materials Letters* (Echeverria Molina, Komvopoulos 2022).

Chapter 4 investigates the degradation behavior of the electrospun bilayer PLLA scaffold in physiological conditions over an extended period. Fiber alignment was quantified in the as-fabricated scaffolds (day 0), while fiber diameter, morphology, molecular weight, crystallinity, and thermomechanical properties were tracked across degradation time points by scanning electron microscopy, differential scanning calorimetry, gel permeation chromatography, and tensile testing. Mass loss was determined gravimetrically. Testing shows that scaffold degradation proceeds through an interplay between chain scission and orderly chain rearrangement within the polymer, leading to coupled changes in molecular weight, crystallinity, mass loss, and thermomechanical properties. Moreover, the scaffold retains both its structural morphology and adequate matrix stiffness over the degradation period studied. This chapter is based on the paper "In Vitro Degradation of Fibrous Bilayer Poly-L-Lactic Acid Scaffolds" by Maria I. Echeverria Molina and Kyriakos Komvopoulos, published in the *Journal of Biomechanics* (Echeverria Molina, Komvopoulos 2023).

Chapter 5 examines how scaffold topography and culture duration shape fibroblast morphology on the bilayer scaffold. Fibroblasts were seeded onto both the aligned and randomly oriented fiber surfaces and cultured for 1, 3, 6, and 9 days, and nuclear and cytoskeletal morphologies were quantified using shape descriptors including roundness, eccentricity, aspect ratio, and area ratio. Fiber alignment was found to be a strong determinant of cell shape, as cells on aligned fibers adopted elongated and oriented morphology, whereas those on randomly oriented fibers spread in a branched, multidirectional manner. Culture duration emerged as a second governing factor, with cells on both surfaces converging toward rounder, stabilized morphologies by day 6, indicating a progressive remodeling of the cell-scaffold interaction over time. This chapter is based on the paper "Influence of Scaffold Topography and Culture Duration on Fibroblast Morphology in Tissue Engineering" by Maria I. Echeverria Molina and Kyriakos Komvopoulos, published in *Tissue Engineering Part A* (Echeverria Molina, Komvopoulos 2025).

Chapter 6 extends this investigation to the combined effects of scaffold architecture and applied mechanical loading. Bilayer scaffolds were characterized by scanning electron microscopy and two-dimensional fast Fourier transform analysis at 0%, 10%, and 20% elongation, and adult human dermal fibroblasts cultured on both aligned and randomly oriented fiber surfaces were assessed under unstretched conditions and under sustained 10% uniaxial strain. The analysis performed showed that stretching promotes alignment of initially random fibers while preserving the orientation of pre-aligned regions. At the cellular level, nuclear morphology showed little dependence on scaffold architecture when unstretched but responded markedly to applied strain. In contrast, cell morphology was governed primarily by fiber alignment, showing limited sensitivity to sustained loading. The results confirmed that scaffold architecture and mechanical stretching regulate organization, from scaffold microstructure to cellular and nuclear morphology, by distinct yet complementary mechanisms. This chapter is based on the paper "Scaffold Fiber Architecture and Uniaxial Stretch Differentially Regulate Cell and Nuclear Morphology in Human Dermal Fibroblasts" by Maria

Echeverria Molina and Kyriakos Komvopoulos, published in *Tissue Engineering Part A* (Echeverria Molina, Komvopoulos 2026).

Chapter 7 presents the conclusions of the dissertation, accompanied by a summary of the main findings of each chapter, and outlines directions for future work based on the results and limitations of the studies presented.

Chapter 2

Design Challenges in Polymeric Scaffolds for Tissue Engineering

The content of this chapter was published in *Frontiers in Bioengineering and Biotechnology*, 9, 617141 (2021), as "Design Challenges in Polymeric Scaffolds for Tissue Engineering" by Maria I. Echeverria Molina, Katerina G. Malollari, and Kyriakos Komvopoulos.

2.1 Introduction

The human body is by far the most sophisticated autonomous system consisting of billions of molecular nanomachines built from the DNA code of a person's zygote, which not only can renew certain types of cells in a complex programmable manner but also repair damaged tissue. However, this self-healing capacity is limited to the type of cells comprising the tissue and the multiple factors controlling tissue self-repair, including degenerative diseases, traumatic events, and age. In fact, some tissues do not exhibit a self-healing capability. To this end, tissue engineering (TE) plays a vital role in the development of functional constructs that can promote the generation of tissue and organ equivalents, or enhance tissue regeneration to restore and/or improve the functionality of damaged tissues and organs, ultimately replacing autografts, allografts, or even whole organs. Examples of engineered tissue applications include skin, cartilage, veins, arteries, brain, gastrointestinal tissues, and cornea. Although some of the aforementioned engineered tissues have been approved for human use, successful transplantation and, especially, implant longevity are limited due to complications leading to biomaterial rejection by various complex mechanisms (Sheikh et al. 2015; Anderson, Jiang 2017).

The increasing demand for human tissues and organs highlighted in a recent report (Israni et al. 2020) and the acceleration of deaths due to acute illnesses, such as ischemic coronary diseases (World Health Organization 2018), have increased the market demand for TE (Grand View Research 2020), highlighting the importance of tissue regeneration

and repair. TE is a multidisciplinary field concerned with the creation of tissue by different techniques that depend on cell seeding of non-woven, porous scaffold biomaterials and the incorporation of various growth factors that promote tissue growth. Scaffolds are 3D constructs that mimic the extracellular matrix (ECM) of native tissue, typically made of biodegradable and biocompatible polymers. A polymeric scaffold material must be characterized by multiple attributes, such as no chronic inflammatory response and/or rejection by the surrounding tissue, degradation rate that matches the healing or growth rate of the tissue, non-toxic byproducts that can be expelled by the body in a timely fashion, acceptable shelf life, good mechanical properties compatible with those of the native ECM which do not impede cell interaction, and no changes in architecture and properties due to sterilization (Pruitt, Chakravartula 2011). However, cell culture, tissue growth, and implantation may affect the scaffold properties and performance due to material degradation and ever-changing interfaces. The scaffold performance is quantified in multiple ways, especially by the cell behavior that it can stimulate and how closely it mimics the native ECM of the generated tissue.

Important developments in TE have been encountered in the past two decades, largely due to significant advances in biomaterials, fabrication, and techniques designed to instigate specific cellular behaviors that stimulate the formation of tissue analogs. Biomaterials showing a versatile performance depending on the biological environment have been developed by modifying their chemistry. Examples include the assimilation of specific surface cues by plasma treatment, layer-by-layer deposition or surface functionalization with polydopamine (PDA), and the so-called "click" chemistry, which can impart specificity for multiple cues (e.g., drug delivery, crosslinking, and cell attachment) to the bulk and the surface of polymeric scaffolds. Hydrogels are a special class of materials that have attracted considerable attention as scaffolds because they can be delivered to the desired site by minimally invasive methods (e.g., by injection) and doped with drugs, cells, and growth factors, therefore showing high potential for many TE applications, such as brain and skin tissues. Notable breakthroughs in TE have also been accounted as a result of significant progress in the development of versatile fabrication methods for scaffold engineering (Dutta et al. 2017; Walker, Santoro 2017; Zhao et al. 2018). For example, 3D printing techniques have provided capabilities to create specific and controlled geometries and shapes of constructs and to simultaneously use biomaterials, growth factors, and cells to create composites that exhibit unique degradation rates, enhanced cell differentiation, specific biological cues, and excellent biomechanical properties throughout the scaffold's lifetime (Do et al. 2015; Di Luca et al. 2016c; Bittner et al. 2018; Ng et al. 2018; Han et al. 2021). Other less common and/or new fabrication techniques, such as multiphoton, laser-assisted, and computed axial lithography, have also been used to create scaffolds for TE (Liang et al. 2021). In addition, conventional methods modified to incorporate cells and growth factors in polymeric constructs, such as electrospinning and gas foaming, have gained attention recently (Costantini, Barbetta 2018; Hong et al. 2019; Karpov et al. 2020).

The understanding of the function of different cells that form a tissue or an organ, the improved techniques for harvesting cells, and the insight into how the healing multifactorial

process works as well as the interplay of the physicochemical properties and morphology of biomaterials have led to the development of scaffolds that can stimulate the desired cellular behavior, while providing the chemical and mechanical cues for achieving tissue growth and regeneration. However, the difficulty to reproduce the complex biological environment during in vitro testing inhibits direct comparisons with the material's behavior in vivo. Developments in bioreactors have enabled the incorporation of in vivo-like signals, such as static and dynamic electromechanical cues and control of the pH, temperature, gene expression, and growth factors, which are closely associated with the initial stages of cell differentiation. More importantly, because most of the engineered tissues are small versions of human counterparts, they can only be tested in animal models, with most of the attempts to create full-size organs being largely ineffective with only a few exceptions, such as 3D printed human ears (Zhou et al. 2018). Nevertheless, some of the engineered tissues (e.g., skin, cornea, and vascular grafts) have reached pre-clinical trials or commercial application, despite the fact that they cannot be implanted to all patients and/or fully restore normal tissue function, thus illuminating the complexity to recreate totally functional tissues. However, despite significant progress in the development of organ-on-chip platforms that can more closely reproduce physiological settings in vitro (Zhang et al. 2018; Wu et al. 2020), animal models are still a fundamental part of the research needed to better understand diseases and to develop more effective drug delivery methods.

Because scaffold design can greatly affect cellular behavior from its inception, there are many critical factors to consider in TE. The objective of this chapter is to provide an appraisal of the current state-of-the-art in TE, specifically focusing on the correlation of scaffold parameters and cell fate, the types of polymeric materials currently used in scaffold engineering, and the effects of biochemical characteristics, structure architecture, biodegradability, and mechanical behavior of scaffold materials on the resulting biomimicry cues and their ability to stimulate specific cell behaviors. In addition, two important soft tissue application areas, namely skin and brain scaffold engineering, are discussed in the context of associated anatomy and biological functions, and the design challenges of scaffolds intended for these TE applications are interpreted in the light of recent advances in scaffold engineering.

2.2 Scaffold Main Characteristics

Scaffolds play a fundamental role in TE because they provide mechanical support, allow perfusion of nutrients and oxygen, transfer biochemical signals that modulate cell behavior (e.g., attachment, motility, proliferation, and differentiation), and can be used to release drugs and growth factors. A scaffold must mimic the ECM by exhibiting the biological, chemical, and mechanical cues that influence cell phenotype and tissue formation. Biomaterials for tissue generation must exhibit tailorable properties to enhance cell attachment, migration, growth, and differentiation, prevent undesirable host responses that lead to chronic inflammation at the biomaterial interface, display chemical and mechanical stability for providing structural support while demonstrating controllable microstructure and adequate porosity, and show

good biodegradability without producing toxic residues and byproducts. Biomaterial scaffolds for TE must be developed according to the aforementioned design criteria by integrating engineering and biological principles and molecular cues that imitate critical structural aspects of the native tissue and can effectively direct cellular behavior and functionality. Based on the preceding requirements, biomaterial scaffolds can be classified into three main material categories, namely architectured materials with fibrous and porous structures, hybrid or composite materials, and hydrogels.

Architectured materials are mainly synthetic biodegradable polymers characterized by 3D fibrous networks. Natural ECM decellularized tissue materials (typically powdered) also belong in this category. These materials can be formed by various fabrication techniques, such as electrospinning, freeze-drying, gas foaming, solvent casting, particulate or porogen leaching, phase separation, self-assembly, and 3D printing. Polymers that belong in this category are synthetic biodegradable polymers, such as poly(lactic acid) (PLA), poly(glycolic acid) (PGA), poly(ε-caprolactone) (PCL), polyvinyl alcohol (PVA), polyethylene glycol (PEG), polyethylene oxide (PEO), polyurethane (PU), and polyvinylpyrrolidone.

Hybrid materials encompass blends of synthetic polymers, natural polymers, and decellularized tissue with one or few solvents. Alternatively, composite materials include the same polymer-based constituents as hybrid materials, but possess either layered or multi-material structures made by various processes. Hybrid and composite materials are typically produced by fabrication methods designed to synthesize architectured biomaterials, with a few exceptions, such as hydrogel-based hybrid materials.

Hydrogels are swollen natural or synthetic polymer networks crosslinked by physical and/or covalent bonds, which show a high potential for tissue repair because they form ECM-like architectures and can serve as platforms for minimally invasive delivery of macromolecules to the injury site (Hsieh et al. 2017; Chen et al. 2019; Peppas, Hoffman 2020). Polymer-based hydrogels show numerous advantages over architectured and hybrid/composite materials, such as different chemical, mechanical, and spatial cues for encapsulating cells, and can provide bioactive signals to the host tissue. The capability of hydrogels to modulate nutrient diffusion and cell motility and their mechanical stability depend on the crosslink density and mesh size, which can be tuned during the fabrication.

Basic understanding of how a scaffold can be modified to elicit the cellular response needed for a specific TE application is of paramount importance in scaffold engineering and requires insight into the effects of the biochemical characteristics, structure and morphology, biodegradability, and mechanical behavior on the scaffold performance. The main design characteristics of scaffolds intended for the TE applications discussed in this section are depicted in Figure 2.1.

Biochemical Behavior

The affinity of the cells for a scaffold greatly depends on the chemical and topological surface and bulk cues of the scaffold material. Specifically, the hydrophilicity, charge density, and chemical specificity of the scaffold surface affect cell attachment, whereas the bulk chemi-

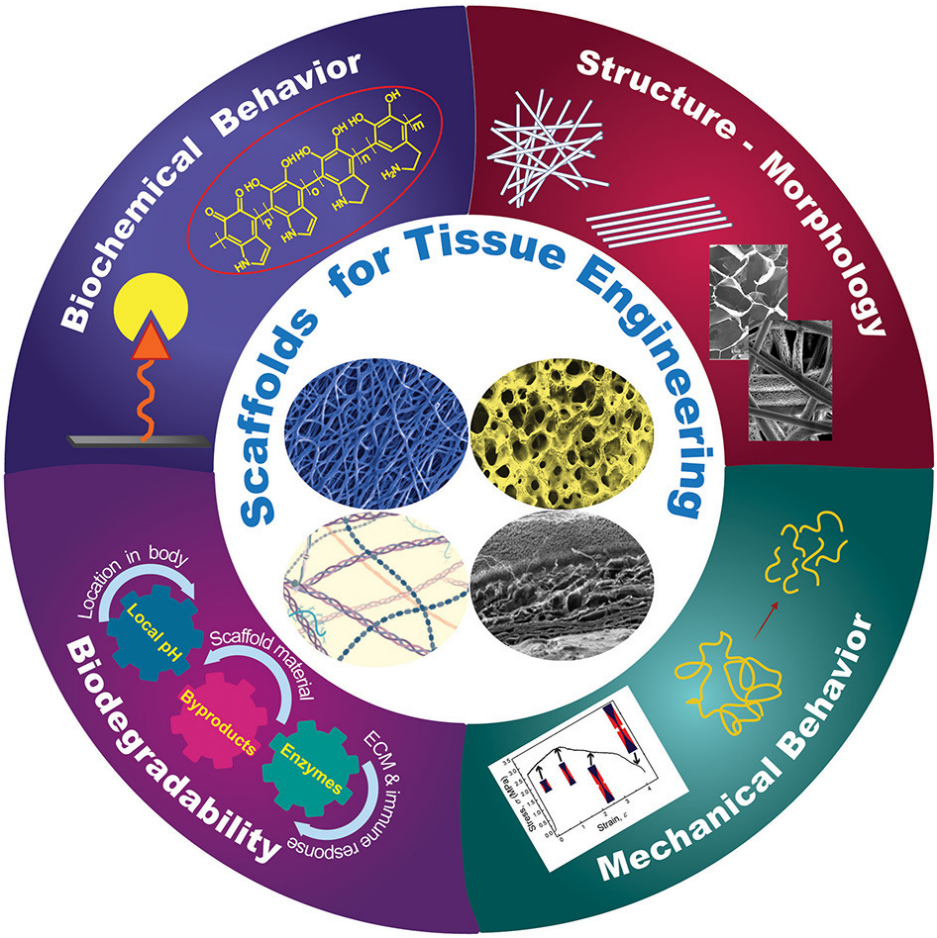

Figure 2.1: Schematic representation of different design characteristics of biomaterial scaffolds that are necessary for eliciting the cellular behavior required for a specific tissue application. Effective tuning of the parameters described in each category plays a critical role in the performance of architectured (fibrous and porous), hybrid, and hydrogel scaffolds for tissue generation and repair.

cal characteristics influence cell signaling and infiltration. Both surface and bulk chemistry synergistically regulate cell growth, migration, differentiation, ECM synthesis, and tissue morphogenesis and are critical to achieving scaffold biocompatibility. Scaffold chemical modification has emerged as an effective means of producing biochemical specificity and recognition, with chemical moieties incorporated in the bulk and/or surface of the scaffolds to mediate cell behavior and functionality, direct inflammatory and immunological response, and ameliorate foreign body reaction at the scaffold-tissue interface (Allen et al. 2006; Anderson, Rodriguez, Chang 2008; Owen, Shoichet 2010; Nimmo, Owen, Shoichet 2011; Lanza et al. 2020).

Kolb, Finn, Sharpless (2001) and Zou et al. (2018) established click chemistry as a potent chemical modification strategy for scaffold biochemical functionalization, primarily because it demonstrates modularity, high reactivity, superb selectivity, high yield, and mild reaction conditions (Jiang et al. 2014). This approach offers many attractive possibilities for bioconjugation, accordingly enabling tailored and well-defined properties of polymeric scaffolds to be acquired via a wide range of surface and bulk functionalizations. Various click chemistry tactics, including copper(I)-catalyzed azide-alkyne cycloaddition (CuAAC) (Meldal, Tornøe 2008), strain-promoted alkyne-azide cycloaddition (SPAAC) (Prescher, Dube, Bertozzi 2004; Laughlin et al. 2008), thiol-X reaction (Hoyle, Lowe, Bowman 2010; Daniele et al. 2014), Diels-Alder (DA) reaction (Nimmo, Owen, Shoichet 2011; Tasdelen 2011), and oxime ligation (Kalia, Raines 2008), have been used to modify the chemistry of biomaterials (Xi et al. 2014; Zou et al. 2018) (Figure 2.2A). In the CuAAC chemistry reaction, a terminal alkyne reacts with an azide group to form a stable triazole ring. CuAAC chemistry has been used to attach functional ligands to the surface of PCL fibers (Lancuški, Bossard, Fort 2013); specifically, the PCL was end-functionalized with an azide moiety before electrospinning and, subsequently, bioactive groups containing alkyne moieties were conjugated at the fiber surface. The enhanced surface hydrophilicity imparted by the conjugated bioactive groups promoted cell attachment without reducing the molecular weight (Lancuški, Fort, Bossard 2012). Because of the toxicity of Cu(I) in biological systems, the SPAAC reaction has gained increased interest as a metal-free alternative approach, extending the usage of click chemistry in physiological settings. SPAAC has been used to functionalize the surfaces of fibers and develop in situ hydrogels with controlled crosslink densities (Zheng et al. 2012). Additionally, the functionalization and synthesis of polymeric materials by thiol-X reactions under mild conditions are characterized by simplicity and efficiency (Lowe 2010). Among different thiol-based reactions, radical-mediated thiol-ene and thiol-yne are the most exploited in TE applications. However, because the former treatment uses UV light that may damage the cells and the tissue, the applicability of this chemical method is limited. In view of this obstacle, nucleophile-mediated thiol-X reactions, such as thiol-Michael addition, have been considered as plausible substitutes (Hoyle, Lowe, Bowman 2010). In addition, oxime ligation is a reaction that can be safely implemented both in vitro and in vivo, because it can be performed at room temperature without the need of a metal catalyst and the application of UV light.

Click chemistry can be applied during the scaffold fabrication to modulate crosslink poly-

merization of functional monomers, or as a post-click functionalization strategy to impart the surfaces of polymeric scaffolds with specific functional groups to elicit cell attachment (Figure 2.2B). The high-efficiency reactions and excellent bond stability that characterize this method enable the crosslinking reactions to be precisely controlled to achieve tunable crosslink densities. Accurate tuning of the crosslink density is critical in the fabrication of hydrogel scaffolds. For instance, azide or alkyne terminal functionalities can be introduced in macromolecules, such as PEG and hyaluronic acid (HA), or in the presence of Cu(I) through the CuAAC crosslinking reaction, producing "clickable" hydrogels with tunable morphological and mechanical properties (Crescenzi et al. 2007; Gopinathan, Noh 2018). Click chemistry also provides a facile way to introduce reactive and clickable sites directly on functional polymers. An example is the incorporation of free thiol groups in poly(3-mercaptopropyl) methylsiloxane-based fibers partially photo-crosslinked by UV illumination during electrospinning, followed by maleimide terminated poly(N-isopropyl acrylamide) brushes added to the fiber surface via a thiol-Michael addition reaction (Yang et al. 2012). The resulting fibers exhibit a thermosensitive behavior that may be desirable in several TE applications (Yang et al. 2012). In addition, because most synthetic polymers utilized in TE are lacking cell-binding moieties and often exhibit hydrophobic behavior, click chemistry can be used to decorate scaffolds with short amino-acid sequences that bind to the receptors on the cell surfaces and mediate cell attachment via specific surface-ligand biological signals. The most commonly immobilized peptide for surface and bulk modification is arginylglycylaspartic acid (RGD), for which the signaling domain is derived from fibronectin and laminin. In addition, several other peptide sequences, such as the Tyr–Ile–Gly–Ser–Arg (YIGSR) and the Ile-Lys-Val-Ala-Val (IKVAV), have also been immobilized on the surface of various biomaterials (Shin, Jo, Mikos 2003).

Although in vivo studies are critical for evaluating the performance of a scaffold, decoupling and elucidating all possible mechanisms that dictate cell fate is cumbersome because of the complex and sophisticated nature of most native biological environments. To disentangle the complexity of in vivo phenomena and elucidate how cells receive and transmit information, it is imperative to employ systems that can assay cell functions in well-defined settings that imitate native environments. To face this challenge, click chemistry has been used to functionalize specific scaffold sites and create 3D patterns for in vitro replicating and evaluating biological processes and environments (Wylie et al. 2011; Azagarsamy, Anseth 2013; Truong et al. 2015). For instance, 3D-patterned hydrogels have been produced from biocompatible click reactions in conjunction with orthogonal photo-chemistries to sequentially introduce and remove biochemical and biophysical signals with precise spatiotemporal control (DeForest, Polizzotti, Anseth 2009; DeForest, Anseth 2011; DeForest, Anseth 2012; Ruskowitz, DeForest 2018). Enzymatically degradable hydrogel platforms with photo-patterned biomacromolecules introduced by sequential click reactions have enabled the detection and promotion of specific cellular functions and the direct observation of cellular processes, such as migration, proliferation, and morphology evolution (DeForest, Anseth 2012). The SPAAC reaction has been used in hydrogel synthesis and the thiol-ene reaction to conjugate biomolecules (DeForest, Anseth 2012). Thiol-ene reactions have also

been used to introduce bioactive peptides in photo-degradable hydrogels, which were then photo-cleaved from the hydrogel network by UV radiation, enabling spatiotemporal control over peptide concentration (DeForest, Polizzotti, Anseth 2009; DeForest, Tirrell 2015). The foregoing studies have demonstrated that cell attachment, proliferation, and motility can be controlled, and cell behavior can be confined to patterned regions to provide platforms for studying how cells respond to chemical and mechanical cues (Figure 2.2C).

In addition to the click chemistry, which has been rapidly implemented in various biomaterial functionalizations, PDA treatment has also emerged as a facile and versatile chemical functionalization method (Madhurakkat Perikamana et al. 2015; Cheng et al. 2019; Mallollari et al. 2019). The principal chemical modification strategies before the introduction of PDA were deposition of self-assembled monolayers (SAMs), plasma-assisted surface chemistry modification (PASCM), and layer-by-layer (LBL) deposition. However, SAMs require compatible chemistry between the surface and the absorbate, surface chemistry functionalization by PASCM is susceptible to alteration with time, and LBL deposition requires multiple coating cycles (Ryu, Messersmith, Lee 2018). Since its introduction (Lee et al. 2007), PDA has been extensively used to functionalize a broad range of surfaces, including metals and ceramics, as well as materials exhibiting low surface energy. Depositing a conformal PDA coating to the surfaces of the latter materials not only improves the solubility and stability of the scaffold, but also provides multi-functionality. This is because the reactivity of the chemical residues in the PDA structure toward nucleophilic amines and thiols yields a superior capacity for immobilizing and conjugating a variety of molecules through Michael addition and Schiff-base formations (Yang, Stuart, Kamperman 2014). DNA, drugs, cells, minerals, peptides, and proteins have been functionalized on PDA-modified substrates for diverse TE applications (Ryu et al. 2010; Tsai et al. 2014; Cheng et al. 2019; Li et al. 2020; Rühs et al. 2020). It has been reported that PDA can promote cell adhesion to various substrates (Ku, Park 2010). In fact, the former study showed that glass, polydimethylsiloxane, silicone rubber, polytetrafluoroethylene, and polyethylene, which are highly resistant to cell attachment (adhesion), when coated with PDA demonstrate cell adhesion characteristics comparable to those of gelatin-coated substrates seeded with human umbilical cord vascular endothelial cells.

It is also known that PDA enhances cellular interaction with biomaterials by immobilizing cell adhesive ECM biomolecules. Specifically, PDA can serve as a primer for the subsequent conjugation of different cell adhesive moieties via covalent interactions between catechols and the amines or thiols of biomolecules (Figure 2.2D). Several PDA-coated polymer substrates can be functionalized with adhesive peptide sequences derived from ECM-based biomolecules, such as fibronectin, laminin, and growth factors (Cai et al. 2013). For example, it has been observed that PDA-coated poly(lactic acid-co-ε-caprolactone) immobilized dual bioactive factors, i.e., cell adhesive RGD-containing peptide and basic fibroblast growth factor (bFGF) for vascular grafting (Lee et al. 2012). The immobilization of RGD and bFGF influenced cell migration and proliferation, respectively, whereas the co-immobilization exhibited a synergistic effect, confirming that PDA can serve as a functionalization platform for vascular grafts. While PDA has been mostly used for post-functionalization, it is also

of particular interest in hydrogel fabrication. For instance, PDA-crosslinked hydrogels, such as HA-catechol hydrogels, confer high stability, tunable mechanical properties, and minimal toxicity (Ryu et al. 2011; Hong et al. 2013). Although PDA has been proven to be a multifaceted chemical toolbox and PDA-coated scaffolds demonstrate enhanced adhesion, proliferation, and differentiation of various cells, the long-term in vivo toxicity and integrity of PDA during scaffold degradation require further in-depth investigation.

The above synopsis of surface and bulk chemical modification methods of the scaffold surfaces discloses a strong correlation between the scaffold chemistry and the host tissue response. The immunological response of the host tissue following scaffold implantation or injection can affect tissue regeneration. Consequently, a fundamental understanding of the effect of scaffold surface chemistry on cellular behavior is of utmost importance in the design of biomaterials that can modulate host immune reactions.

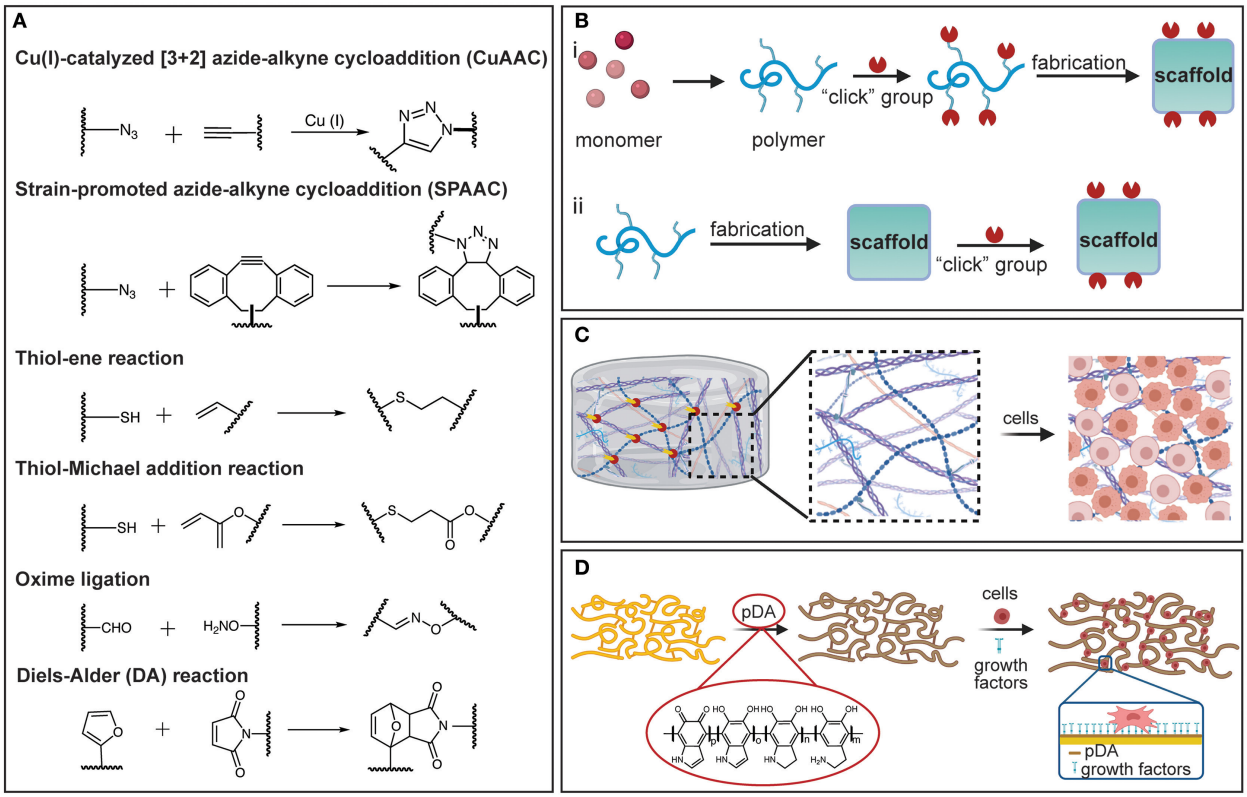

Figure 2.2: (A) Representation of various click chemistry reactions used in the fabrication of polymeric scaffolds. (B) Fabrication strategies based on click chemistry: (i) pre-click and (ii) post-click. (C) Schematic illustrating a hydrogel crosslinked by click chemistry and functionalized with ECM-based molecules to promote cell attachment and differentiation. (D) Schematic showing a PDA-coated electrospun scaffold decorated with growth factors to promote cell differentiation. [Panels (B)–(D) were created with BioRender.com].

Structure and Morphology

The materials and fabrication methods used in scaffold engineering must be versatile to allow tailoring of various key structure parameters (e.g., fiber diameter, porosity, and fiber alignment) and, thus, produce a scaffold that closely mimics the ECM of the tissue of interest. Variations of these parameters lead to different cellular responses (Jenkins, Little 2019). One of the tunable parameters in fibrous scaffolds is the fiber diameter that has been proven to modulate cell differentiation (Christopherson, Song, Mao 2009; Wang et al. 2012; Bean, Tuan 2015; Ghanian et al. 2015; Nguyen, Sathe, Yim 2016; Narayanan et al. 2020) and can be controlled by adjusting the fabrication process conditions (Elkasaby et al. 2018) and the degree of crosslinking (Shields et al. 2004; Gonçalves de Pinho et al. 2019). As an example, the alignment of 3 µm-diameter fibers was found to enhance the arrangement, growth, and differentiation of myoblasts, contrariwise to 300 nm-diameter aligned fibers (Narayanan et al. 2020). Changes in fiber diameter have also been observed to impact gene expression and phenotypic markers (Bashur et al. 2009; Noriega et al. 2012; Erisken et al. 2013; Lee et al. 2017). Similarly, fiber diameter has been shown to affect cell adhesion and proliferation (Erisken et al. 2013; Entekhabi et al. 2016). For instance, tendon fibroblast seeding on electrospun scaffolds consisting of poly(lactic-co-glycolic acid) (PLGA) nanofibers demonstrated an enhancement of cell proliferation, total collagen, and proteoglycan, whereas their microfibrous version demonstrated increased expression of phenotypic markers, such as collagen I, II, and V and tenomodulin (Erisken et al. 2013). These findings indicate that nanofibers resemble an injured ECM and stimulate regeneration, whereas microfibers aid to maintain the fibroblastic phenotype. The fiber diameter also exhibits a significant effect on cell infiltration, which is critical to 3D scaffold engineering. Indeed, it has been discovered that the larger the fiber diameter the better the infiltration of human venous myofibroblasts and more homogeneous the cell delivery in the scaffold (Balguid et al. 2009). Other studies have revealed a considerable effect of fiber diameter on the cell morphology and size (Bashur et al. 2009; Hsia et al. 2011; Daud et al. 2012; Kuppan, Sethuraman, Krishnan 2015; Lee et al. 2017) as well as on the cell migration velocity and distance range (Wang et al. 2010; Binder et al. 2013; Kievit et al. 2013; Meehan, Nain 2014; Ottosson, Jakobsson, Johansson 2017; Estabridis et al. 2018). However, fixing the fiber diameter for a particular cell behavior is not possible because it depends on the type, size, and shape of cells, the scaffold material, and the fabrication process, which affects the scaffold structure and fiber diameter (Noriega et al. 2012; Zouani et al. 2012).

Similar to the fiber diameter, microgroove patterns can influence the cell morphology and, in turn, the proliferation rate and spreading of the cells (Thakar et al. 2009) as well as cell differentiation (Watari et al. 2012; Abagnale et al. 2015). For instance, seeding of human mesenchymal stem cells (hMSCs) isolated from lipoaspirates and cultured in a differentiation medium on topographically patterned structures with grooves 5 µm in width and ridges of different widths promoted osteogenesis for 2 µm-wide ridges and adipogenesis (fat cell formation) for 15 µm-wide ridges, whereas 650 nm-wide ridges stimulated differentiation toward osteogenic and adipogenic lineages (Abagnale et al. 2015), in contrast with the findings of a

previous study (Watari et al. 2012).

Another scaffold parameter that can be adjusted is the fiber alignment or the structure morphology, which have also been correlated with various cellular responses (Sundararaghavan et al. 2013). In particular, aligned fibers have been observed to enhance stem cell differentiation conversely to randomly oriented fibers (Christopherson, Song, Mao 2009; Tijore et al. 2015; Abarzúa-Illanes et al. 2017; Sperling et al. 2017). However, other findings suggest that random fibers represent a more suitable environment for stem cell differentiation (Lins et al. 2017). Enhanced cell proliferation has also been linked to fiber alignment, although there have been reports of increased cell affinity to attach on either aligned or randomly dispersed fibers (Lim et al. 2010; Ren et al. 2013; Lins et al. 2017). For instance, while increased keratocyte proliferation occurred on the aligned nanofibers of a gelatin/poly(L-lactic acid) (PLLA) scaffold, corneal epithelial cells exhibited a higher proliferation on randomly oriented fibers of the same material (Yan et al. 2012), revealing a unique cell response to scaffold fiber alignment. Moreover, correlations between cell shape and fiber orientation have been observed in several investigations. Typically, cells tend to elongate in the direction of fiber alignment and assume a spherical or polygonal shape when seeded on scaffolds with randomly oriented fibers (Bashur et al. 2009; Vimal, Ahamad, Katti 2016). Surprisingly, while keratocytes spread randomly on fibers oriented in various directions and elongate along the direction of aligned fibers, corneal epithelial cells remain large, round, and flat on both randomly oriented and aligned fibrous gelatin/PLLA scaffolds (Yan et al. 2012). Additionally, the fact that cell migration occurs faster in the direction of fiber alignment (Ottosson, Jakobsson, Johansson 2017) reveals a dependence of cell migration on both fiber diameter and alignment and highlights the importance of optimizing the scaffold morphology during the fabrication.

Pore scaffold architecture, including pore size, shape, and density, is of principal importance in cellular behavior. Generally, high porosity and large pores are associated with increased proliferation, differentiation, and gene expression (Lowery, Datta, Rutledge 2010; Zhang et al. 2010; Zhang et al. 2014; Nunes-Pereira et al. 2015; Di Luca et al. 2016c; Di Luca et al. 2016d), although an opposite trend has been reported in some studies (Mandal, Kundu 2009; Ng et al. 2018). For instance, in the case of silk fibroin porous membranes of fixed porosity fabricated by freeze-drying, large pores enhanced the proliferation of human dermal fibroblast (HDF) cells compared to membranes with small pores; however, membranes with high porosity and interconnectivity showed increased cell proliferation and cellular migration even for a much smaller pore size (Mandal, Kundu 2009). These results suggest that high porosity and interconnectivity assist cell migration within the construct, facilitating cell growth in a compatible environment. Moreover, the pore size may exhibit a more profound effect on the proliferation of HDF cells compared to the fiber diameter and may also affect the cell morphology. For example, while 20 µm pores promoted cell elongation along the fibers of electrospun PCL scaffolds, 6.5 µm pores resulted in cell spreading across the fibers (Lowery, Datta, Rutledge 2010). In general, pores larger than the cell stimulate cell alignment along a single fiber, whereas pores smaller than the cell favor cell bridging across fibers, resulting in slower movement and longer migration distances. This behavior may be attributed to the

fact that large pores promote single-fiber cell attachment, which is conducive to faster cell migration. Nonetheless, the pore size effect on the cell behavior is strongly depended on the cell type and scaffold material (Nunes-Pereira et al. 2015).

Pore size and shape gradients are also important scaffold characteristics affecting cellular behavior. For example, in vitro experiments with hMSCs seeded on 3D printed PCL scaffolds with ∼73% porosity and square or rhomboidal pores exhibited differentiation to chondrogenic and osteogenic cells, respectively (Di Luca et al. 2016b). Pore size gradients have also been linked to specific cellular differentiation and gene expression (Oh et al. 2007; Di Luca et al. 2016c; Di Luca et al. 2016d), whereas radially varying porosity has been reported to yield cell behaviors characterized by gradient gene expression and cell differentiation and proliferation (Di Luca et al. 2016a). Through-thickness variation of the porosity and the fiber density accomplished by combining aligned and randomly oriented fibers in the scaffold structure and the incorporation of surface microwells have been correlated with increased cell migration and proliferation compared to controls of lower porosity consisting of randomly oriented fibers fabricated under the same conditions (Cheng et al. 2013a; Pu, Komvopoulos 2014; Pu et al. 2015).

Surface roughness is another scaffold parameter that strongly affects gene expression (Chen et al. 2017b) and the adhesion (Milleret et al. 2012), morphology (Chen et al. 2017b), differentiation (Faia-Torres et al. 2015), and proliferation (Ribeiro et al. 2015) of the cells. It has been found that rough and smooth surfaces prompt different cell responses. For instance, an investigation of the effect of surface roughness of electrospun poly(ethylene oxide terephthalate)/poly(butylene terephthalate) scaffolds on gene expression, differentiation, and morphology of hMSCs showed that relatively high surface roughness [i.e., root-mean-square (rms) roughness = 71(11) nm] was beneficial to some osteogenic genes, whereas low roughness (i.e., rms roughness = 14.3(25) nm) led to the expression of other osteogenic genes and a chondrogenic gene of the hMSCs, with the cells exhibiting a small spindle shape on the rough surfaces as opposed to an elongated and multipolar shape on the smoother surfaces (Chen et al. 2017b). In other studies, increasing the roughness of electrospun PLLA scaffolds decreased osteoblast proliferation but increased fibroblast proliferation (Ribeiro et al. 2015). The discrepancies about the effect of surface roughness on the cellular response, such as higher osteoblast proliferation and lower fibroblast proliferation on rough and smooth microporous poly(hydroxybutyric acid) membrane surfaces, respectively (Huaga et al. 2009), can be attributed to complex cell effects depending on the cell line and different chemical, topographical, and mechanical surface cues.

All of the foregoing studies substantiate that the architecture, fiber diameter and alignment, pore size and shape, and surface roughness cannot be uniquely specified for all types of cells. Consequently, designing scaffolds to direct and promote specific cell behavior and morphology depends on the intrinsic specificities of the targeted application. Figure 2.3 provides a synopsis of the important structure and morphology parameters affecting cellular behavior in TE that were discussed in this section.

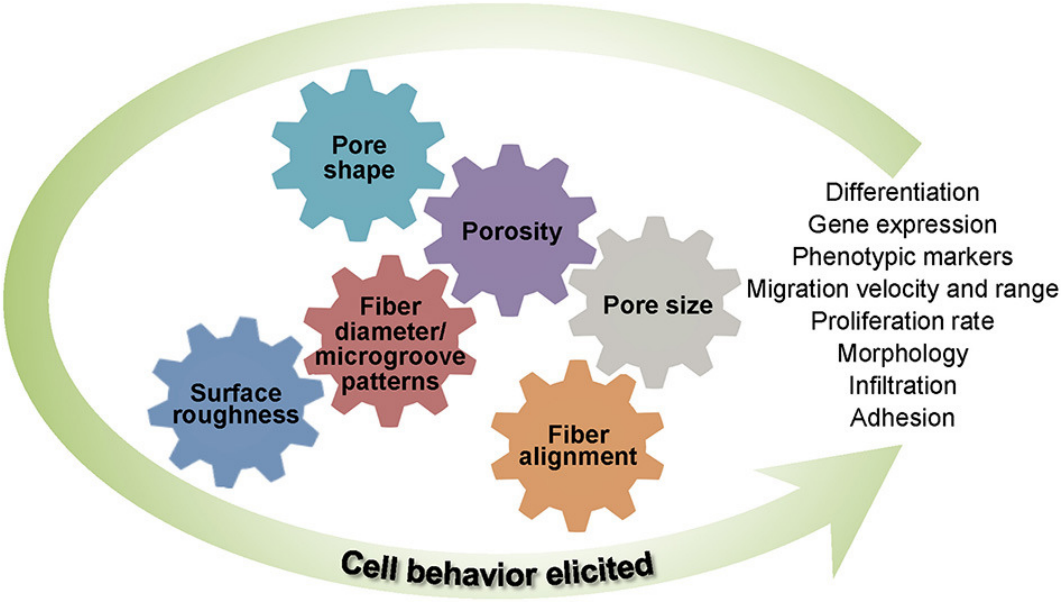

Figure 2.3: Important structure and morphology scaffold parameters affecting cell behavior.

Biodegradability

Biodegradability is of particular importance in scaffold engineering because it must be coordinated with tissue generation for the construct to maintain sufficient strength and effectively sustain the mechanical stresses in the tissue environment. Importantly, the byproducts of polymer biodegradation must be non-toxic to avoid an immune response and also extractable through normal body function. The degradation rate of biopolymer scaffolds is therefore of utmost significance because it is intertwined with the tissue viability. Specifically, if scaffold degradation is faster than wound healing and native tissue regeneration, the cells will be deprived of the ECM-like structure, the formed tissue can be defective or unfeasible, and the produced byproducts may not be promptly expelled from the body (Cajori, Crouter, Pemberton 1924; Pucino et al. 2019). Alternatively, too slow scaffold degradation may lead to scaffold encapsulation, triggering an immune response and poor integration or rejection from the host tissue (Balguid et al. 2009; Sanz-Herrera, García-Aznar, Doblaré 2009; Park et al. 2010; Holloway et al. 2014). The degradation rate is controlled by the material composition (functional groups), the scaffold environment (pH and enzymes) and structure (porous, hydrogels, and bulk), the surface and bulk chemical modification of the scaffold, the mechanical environment (physical loading), and the type of external intervention (e.g., ultrasound, heat, radiation, etc.), as illustrated in Figure 2.4. The degradation rate is typically quantified as a mass loss, despite the fact that it not only affects the mass but also the crystallinity, geometry (shape), and topology of the scaffold (Suuronen et al. 1998; Annor et al. 2012; Zhang, Zhou, Zhang 2014; Milošev et al. 2017). Other factors affecting the rate of scaffold

degradation include the implant location and the patient's age, gender, and comorbidities (Roman et al. 2017).

The degradation rate of polymeric scaffolds strongly correlates with the material composition, the polymer molecular architecture (e.g., side groups, aromatic groups, double or triple bonds, and crosslinking), and the fabrication method (e.g., blending and copolymerization), which controls the degree of chain scission (Liu, Wang, Qi 2012; Ferrari et al. 2017; Ferreira et al. 2019; Keirouz et al. 2020; Sadeghi-Avalshahr et al. 2020) and modulates the biodegradability, hydrophilicity, and biocompatibility as well as cell adhesion, proliferation, growth, and antibacterial activity in TE applications (Gao et al. 2019). Polymer crosslinking reduces the degradation rate (Bi et al. 2011; Kishan et al. 2015; Chen et al. 2020), whereas the incorporation of a high fraction of nanoparticles (NPs) to play the role of bioactive sites in the scaffold may increase the degradation rate (Mehrasa et al. 2016; Radwan-Pragłowska et al. 2020), although some studies have shown an opposite effect (Mehrasa et al. 2016; Park et al. 2018). The degradation rate can also be tuned by chemical modification methods or by adding NPs that can neutralize acidic products (Zhang, Zhou, Zhang 2014; Shuai et al. 2019).

Biopolymer degradation is a manifestation of several distinct but non-mutually exclusive mechanisms, namely hydrolytic degradation (chain scission by water molecules), enzymatic degradation (enzyme catalysis), oxidative degradation (radicals produced from peroxides), and physical degradation associated with various factors, such as loading, wear, and swelling (Brannigan, Dove 2017). The most common synthetic polymers used in TE, i.e., polyhydroxy esters, such as PLLA, PCL, PGA, PEO, and PVA, degrade abundantly by hydrolytic chain scission, where the loss of monomers and oligomers activates bulk or surface erosion mechanisms, depending on the dynamics of diffusion-reaction phenomena (Drury, Mooney 2003; You et al. 2005; Annor et al. 2012), and generates acidic byproducts (Idaszek et al. 2013; Kianpour et al. 2020). Alternatively, because the macromolecules of natural polymers, such as collagen, HA, alginate, and chitosan, are similar to the native ECM, they are prone to enzymatic degradation (Lam et al. 2009; Annor et al. 2012). Particularly, collagen is naturally degraded by collagenase and proteases, allowing for locally controlled degradation by the cells in the tissue (Drury, Mooney 2003; Annor et al. 2012). Accordingly, to tailor the degradation rate, natural polymers have been used in conjunction with synthetic polymers (Wan et al. 2008; Fu et al. 2014).

Degradation also changes intrinsic topography features of the scaffold, such as fiber roughness and diameter, porosity, and wettability, depending on the surface area-to-volume ratio of the scaffold, consequently affecting the cellular behavior (Lam et al. 2009). A larger surface area-to-volume ratio typically leads to faster degradation. Indeed, a comparison between electrospun biodegradable L-tyrosine-based PU membranes and thin films of the same material revealed a higher degradation rate for the electrospun membranes than the films, with the hydrolytic degradation rate of the membranes showing a dependence on blending ratio (Spagnuolo, Liu 2012). The surface area-to-volume ratio is linked to the wetting angle (hydrophilicity/hydrophobicity) and water intake (swelling) of the scaffold. For instance, electrospun poly(D,L-lactic acid) (PDLLA) and PEO/PLA (PELA) block copoly-

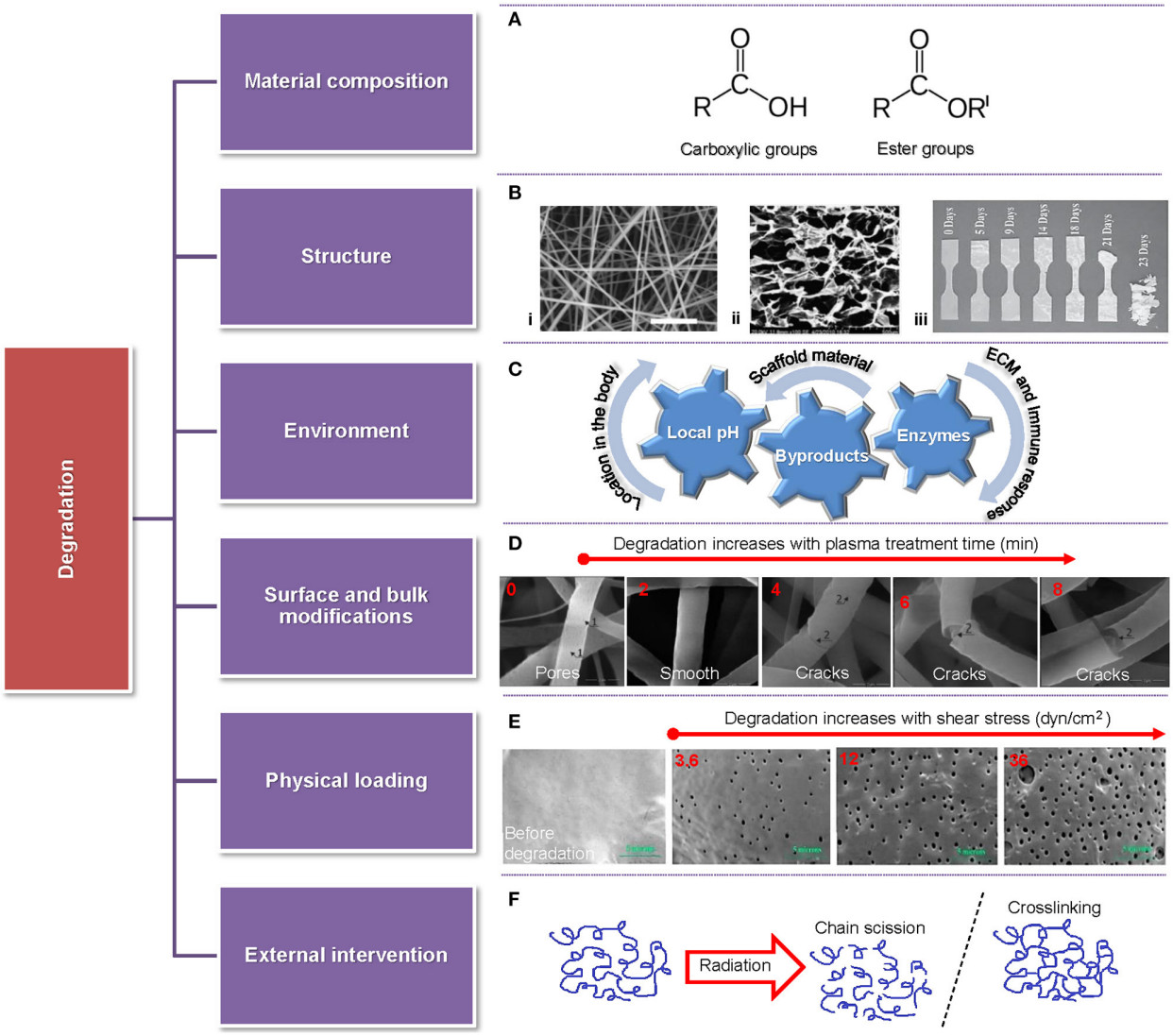

Figure 2.4: Overview of parameters affecting the degradation rate of scaffolds accompanied by representative examples. (A) Highly reactive functional groups attacked by water molecules. (B) Different scaffold structures: (i) fibrous (Pu, Komvopoulos 2014), (ii) porous (Han et al. 2014), and (iii) solid (Weir et al. 2004). (C) Various environmental factors (local pH, byproducts, and enzymes) affecting scaffold degradation. (D) Fiber morphology vs. time of plasma treatment showing fiber degradation after a short treatment time and fiber cracking and breakage after long treatment time (Bolbasov et al. 2018). (E) Comparison between a fresh sample and samples degraded for 28 days in PBS at 32 °C for shear stress increasing from 3.6 dyn/cm^2 (left) to 36 dyn/cm^2 (right) (Zheng et al. 2017). (F) Schematic of chain scission and crosslinking induced by radiation.

mer scaffolds have been reported to demonstrate faster degradation compared to cast film counterparts, especially in the early stage of the hydrolysis process, with the difference in degradation rate between the two materials decreasing after 10 weeks of incubation in phosphate buffered saline (PBS) at 37 °C. It was also reported that the fibrous PDLLA exhibited a larger wetting contact angle than the fibrous PELA and even larger than the cast PDLLA (Cui et al. 2008), in agreement with the findings of an earlier investigation (Cui et al. 2006).

Loading effects on scaffold degradation have received relatively less research attention. Degradation studies of 3D printed PLGA in a PBS solution have shown faster scaffold degradation in a shaking incubator than in a microchannel with recirculating solution or static incubators, with the degradation rate of the samples in the static incubator being between those of the other two cases, illuminating the importance of the effects of fluid flow and loading on the degradation of PLGA scaffolds (Ma et al. 2018). Similarly, cyclic loading has been observed to accelerate PLGA degradation compared to static loading (Yang et al. 2010), whereas high fluid shear rates in drug-releasing PLGA films used in vascular drug-eluting stent applications have been correlated to a faster release of sirolimus particles from the films, matching the degradation rate of the PLGA matrix (Zheng et al. 2017).

Various external factors (e.g., ultrasound, heat, and radiation) encountered during scaffold sterilization, patient therapy, and scaffold surface modification can also influence the rate of scaffold degradation by indirectly affecting the aging, crosslinking, morphology, hydrophilicity, and physical, chemical, and mechanical properties of the polymer material in combination with the cellular behavior (Yixiang et al. 2008; Rediguieri et al. 2016). For instance, under typical cancer therapy radiation levels, PCL undergoes backbone changes that have been associated with crosslinking and faster degradation (Cooke, Whittington 2016). In vivo studies of electrospun PLLA scaffolds coated with titanium by reactive magnetron sputtering in nitrogen plasma atmosphere have shown that plasma treatment can mitigate inflammatory response, increase wettability, and stimulate cell attachment to the scaffolds, while, at the same time, expediting the commencement of scaffold degradation (Bolbasov et al. 2018).

The degradation byproducts may modify the local pH of the media surrounding the cells, consequently affecting cell energy metabolism, matrix synthesis, and cell behavior (Jones, Cochrane, Percival 2015). An acidic pH environment may promote fibroblast proliferation and the migration and regulation of bacterial colonization, with keratinocytes showing optimal migration at more alkaline pH levels, e.g., pH $\approx$ 8.5 (Sharpe et al. 2009). Furthermore, enzyme activity is pH sensitive. For instance, protease exhibits a peak activity in the pH range of 7–8 and a decreased activity in acidic media, suggesting the need for a balanced pH for this enzyme because an excess of proteases hinders the wound healing process (Greener et al. 2005). Investigations of the pH effect on the metabolism of chondrocytes embedded in agarose gel have shown that even for a narrow pH range of 6.6–7.3 acidic pH suppresses the production of lactate and increases glycosaminoglycan synthesis without affecting the synthesis of collagen, suggesting that metabolic activities and the biosynthetic ability of chondrocytes are strongly influenced by the media pH (Wu et al. 2007). As mentioned earlier, many synthetic polymers generate acidic byproducts upon degradation, consequently stimulating

local inflammation and interfering with the healing process. Therefore, other biopolymers, such as biodegradable PU foams and polycarbonate, which exhibit good biocompatibility, reduced inflammatory response, and controlled degradation to non-cytotoxic byproducts, have been used to promote cell attachment, collagen deposition, and keratinocyte growth and retention, especially for skin TE applications (Hafeman et al. 2011; Greenwood, Wagstaff 2016; Xu, Guan 2016; Brannigan, Dove 2017).

Several studies have been focused on the effect of the scaffold degradation rate on cellular behavior, including adhesion, proliferation, differentiation, and metabolism. For example, the slow degradation of electrospun PCL scaffolds maintained the rigidity needed for myofibroblast differentiation and the secretion of higher levels of matrix components, whereas the decreased rigidity of the faster degrading poly(glycolic acid)-poly(4-hydroxybutyrate) scaffolds led to the accumulation of acidic byproducts, reduced matrix production, poor cell proliferation and differentiation, and undesirable collagen crosslinking (Balguid et al. 2009). Porous silk fibroin scaffolds prepared with the salt leaching process and two different solvents (i.e., hexafluoroisopropanol and aqueous solution) demonstrated remarkable differences in degradation rate exclusively due to the process condition (solvent), conversely to chemical modification followed by in vitro seeding with human bone marrow stem cells in an osteogenic medium for 56 days, where the faster degrading aqueous-derived scaffold exhibited a higher metabolic rate (i.e., higher glucose consumption and lactate production) during osteogenesis due to the enhancement of proliferation and osteoblastic differentiation (Park et al. 2010). In another study, 3D printed porous PLGA scaffolds showed similar degradation rates with that of new bone generation and maturation after 24 weeks of implantation in a rabbit model (Ge et al. 2009). The degradation of injectable porous hydrogels is another emerging application area. This is because TE relies on the scaffold's capacity to effectively release drugs, proteins, and nanoparticles to aid the wound healing process. An in vitro study of two porous injectable hydrogels, namely serum bovine albumin (BSA) and vascular $K_2(SL)_6K_2$ polypeptide/BSA (KK-BSA) crosslinked via sulfydryl groups by Ag^+ ions, showed that KK-BSA hydrogel degraded faster than the BSA and completely within 7 days of soaking in PBS, suggesting that antibacterial units (Ag^+) and vascular polypeptide can be released in the early stage of wound healing, matching the physiological drive for wound healing (Cheng et al. 2020).

Mechanical Behavior

The cells sense the physicochemical characteristics of their microenvironment via surface mechanoreceptors and accordingly respond by actively remodeling it. Although various factors of a cellular microenvironment (e.g., cell interactions, growth factors, and ECM biochemistry and structure) contribute to vital signaling for the cells, the signals generated by the ECM play a particularly crucial role in the biochemical response of the cells (Dvir et al. 2011). The ECM influences the basic biological functions and the fate of the cells through both biochemical interactions (e.g., growth factors and adhesive motifs) and mechanical cues (e.g., stiffness and deformability). Mechanical signals have profound effects on cell

differentiation, proliferation, and death, greatly affecting tissue growth in vivo (Vogel, Sheetz 2006; Wang, Tytell, Ingber 2009). In the design of scaffolds for TE it is often required to recapitulate the modulus and ductility of a range of native environments. However, the complexity of the cellular environment requires an awareness of its physical, biochemical, and mechanical properties for the successful fabrication of functional tissue analogs.

One of the main aspects affecting cell micromechanics is the scaffold structure characteristics, such as porosity, pore size, fiber diameter, and fiber alignment (Kennedy, Bhaw-Luximon, Jhurry 2017). For fibrous constructs, such as electrospun scaffolds, altering the fiber diameter influences both the cell behavior and the cell morphology, such as the cytoskeletal arrangement and adhesion sites, ultimately changing the intracellular tension forces that direct cell phenotypes (Badami et al. 2006; Noriega et al. 2012). Changes in the fiber diameter can greatly affect the fiber stiffness. Indeed, because large-diameter PCL and PVA fibers are more amorphous due to the fact that they possess a less aligned molecular structure, they exhibit a lower elastic modulus compared to small-diameter PCL and PVA fibers that show increased crystallinity and, accordingly, higher elastic modulus (Wong, Baji, Leng 2008; Stachewicz et al. 2012). It is well-accepted that cell-matrix interactions depend on the degree of fiber alignment (Baji et al. 2010; Wen et al. 2014). Fiber alignment in scaffolds that mimic the ECM of the tissue, such as blood vessels (Ma et al. 2005) and nerve tissue (He et al. 2010), have been found to direct cell phenotypes. Even though the fiber alignment does not directly impact the elastic modulus of the fibers, it influences the stiffness experienced by the cells. Because the fibers display a higher effective stiffness in the longitudinal direction than the transverse direction, cell attachment and migration mostly occur along the axial direction of the fibers. Moreover, the packing density of the fibers may also influence the effective stiffness. For instance, bundling of collagen fibers increases the effective stiffness (from $\sim$1 kPa for a single fiber to $\sim$5 kPa for fiber bundles), enhancing the cell adhesion and migration rate (Doyle et al. 2015).

While changing key structure parameters of scaffolds, such as the pore size, fiber diameter, and fiber alignment, is an effective method for tuning the mechanical properties of scaffolds, the material chemistry can also be used to independently modify the mechanical behavior of the scaffolds. Thus, the mechanical properties of polymeric scaffolds can be altered by changing the photopolymerization time or the number of photoreactive groups (Kennedy, Bhaw-Luximon, Jhurry 2017). These approaches can be employed during the formation of hydrogels or electrospun scaffolds to control the mechanics while maintaining the structure architecture. For example, a PEG dimethacrylate nanofiber hydrogel matrix with tunable elasticity fabricated by integrating electrospinning with photopolymerization was used to study the effects of scaffold elasticity on the differentiation rate of hMSCs to vascular cells in vitro (Wingate et al. 2012). An increase in polymerization time enhanced the degree of crosslinking, producing scaffolds with elastic modulus in the range of 2 kPa to 15 kPa, consistent with in vivo stiffness. It was also found that the matrix elasticity instigated the cells to express different vascular phenotypes that demonstrated high differentiation efficiency, with softer scaffolds resulting in upregulation of the endothelial cell markers (Flk-1) and stiffer scaffolds eliciting smooth muscle cell (SMC) markers. The former

study (Wingate et al. 2012) also illuminated the importance and capacity of local elasticity to control MSC differentiation to endothelial or SMC-like cells, leading to a vascular tissue regeneration in which the endothelial cell layer was softer than the SMC layer. In another investigation, electrospun photoactivatable methacrylated HA scaffolds induced chondrogenic differentiation of hMSCs by altering the fiber mechanics through the crosslink density and the cell adhesiveness mainly through the concentration of conjugated tripeptide RGD motifs (Khetan et al. 2013). It was also shown that fiber mechanics govern gene expression, with softer fibers promoting the expression of chondrogenic markers and the adhesive motifs at the fiber surface directing cell adhesion, proliferation, and migration. Studies dealing with the effects of the matrix stiffness and spatial distribution of cell-adhesive motifs on the attachment and differentiation of stem cells have demonstrated that both the matrix stiffness and the presence of adhesive cues can override other physical effects affecting the stem cell fate (Ye et al. 2015; Yevick et al. 2015). The scaffold mechanics can also be adjusted by varying the weight ratio of polymer blends (Vatankhah et al. 2014), although this may alter the surface roughness and hydrophilicity of the scaffold and, consequently, change the cell behavior.

Likewise, both the strength and the stiffness of bulk hydrogel scaffolds depend on the rigidity of the polymer chains and the crosslink density. Sequential photopolymerization allows for spatiotemporal control of the hydrogel stiffness (Leijten et al. 2017). The degree of photopolymerization, which depends on the irradiation dose and the crosslink density, can be tuned to produce unreacted functional groups in the matrix, which can enhance the hydrogel's mechanical properties through a second crosslinking reaction at a certain time (Guvendiren, Burdick 2012; Guvendiren et al. 2014). In a specific case, matrix metalloproteinase (MMP)-degradable PEG hydrogels of different stiffness were used to examine the effect of the matrix modulus on the behavior of valve interstitial cell myofibroblasts seeded in 3D scaffolds as compared to flat hydrogel counterparts (Mabry, Lawrence, Anseth 2015). It was found that in situ stiffening of cell-laden PEG hydrogels by thiol-ene chemistry is an effective means of independently varying the scaffold mechanics at different length scales. The former study also provided insight into how cells sense mechanical signals originating from multiple length scales. While chemistry can be a powerful approach when modulating the micromechanical characteristics of scaffolds, modifying the mechanics by either blending or photopolymerization introduces a new surface chemistry, which may affect the cell behavior, the cell affinity to attach onto the scaffold surface, and the interaction of the cells with their microenvironment.

Although scaffolds undergo dynamic mechanical changes due to degradation and loading effects, the cells can also change the mechanical properties of scaffolds through the deposition of ECM, the application of cellular tractions, or even the reconstruction of the surrounding tissue. A scaffold implanted in the body experiences physiological loads (e.g., shearing by body fluids) that depend on the host tissue and/or cellular traction forces, which can induce deformations in the surrounding environment. Cellular traction forces manifest themselves during cell attachment. Cell seeding can result in scaffold contraction when there is a scaffold-tissue stiffness mismatch and the scaffold elasticity is inadequate to absorb the forces exerted

by the moving cells. However, a small degree of local contraction is needed to assist cell migration and differentiation (Ulrich et al. 2010). In a study with a new dextran methacrylate hydrogel system that resembled the fibrous architecture of native ECM where the fiber stiffness, diameter, and alignment were controlled, lower fiber stiffness caused the cells to recruit neighboring fibers, effectively increasing the adhesive ligand density and enhancing cell adhesion and spreading (Baker et al. 2015). It was also shown that increasing the stiffness of the 3D fibrous constructs suppressed cell spreading and proliferation, whereas increasing the stiffness of flat hydrogel counterparts was conducive to MSC spreading and proliferation. The mechanical properties of scaffolds can also be affected by hydrolytic and/or enzymatic scaffold degradation, with the degradation rate exhibiting material dependence. For instance, PCL is a slowly degrading polymer that preserves its bulk mechanical properties for an extended period ($\sim$65 days), as opposed to PCL-PLGA blends that display significant deterioration of the mechanical properties and considerable mass loss (Baker et al. 2009).

It is well-known that cells are dynamic systems responding to changes of their microenvironment by altering their morphology and applying tractions or by modifying their microenvironment through cell-mediated enzymatic degradation. However, more studies are needed to better understand the interplay between local degradation and cellular tractions and how the latter can influence differentiation and other cellular behaviors. Nevertheless, most studies conducted so far have established that the mechanical properties of synthetic scaffolds can dictate the cell fate and regulate the cell response. Figure 2.5 summarizes the parameters that play an important role in the mechanical behavior of scaffolds discussed in this section, including the cell-scaffold interface.

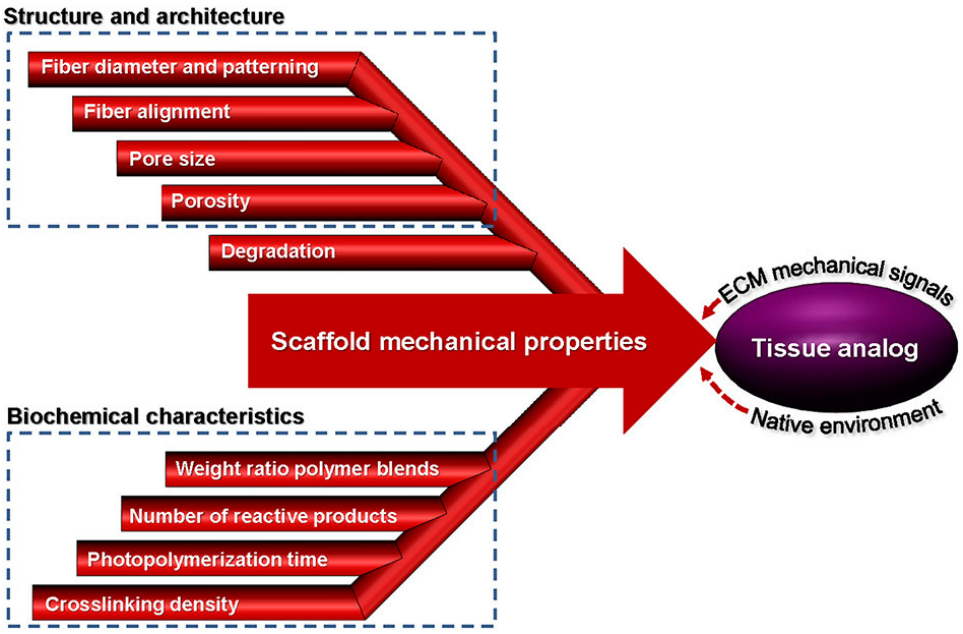

Figure 2.5: Parameters affecting the mechanical properties of scaffolds from fabrication to implantation used to create a tissue analog.

2.3 Immunomodulation

Biomaterials for TE aim to replace damaged or diseased tissues with functional site-specific tissues. Although biomaterial properties, such as strength, porosity, degradability, and chemistry, are considered to be the main design principles for tuning the response of seeded cells and mimicking the nature of the native tissue, another critical factor for achieving successful clinical outcomes is the host tissue response to the implanted biomaterial. The immune system plays a vital role in host defense against pathogens, foreign bodies, and the tissue healing response following injury (Dellacherie, Seo, Mooney 2019). Since biomaterials are essentially foreign bodies, the immune-mediated tissue reaction to the presence of the foreign body is of utmost importance for the success of the TE strategy. Historically, in TE and regenerative medicine fields, immune responses were considered as challenges that had to be overcome because immunological reactions usually lead to restricted integration and regeneration of transplanted cells, tissues, and organs. However, in recent years, the design of biomaterials has shifted from suppressing the immune response to actively modulating it to promote synergy with the host environment (Sadtler et al. 2019; Stabler et al. 2019). Therefore, immunomodulatory biomaterials which promote or facilitate desired activation state or phenotype within the host immune cells have acquired widespread attention in the development of more effective biomaterials (Andorko, Jewell 2017; Dziki, Badylak 2018). To address the importance of immunomodulation in biomaterials design for TE applications, a

brief overview of the role of the immune system in tissue repair and the role of physicochemical properties of scaffolds in directing immune responses is provided next.

The immune system continually surveils the body to detect the invasion of harmful pathogens or tissue damage, and upon recognition of a threat, it activates an orchestrated inflammatory cascade of events (Medzhitov 2008). The recognition of pathogens occurs through the release of molecules by dying cells that are uncommon and not typically found in the body. These molecules are referred to as danger-associated molecular patterns (DAMPS) and pathogen-associated molecular patterns (PAMPS) when occurring from various species of bacteria, viruses, and parasites (Iwasaki, Medzhitov 2010), as shown schematically in Figure 2.6. During the innate immune response (i.e., the segment that provides rapid but less specific reaction) these patterns are recognized by tissue-resident immune cells that trigger the secretion of inflammatory signals, which are picked up by antigen-presenting cells, such as dendritic cells (DCs) and macrophages. Initially, neutrophils infiltrate the injury site and act non-specifically to clear pathogens associated with the injury, while secreting cytokines that recruit other immune cells, such as macrophages that clear up the cellular debris (Nathan 2006; Selders et al. 2017). When the macrophages arrive at the injury site, they exhibit inflammatory M1 phenotype and clear up the cellular debris and phagocytose pathogens. Once the threat is eliminated, phagocytes transition to anti-inflammatory phenotype M2, promoting tissue repair and generation of new blood vessels. While neutrophils and phagocytes comprise the first line of defense, they act with non-specificity because they cannot identify the pathogen they encounter. As described previously, during infection or acute injury during biomaterial implantation, pathogens or dying cells release antigens and threat signals. In the innate immune response phase, DCs, which are antigen-presenting cells, pick up the pathogen-derived antigens and threat signals and present them as surface activation signals on their membrane, including signals that induce their maturation and migration to the lymph nodes as well as major histocompatibility complexes responsible for presenting antigens to immature B and T cells (Dellacherie, Seo, Mooney 2019), as shown in Figure 2.6. Antigens and threat signals can also drain to the lymph nodes, where they bind and activate B cells to produce antibodies and/or activate resident antigen-presenting cells to prime T cells. Priming of immature T and B cells leads to the development of effector T cells and plasma cells and the development of memory T and B cells that can be activated when the same antigen is encountered (Kurosaki, Kometani, Ise 2015). The effector T cells and antibodies home to the affected tissue and participate in the adaptive immune effector phase.

Scaffolds for TE applications incorporate signals or cells which, upon implantation or injection, induce proliferation of the encapsulated cells, alter the phenotype of the infiltrating cells, and promote changes in tissue growth and function. Similarly, altering the physical properties of biomaterials can affect the immune response. Alteration in size and shape, composition, charge, and topography of biomaterial constructs can impact the intrinsic immunogenicity. For instance, physically confining the macrophage shape by micropatterning (i.e., elongated or pancake-like shapes) can affect the phenotype without the need to add exogenous cytokines (McWhorter et al. 2013). Also, the pore size of scaffolds can

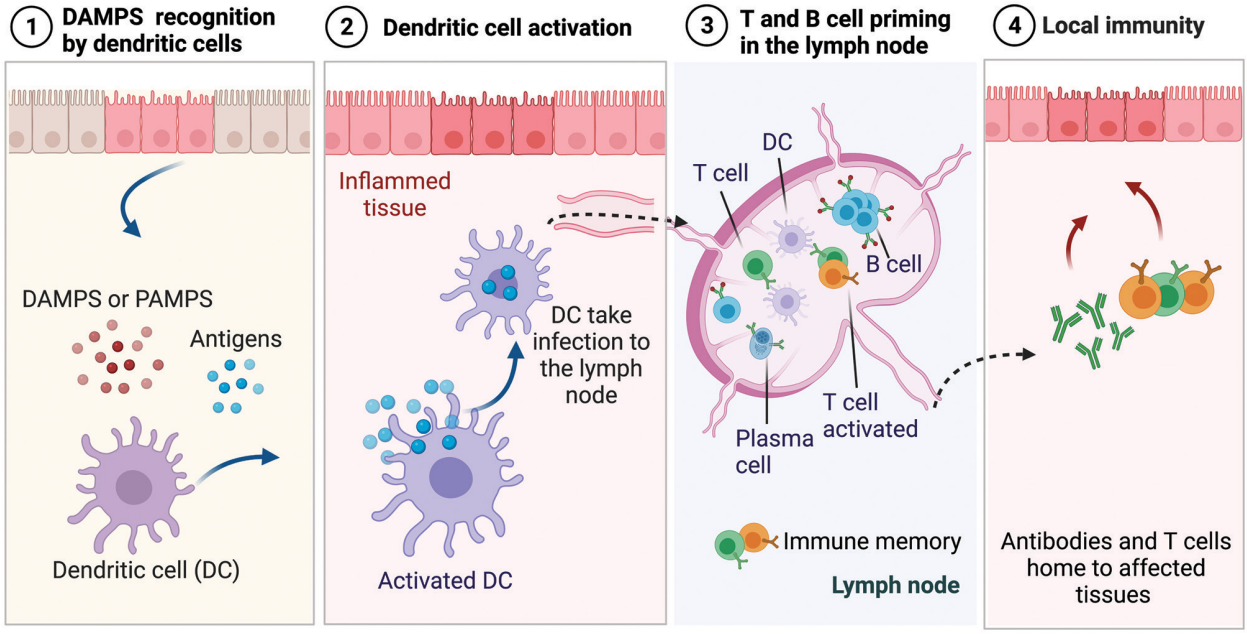

Figure 2.6: Overview of innate immune response upon injury or infection.

impact fibrotic capsule formation and shift macrophage phenotype. Studies have revealed a correlation between increased pore size of electrospun scaffolds and a shift toward M2 macrophage phenotype (Garg et al. 2013; Sussman et al. 2014). However, while porosity can be tuned to promote a regenerative environment by modulating macrophage phenotype, it may negatively impact the mechanical strength of the construct, which may be detrimental for recapitulating the strength of the native tissue. Changes in stiffness can also modulate host immune interactions, impacting both the biomaterial mechanics and its degradation rate. Modifying the extent of crosslinking and, in turn, the biomaterial stiffness can affect the M2-to-M1 macrophage ratio while, at the same time, altering the type of crosslinking; consequently, degradability can also influence immune cell recruitment and inflammatory response. For instance, changing the crosslinking of collagen scaffolds from glutaraldehyde to hexamethylene diisocyanate resulted in a 10-fold enhancement of neutrophil recruitment even after 28 days of subcutaneous implantation (Ye et al. 2010). Additionally, tuning the chemical properties of scaffolds can have a dramatic effect on the host response. Crosslinking agents, including carbodiimide or glutaraldehyde, which aim to strengthen ECM-based scaffolds, have been shown to promote an early pro-inflammatory immune cell phenotype and inhibit the degradation of ECM by macrophages (Valentin et al. 2009; Brown et al. 2012; Sadtler et al. 2016). Furthermore, the size and geometry of scaffolds affect responding immune cell phenotypes by altering foreign body reaction and fibrosis. Tuning the geometry of implanted materials can influence their host recognition and propagation of foreign body reactions. For instance, it has been shown that increasing the implant size is insufficient

in battling foreign body responses and that spherically-shaped implants are essential for resisting host fibrosis (Veiseh et al. 2015). Also, the degradation products of ECM-based hydrogels have been reported to have a diverse effect on macrophage phenotype compared to particulate powder ones (Dziki et al. 2017; Sadtler et al. 2017).

The design of biomaterials which can actively modulate the immune response rather than circumvent or suppress it is of paramount importance to achieving tissue repair and regeneration. Leveraging the immunomodulatory capabilities of biomaterials requires control over their physicochemical features, careful design and selection of their morphology and architecture, and thorough in vitro and in vivo studies to reveal the interplay between the biomaterial and the resulting immune response.

2.4 Outlook and Future Perspectives

The foregoing synopsis elucidates some of the most important accomplishments, the current demands, and the existing challenges regarding biomaterial scaffolds used in various TE applications. The development of such functional constructs for augmenting or replacing native tissues lies at the crossover of biology, medicine, materials science, and engineering. Numerous new strategies have been advanced to fabricate highly tunable and functional scaffolds. However, despite the outstanding progress achieved to date, there are still numerous challenges that must be overcome before scaffold-based TE technologies can attain broad clinical usage and commercialization. Several design considerations that are undistinguishably linked to the formation, function, and implant location of native tissue must be addressed to further advance scaffold engineering. The chemical, morphological, and mechanical properties of scaffolds must be tuned to optimize interactions with the cells and the surrounding tissue, whereas the biodegradation rate must be controlled to preserve the scaffold's integrity until the maturity of the growing tissue. Scaffolds should be designed with an appreciation of the bio-chemo-mechanical properties of the native tissue and the complex mechanisms that control cell interactions. Furthermore, the composition and micro/nanostructure of the ECM of different tissues vary significantly. Therefore, recapitulating the biological roles of the native tissue through a synthetic construct should recognize the structure architecture of the tissue of interest and its biological role. Clearly, there are no universal design criteria that fit all of the tissue characteristics. Because native tissues are characterized by a wide range of functions and compositions, the same scaffold materials cannot be used for all tissues. When selecting and developing new materials for TE, it is imperative to simultaneously consider the complex biochemistry, morphology, mechanical behavior, and biodegradation characteristics of the scaffold (Figure 2.7).

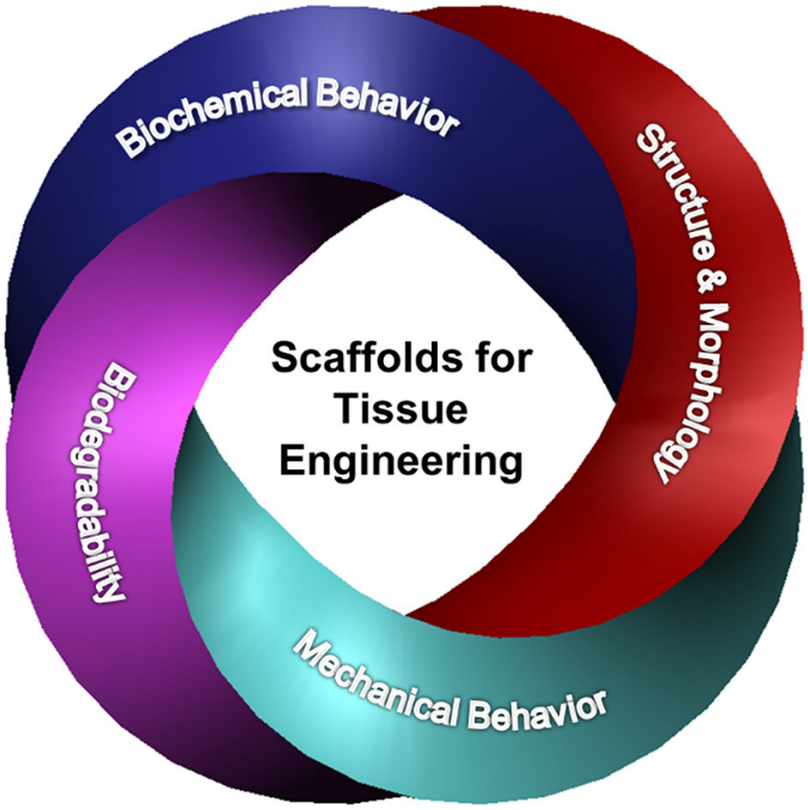

Figure 2.7: Synergy between biochemical behavior, structure and morphology, biodegradability, and mechanical behavior of scaffolds activates cellular behavior, controls cell fate, and drives TE advancement.

The interactions between the native cells and the scaffold promote distinct cell phenotype changes and affect the regeneration of the tissue. While these effects were initially attributed to interactions at the cell-scaffold interface, cumulative evidence suggests that the 3D structure architecture of the scaffold plays a crucial role. The biochemical behavior of the scaffold dictates whether the cells will proliferate, change the types of ligands and receptors present at their surfaces, or change function. If the scaffold does not possess the right cues, the cells may detach from the matrix and undergo apoptosis. In view of the scaffold-dependent cell behavior, it is imperative to characterize scaffold materials for both short- and long-term cell phenotype effects. Strategies to control and recap cell-material interactions should account for the effect of scaffold structure across multiple length scales.

The necessity for scaffolds that can deliver oxygen and nutrients while removing cell products and waste has been a central theme in multiple TE efforts. Increasing the cellular density in a scaffold to mimic the density of the native tissue may produce a hypoxic core that usually leads to cell dysfunction and death. It is vitally important that a blood supply is within the vicinity of the cells so that they can sense the physiological cues and access

the oxygen and nutrients that are necessary for their long-term viability (Lokmic, Mitchell 2008). In native tissues, the cells are in proximity of a few hundred micrometers from a flowing blood supply, because mass transport is insufficient for a larger distance (Folkman, Hochberg 1973). Therefore, the fabrication of viable tissue-engineered constructs of a size larger than the latter distance range appears to be inconceivable in the absence of a natural vascular network, including vasculogenesis and angiogenesis. Vasculogenesis generates new vascularization in the absence of preexisting blood vessels, whereas angiogenesis is defined as the formation of new vessels from an existing vascular network (Auger, Gibot, Lacroix 2013). The vascular networks play a pivotal role in the survival of cells; however, their quality is more critical than their quantity. When aiming for vascular networks in engineered tissues, the blood perfusion and distribution over a tissue volume is more important than the number of vascular structures. An optimal vascular network must be highly organized and include capillaries, venules, and arterioles to sufficiently supply the cells with oxygen and nutrients. Besides vascular organization, other key parameters, such as perfusability and barrier function, must also be taken into account. In addition, there is a need for an optimum balance between vascular organization in engineered tissues before implantation and vascular remodeling after implantation. An initial degree of vascular organization is necessary for supplying the cells with nutrients, whereas vascular remodeling after implantation is critical to adapting to the post-implantation environment. Likewise, while it is clear that endothelial cells are needed to form the lining of the structures, it is essential to investigate which combination of cell types (i.e., macro/microvascular and progenitor based) can lead to the formation of an optimal vascular network for a specific tissue (Rouwkema, Khademhosseini 2016). Therefore, a scaffold intended for completely tissue-engineered organs requires spatial control over different tissue layers and types and the incorporation of perfused vascularization to promote tissue health and recapitulate tissue function.

Despite several decades of intense research, the widespread use of TE remains encumbered not only due to the engineering design constraints highlighted in this chapter but also because of several regulatory hurdles. Concerns regarding cell seeding, poorly defined degradation products, and the need for extensive pre-clinical data increase both the time and the cost to achieve regulatory approval for clinical translation of scaffold-based TE technologies. Furthermore, most of the conducted studies have relied on scaffold implantation in animal models like rodents and rabbits. This raises many concerns about the performance of engineered scaffolds in the human body due to interspecies variability between animal models and human immunology (Mestas, Hughes 2004; Seok et al. 2013). Therefore, more efforts must be devoted to the implementation of animal models that closely resemble human physiology, and pre-clinical data of the scaffold efficacy should be acquired from multiple animal models across various species. Finally, it is critical to understand that the majority of TE approaches combine cells seeded into scaffolds with signaling cues and chemical functionalities or drugs, thereby rendering the regulatory pathways more complex and necessitating the use of costly methods to demonstrate implant safety.

As the medical challenges become more abundant, the need to improve the quality of life for patients worldwide through TE innovation is becoming more evident. The limited clinical

success of TE thus far signifies the enormous scientific, medical, and financial challenges faced in this field and underlines the importance of collaboration among scientists, engineers, and physicians more than ever. It is critically important that the requirements of medical groups are aligned with the responses of biomaterial groups and that a strong commitment exists among financial partners, government agencies, and corporations to enable innovative advances in scaffold engineering for a wide range of TE applications.

Chapter 3

An Electrostatic Finite Element Analysis of the Electrospinning Process of Bilayer Constructs Using a Parallel-Plate Collector

The content of this chapter was published in *Materials Letters*, 313, 131649 (2022), as "An Electrostatic Finite Element Analysis of the Electrospinning Process of Bilayer Constructs Using a Parallel-Plate Collector" by Maria I. Echeverria Molina and Kyriakos Komvopoulos.

3.1 Introduction

Electrospinning is a conventional yet versatile manufacturing process for fabricating fibrous constructs and scaffolds for multiple applications, including aerosol particle filtration, proton exchange membranes for fuel cells, and scaffolds for tissue engineering (Neisiany et al. 2020; Rahmati et al. 2021; Waldrop, Wycisk, Pintauro 2020). Basic knowledge of the electrospinning process is critical because it controls the morphology and physical attributes of the fabricated construct. Specifically, the internal structure and biomechanical properties of electrospun scaffolds strongly depend on the fiber diameter and alignment, porosity, and pore size, which affect the mechanical performance of the scaffold and its affinity to elicit a specific cellular behavior (Echeverria Molina, Malollari, Komvopoulos 2021; Baji et al. 2010). Cell alignment along the fiber orientation, cell infiltration, cell migration to specific directions, and cell differentiation are characteristic examples of the effect of a fibrous scaffold morphology that mimics the extracellular matrix of tissues like cartilage, neural tissue, and bone (Echeverria Molina, Malollari, Komvopoulos 2021). The design challenges and fabrication strategies for polymeric electrospun scaffolds used in tissue engineering are discussed in detail in Chapter 2. Therefore, the design of an electrospinning setup that can produce

constructs with desired morphologies is of paramount importance. For instance, bilayer constructs consisting of aligned and randomly oriented fibers fabricated with a parallel-plate collector demonstrated enhanced cell proliferation and migration (Pu et al. 2015).

Although fibrous constructs possessing various morphologies have been fabricated with different collector designs (Pu, Komvopoulos 2014; Keirouz et al. 2020), knowledge of the effect of the mandrel configuration on the electric field of the deposition process is mostly empirical. Previous simulations have provided insight into the overall electric field intensity but not the directionality (Samadian et al. 2017; Xie, Zeng 2012). Therefore, a comprehensive analysis of the electric field produced by a specific mandrel geometry is essential to understand the physical aspects of the electrospinning process and accordingly guide the design of systems that can produce constructs with versatile fibrous architectures.

The finite element analysis (FEA) is a powerful method for performing electrostatic simulations of the electrospinning process, which can illuminate the effects of the directionality and intensity of the electric field on the construct morphology. Consequently, the objective of this study was to perform FEA simulations of the electrostatic field of the electrospinning process for a parallel-plate collector configuration, used to fabricate bilayer constructs with aligned and randomly oriented fibers (Pu, Komvopoulos 2014). The thickness effect of polymer deposited between the collector plates on the electric field in the vicinities of the needle tip and the plates and the variation of the electric field intensity with the distance from the needle tip, the plate edge, and along the symmetry plane of the electrospinning system are interpreted in the context of FEA results. The simulations provide explanation for the fiber alignment between the plates, and the deposition of randomly oriented fibers beyond a critical polymer thickness due to the diminishing directionality of the electric field.

3.2 Simulation Methodology

The electrostatic analysis of the parallel-plate electrospinning system was performed with the FEA software COMSOL Multiphysics (version 5.6), using the electrostatics module. The setup includes an aluminum mandrel consisting of a 27 mm-diameter shaft insulated with a 10 mm-thick polydimethylsiloxane layer of 2.6 relative permittivity and two parallel plates of 58 mm diameter, 5 mm thickness, and 15 mm distance from each other, a steel needle, and an aluminum holder of the needle. The distance between the needle tip and the shaft axis was kept constant at 120 mm, as in the experiments. The surrounding medium is air. A poly-L-lactic acid (PLLA) layer of 3.51 relative permittivity (Huber et al. 2016) and thickness up to 300 µm is modeled between the plates, with its bottom surface located 100 µm below the inner edge of the plates. The entire electrospinning setup is enclosed in a simulation box (1200 mm × 1000 mm × 600 mm). The foregoing simulation parameters are consistent with the experimental conditions used to fabricate bilayer scaffolds with a layer having fibers aligned between the plates and a layer with randomly oriented fibers. For uniform polymer coverage, the mandrel was rotated at 8.4 rpm. The electrospun solution consisted of 19 % w/v of PLLA and hexafluoroisopropanol solvent. A flow rate of 1 mL h^{-1} was used in all the

experiments.

The electrostatic analysis was performed for a potential of 14 kV applied to the needle holder and grounded collector, using Maxwell's equations and assuming insulated outer surface of the simulation box. The FEA mesh consisted of ∼64,222,393 tetrahedral finite elements (depending on the polymer thickness) with a minimum size of 2 µm (Fig. 3.1a). To improve the accuracy, an algebraic multigrid preconditioned conjugate gradient solver was used at the expense of a longer computational time. Convergence studies confirmed that the results were not affected by the size of the simulation box. Introducing fillets to the inner edge of the plates and the edge of the needle tip decreased the electric field intensity only locally without affecting the observed trends. Accordingly, fillets were not used in the FEA model.

3.3 Results and Discussion

The analyzed electrospinning system resembles a parallel-plate capacitor with the needle and its holder representing the plate to which the potential is applied and the grounded mandrel the other plate of the capacitor, with air or polymer plus air dielectric medium between the plates before and during electrospinning, respectively. Results are presented for the simplifying case of stationary mandrel and in tandem deposition between and at the top of the plates.

Fig. 3.1b shows scanning electron microscopy (SEM) images of aligned and randomly oriented fibers of a bilayer construct fabricated with the aforementioned setup. These fiber morphologies are representative of all regions across the space between the plates. The electric field in the vicinities of the inner edge of the left plate and the needle tip for a 60 µm-thick polymer layer is shown in Fig. 3.1c(i) and 3.1c(ii), respectively. For comparison, the electric field adjacent to the plates and the needle tip for a 100 µm-thick polymer layer is shown in Fig. 3.1c(iii) and 3.1c(iv), respectively. While the electric field intensity decreases near the middle of the distance between the plates, it is still sufficiently strong and directional for aligning the fibers between the plates (Fig. 3.1b(i)). Although the deposited polymer does not affect the electric field at the needle tip, the increase of its thickness weakens the electric field at the top of the plates (Fig. 3.1c). Fig. 3.1d shows that the electric field intensity decreases abruptly with increasing distance from the needle tip up to ∼5 mm, beyond which it decays fairly linearly at a very low rate. Similar results have been reported previously (Samadian et al. 2017; Xie, Zeng 2012). The localized sharp drop of the electric potential in the proximity of the grounded plates (inset of Fig. 3.1d) is due to the abrupt change in dielectric medium from air to polymer.

Fig. 3.2a shows the effect of polymer thickness on the variation of the electric field intensity with the y-distance (defined in the inset). The electric field intensity increases rapidly with the distance up to the polymer/air interface where a sharp drop is encountered. Importantly, the increase of the polymer layer thickness decreases the electric field intensity profoundly. A strengthened electric field arises in the vicinity of the plate edge (antenna

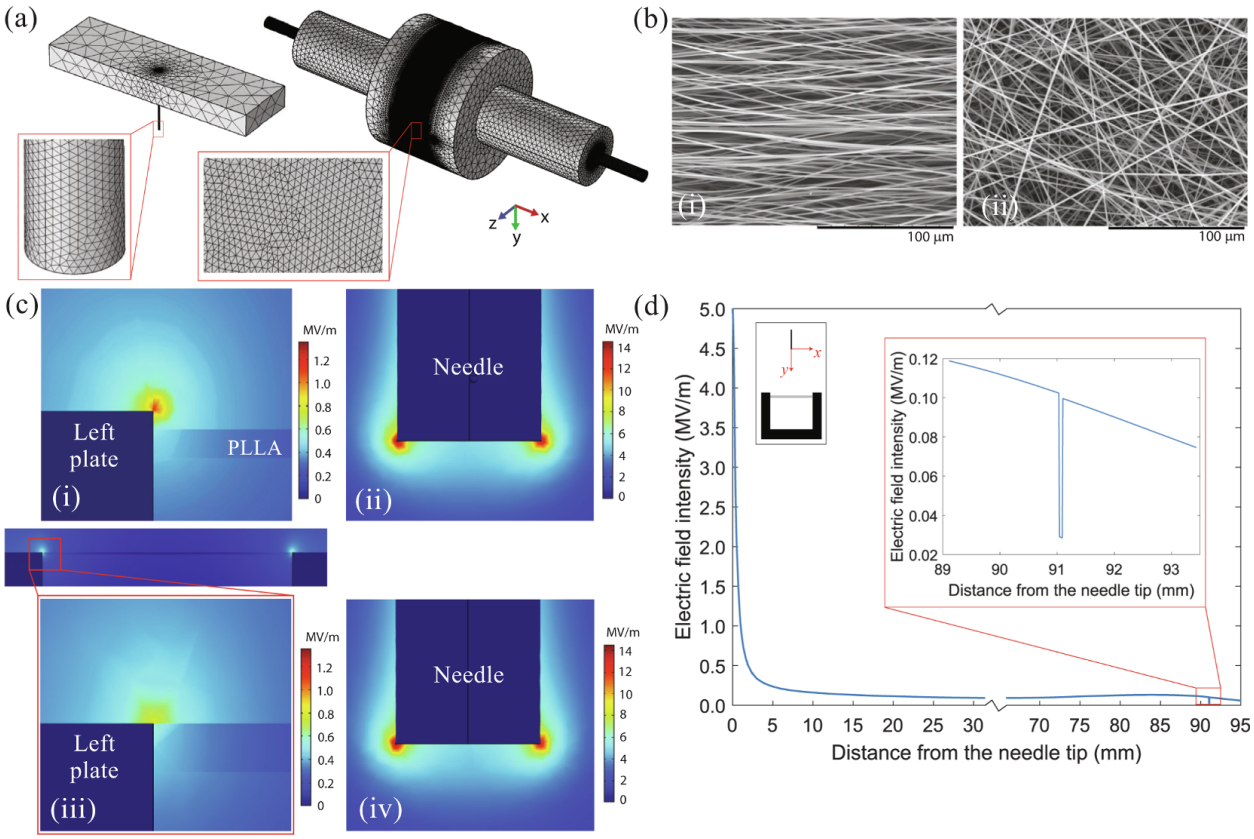

Figure 3.1: (a) Finite element mesh of the needle holder (left) and mandrel assembly with a 60 µm-thick polymer layer between the plates (right). The models are not to scale. (b) SEM images of fiber morphologies representative of all the polymer regions between the plates of a bilayer construct consisting of (i) aligned and (ii) randomly oriented fibers. (c) Electric field intensity in the vicinities of (i) the left plate and (ii) the needle tip for a 60 µm-thick polymer layer, and (iii) between the plates and in the vicinities of the left plate and (iv) the needle tip for a 100 µm-thick polymer layer. These plots were obtained at a plane dissecting the model along the needle axis and the mandrel axis. (d) Electric field intensity versus distance from the needle tip for a 60 µm-thick polymer layer. The distance from the needle tip is measured in the y-direction. The inset shows a cross-sectional view of the mandrel and the (x, y) coordinate system with its origin at the center of the needle tip.

effect) and at the polymer/air interface. For a 40 µm-thick polymer layer, the electric field intensity increases at a lower rate in the area below polymer deposition compared to the significant and abrupt increase of the electric field intensity at the polymer/air interface and the plate edge. A similar result is shown for 60 µm- and 100 µm-thick polymer layers. However, in all cases the electric field decays exponentially with increasing distance from the plate edge.

When the polymer layer thickness exceeds the height of the plate edges, the electric field first weakens as the antenna effect subsides, then increases suddenly due to the transition from polymer to air dielectric medium, and finally exhibits a decreasing trend with increasing distance from the needle tip. The same behavior is observed in all simulations for a polymer layer extending beyond the plate edges (i.e., polymer layer thickness >100 µm), with a higher electric field intensity arising at the polymer/air interface due to the abrupt change in permittivity. In all cases, the electric field intensity demonstrates a similar exponential decay with increasing distance from the polymer layer, asymptotically approaching the curve corresponding to air dielectric, including the cases of polymer layer thickness of less than 100 µm. This result shows a localized polymer effect on the electric field, i.e., the polymer does not affect the electric field in the air medium (Fig. 3.1d (inset) and 3.2b).

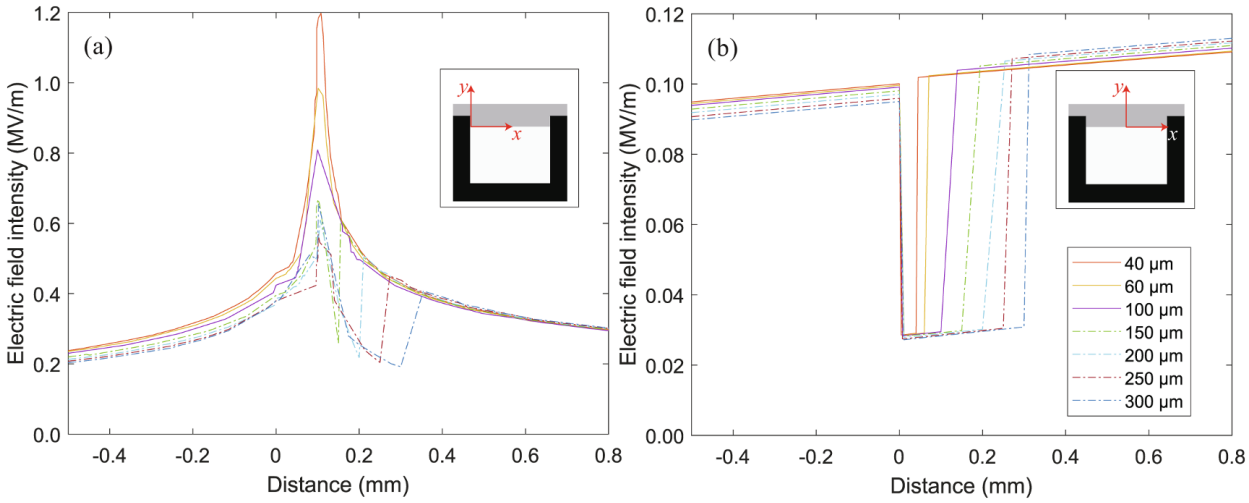

Figure 3.2: Electric field intensity versus distance measured in the y-direction (specified in the insets) and polymer layer thickness (shown in the legend) along (a) the wall surface of the left plate and (b) the axisymmetric axis of the electrospinning system and the needle axis. The insets show cross-sectional views of the mandrel and the (x, y) coordinate system used in each plot. The origin of the coordinate system is 100 µm below the top of the plates and in (a) it is 5 µm to the right from the inner wall surface of the left plate, whereas in (b) it is in the middle of the distance between the plates.

Fig. 3.3 provides further insight into the electric field directionality and intensity at

the collector plates. The electric field direction is perpendicular to the plate walls and intensifies in the vicinities of the plate edges. This behavior was observed in all simulations, including the case of air dielectric (Fig. 3.3a), and indicates that fiber alignment between the plates is due to dipole moments aligned in the direction of the electric field. The results for a polymer layer thickness of 60 µm (Fig. 3.3b) and 100 µm (Fig. 3.3c) indicate that the electric field intensity decreases as the polymer thickens due to the strengthening of the dielectric effect. The weakening of the electric field perpendicular to the plate walls caused by polymer thickening is consistent with the experimentally observed progressive diminution of fiber alignment between the plates. However, because the simultaneous fiber deposition between and at the top of the plates may further decrease the electric field intensity, the thickness of the polymer layer with aligned fibers is limited to ∼50 µm, in agreement with the experiments performed with the particular mandrel configuration (Pu et al. 2015; Pu, Komvopoulos 2014).

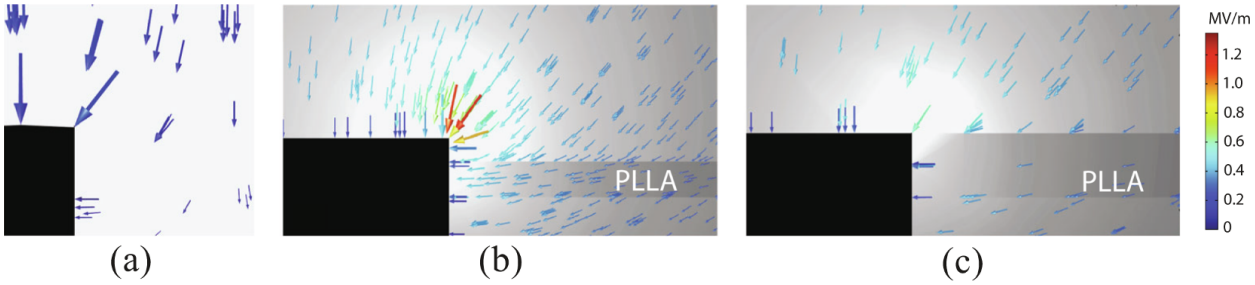

Figure 3.3: Electric field in the symmetry plane of the electrospinning setup defined by the mandrel axis and the needle axis for a polymer layer thickness (a) 0 (air), (b) 60 µm, and (c) 100 µm. The vector scaling factor, geometry scale, and color legend of the electric field intensity in (b) and (c) are the same. Only the left plate is shown in each panel. The color of the vectors in (a) is not representative of their magnitudes; it only shows the directionality of the electric field.

3.4 Conclusions

An electrostatic FEA analysis of the electrospinning process for a parallel-plate collector was performed to elucidate the fabrication of polymeric bilayer constructs with aligned and randomly oriented fibers. Simulations revealed that the electric field directionality controls the fiber alignment between the plates, and that the decrease of the electric field intensity and loss of directionality with increasing polymer thickness leads to the deposition of randomly oriented fibers. The electrospun polymer produces a local electric effect, instigating significant changes in the electric field intensity in the vicinity of the polymer and an asymptotic approach of the electric field to that for air dielectric. The present analysis can be extended

to study other collector configurations, guiding the design of electrospinning systems capable of producing fibrous constructs with various morphologies.

Chapter 4

In Vitro Degradation of Fibrous Bilayer Poly-L-Lactic Acid Scaffolds

The content of this chapter was published in the *Journal of Biomechanics*, 161, 111823 (2023), as "In Vitro Degradation of Fibrous Bilayer Poly-L-Lactic Acid Scaffolds" by Maria I. Echeverria Molina and Kyriakos Komvopoulos.

4.1 Introduction

Polymer degradation and mechanical properties of polymeric scaffolds are two crucial factors in tissue engineering, significantly affecting tissue regeneration. Material degradation must act in consort with tissue regeneration to provide mechanical stability, while also supporting the development of the extracellular matrix (ECM). In the course of polymer degradation, the byproducts released from the polymer system may have a detrimental effect on tissue generation. In tissue engineering, the aforementioned byproducts must be non-toxic to prevent chronic inflammation and immune response, and easily excreted through the body's normal function with no accumulation in other organs (e.g., liver and kidneys). Therefore, the rate at which degradation occurs is of utmost importance because it dictates cellular viability during the creation of new tissue. If the degradation rate is faster than the healing and regeneration rates of the native tissue, the scaffold would fail to effectively support the growing tissue, leading to the formation of defects and/or unfeasibility. This problem can be further exacerbated if the harmful byproducts are not expelled adequately fast from the body (Pucino et al. 2019; Cajori, Crouter, Pemberton 1924). Alternatively, if the degradation rate is too slow, the body's prolonged exposure to the scaffold may lead to adverse reactions, such as chronic inflammation or fibrosis (Holloway et al. 2014; Park et al. 2010; Sanz-Herrera, García-Aznar, Doblaré 2009; Balguid et al. 2009). The degradation rate of the scaffold is influenced by a number of factors including, but not limited to, material and microstructure factors (i.e., chemistry, molecular weight, crosslink density, and chemical

modification), scaffold factors (i.e., 3D structure or shape) and environmental factors (i.e., pH, enzymes, radiation, heat, and applied or residual loading) (Echeverria Molina, Malollari, Komvopoulos 2021); see Chapter 2.

The mechanical support provided by the scaffold to the surrounding tissue during the regeneration process is of critical importance. The mechanical properties of the scaffold indirectly affect cell behavior (e.g., proliferation, migration, differentiation, and mortality) by way of mechanical signals sensed by mechanoreceptors on the cell surface (Dado, Levenberg 2009). For instance, scaffold characteristics, such as fiber diameter, fiber alignment, fiber packing density (porosity), and pore size, direct cell behavior and morphology by impacting the stiffness sensed by the cells in their surrounding environment. On the other hand, the mechanical properties can also be affected by the scaffold chemistry (e.g., weight ratio of polymer blend, photopolymerization time and number of reactive groups, and crosslink density), which can change the fiber stiffness, in sequence affecting cell behavior and phenotype (Echeverria Molina, Malollari, Komvopoulos 2021). Moreover, if a significant mismatch exists between the mechanical properties of the scaffold and the native tissue, deformation of the scaffold may lead to its gross collapse under the weight of the cells and the newly formed tissue, resulting in failure of the tissue regeneration process and the impediment of cell migration and proliferation. More importantly, the decrease of the scaffold's mechanical integrity over time due to degradation could impact ECM cellular secretion and tissue regeneration.

Poly-L-lactic acid (PLLA) is a widely used biodegradable and biocompatible polymer with exceptional mechanical properties and simple degradation products, such as carbon dioxide and water. This biopolymer has been extensively used in many medical applications, including tissue engineering (Liu et al. 2020), bone fracture fixation (Fan et al. 2008; Marumo et al. 2006), and drug delivery (Keirouz et al. 2020; Liu et al. 2020; Tyler et al. 2016). For this reason, developing a deeper understanding of the degradation behavior of PLLA over time is warranted, especially the effects of the evolving degradation process on the mechanical properties of the polymer. PLLA undergoes hydrolytic degradation both in vitro and in vivo, although in vivo degradation may also be catalyzed by ions from body fluids, localized pH changes in the vicinity of implantation due to acute inflammation or infection, enzymes (i.e., hydrolases, such as proteases, esterases, lipases, and glycosidases) (Rosato et al. 2022) or the generation of oxidants from phagocytic processes (e.g., superoxide anion, hydrogen peroxide, hydroxyl radical, and hypochlorous acid). All of the foregoing can lead to hydrolysis of the ester bond and, in the case of oxidative degradation, can result in a highly toxic cell environment (Ratner et al. 2004). Although PLLA degradation has been studied in the past under conditions of accelerated degradation, high-temperature environments, and in the presence of various media (Rosato et al. 2022; Weir et al. 2004; Yuan, Mak, Yao 2002), the reported results were primarily dependent on the multiple abovementioned factors; hence, they were material and application specific and cannot be easily extrapolated.

Indisputably, an optimal balance between material degradation and mechanical properties of a scaffold is crucial for successful tissue engineering. A scaffold that degrades at a rate that matches the regeneration rate of the tissue and provides adequate mechanical

support is more likely to promote successful tissue regeneration. Therefore, the principal objective of this study was to investigate the degradation behavior of previously reported (Pu, Komvopoulos 2014) and tissue engineering promising electrospun PLLA bilayer microfibrous scaffolds consisting of a layer with aligned fibers (AFL) and a layer with random fibers (RFL) exposed to pH-neutral medium. The degradation was evaluated over an extended period of time in terms of changes in the molecular weight, crystallinity, mass loss, and mechanical properties. The obtained results reveal the potential of the investigated PLLA bilayer scaffolds for various tissue engineering applications and establish an effective experimental methodology for exploring material degradation in other fields and applications, such as agriculture, packaging, and disposable products.

4.2 Materials and Methods

Sample Fabrication

Scaffold samples were fabricated by the electrospinning technique using a 19 % w/v solution of PLLA (1.12 $\mathrm{dL\,g^{-1}}$) (Evonik–Lactel Absorbable Polymers, Birmingham, AL, USA) mixed with hexafluoroisopropanol (Thermo Fisher Scientific, Waltham, MA, USA) through sonication at room temperature overnight. The electrospinning setup had an aluminum mandrel consisting of two parallel aluminum plates of 57 mm diameter spaced 15 mm apart and connected by a 15 mm-diameter rod (Echeverria Molina, Komvopoulos 2022). The electrospun samples comprised a layer with aligned fibers, which gradually transitioned to a layer with fully randomly oriented fibers. To prevent fiber deposition in undesired locations and minimize material waste, parts of the mandrel were covered with 1 cm to 1.5 cm-thick polydimethylsiloxane (Sylgard™ 184, Dow, Midland, MI, USA). The mandrel was rotated by an AC motor at a speed of 8.4 rpm, resulting in fiber deposition along the perimeter of the parallel plates, as shown previously (Echeverria Molina, Komvopoulos 2022; Pu, Komvopoulos 2014). A syringe pump was used to deliver the PLLA solution at a rate of 1 $\mathrm{mL\,h^{-1}}$ through a 23G caliber needle with a flat tip located above the mandrel. The distance between the tip of the needle and the center of the mandrel was fixed at 12 cm. A DC power supply (Gamma High Voltage Research, Ormond Beach, FL, USA) was used to ground the mandrel and apply a positive voltage of 14 kV to the needle.

Scanning Electron Microscopy

The electrospun scaffolds were imaged at different magnifications with a scanning electron microscope (SEM) (TM-1000 Hitachi, Tokyo, Japan). SEM imaging included AFL and RFL cross sections of as-fabricated, tested, and degraded samples obtained by cutting the fibrous scaffolds with ultra-sharp double-edge blades.

Characterization of Fiber Diameter and Alignment

The scaffold morphology was described in terms of fiber alignment, fiber diameter, and porosity. The fiber alignment was studied with a modified Fast Fourier Transform (FFT) technique using ImageJ software (version 1.53e, National Institute of Health, USA) and SEM images of the samples at 2000× magnification. The SEM images were converted to grayscale and masked with a circular pattern having a graded periphery (darker in outer ring and lighter in inner ring) using a photo editing software (Adobe Photoshop, Adobe, San Jose, CA). The edited images were imported into ImageJ and converted to frequency domain plots through 2D FFT using the oval-profile plugin of ImageJ (O'Connell 2012), which summed up the pixel intensities of each radian in the 2D FFT images. Due to symmetry of the images of both AFL and RFL sides, frequency plots were obtained in the range of 0° to 180°. To account for differences in original image brightness and contrast, the FFT data were normalized by subtracting the lower intensity from the intensity at each pixel. The percentage intensity in the y-axis of the FFT plots gave a measure of the percentage of fibers aligned in a specific direction. Furthermore, SEM images of 2000× magnification of 3 different scaffolds were used in ImageJ to measure the diameter of at least 30 fibers in each set of scaffolds. The scaffold porosity was determined from the following equations (Pu, Komvopoulos 2014; Zhu et al. 2008):

$$\rho_{\text{app}} = \frac{m_{\text{scaffold}}}{t_{\text{scaffold}} \times A_{\text{scaffold}}} \tag{4.1}$$

where ρ_{app} is the apparent density ($\text{g}\,\text{cm}^{-3}$), m_{scaffold} is the scaffold mass (g), t_{scaffold} is the scaffold thickness (cm), and A_{scaffold} is the scaffold area (cm^2).

$$\phi = \left(1 - \frac{\rho_{\text{app}}}{\rho_{\text{PLLA}}}\right) \times 100\% \tag{4.2}$$

where ϕ is the scaffold porosity and ρ_{PLLA} is the bulk density of PLLA ($\text{g}\,\text{cm}^{-3}$).

Mechanical Testing

The mechanical behavior of the fibrous PLLA scaffolds was examined with an Instron machine (Instron model 3345, Norwood, MA, USA) equipped with a 5 kN load cell. The tests were conducted at room temperature at a strain rate of $0.017\,\text{s}^{-1}$. The samples prepared for mechanical testing were 10 mm in gauge length (measured along the aligned fibers of the AFL), 5 mm in width, and specific thickness (i.e., ∼200 µm for as-fabricated samples) measured with a caliper before testing. The bilayer scaffold samples were placed in the tester with the aligned fibers parallel to the direction of the tensile load. All reported properties represent averages obtained from 3 to 5 tests. The acquired force–displacement data were converted to engineering stress–strain responses.

Degradation Experiments

For degradation testing, fibrous scaffold samples with dimensions 15 mm × 5 mm × 0.2 mm were first weighed and then submerged in Dulbecco's phosphate-buffered saline (DPBS) (21-031-CV, Corning, New York, USA) solution with a pH of 7.4 in a water bath of 37 °C for 35, 147, and 242 days. The DPBS solution whose pH was measured weekly was replaced with fresh solution when the pH dropped below 7.2. After removing the samples from the media at the desired degradation time, they were thoroughly washed with deionized water three times and dried in a vacuum desiccator for at least 5 days. During the drying period, the weight of the samples m_t was measured daily and recorded until no further change in weight was observed. The mass loss Δm, defined by

$$\Delta m = \frac{m_0 - m_t}{m_0} \times 100\% \tag{4.3}$$

where m_0 is the original mass, was calculated as the percentage of the remaining weight using at least 3 samples for each set.

Gel Permeation Chromatography

The average molecular weight of the as-fabricated and degraded scaffold samples was measured by gel permeation chromatography (GPC), performed with a GPC/SEC system (Agilent, Santa Clara, CA, USA) equipped with a refractive index detector, using tetrahydrofuran (THF) (Thermo Fisher Scientific, Waltham, MA, USA) as the eluent at a flow rate of $1\,\mathrm{mL\,min^{-1}}$. The samples were cut into small sections to dissolve in the THF at a concentration of $2\,\mathrm{mg\,mL^{-1}}$ at 40 °C for 2 h. These solutions were thereafter injected for each analysis. Calibration was accomplished with polystyrene standards (Polysciences, Warrington, PA, USA).

Differential Scanning Calorimetry

Differential scanning calorimetry (DSC) was performed with a DSC calorimeter (Mettler-Toledo, Columbus, OH, USA) using a cooling and heating rate of $10\,^{\circ}\mathrm{C\,min^{-1}}$ in flushing nitrogen. Scaffold samples of ∼1.3 mg were sliced into smaller sections to fit the sample holder (aluminum pans). The melting temperature T_m was observed as the temperature at the maximum value of the melting peak. The glass transition temperature T_g, calculated with the calorimeter software (STARe SW 16.00, Mettler-Toledo, Columbus, OH, USA), was defined by the onset temperature. The melting enthalpy ΔH_m of the fibers was found as the corresponding energy (J/g) in the melting range. The crystallinity X_c of the PLLA fibers was calculated by dividing the melting enthalpy of PLLA by $93\,\mathrm{J\,g^{-1}}$ (Fischer, Sterzel, Wegner 1973), i.e.,

$$X_c = \frac{\Delta H_m}{\Delta H_{m,100}} \times 100\% \tag{4.4}$$

where $\Delta H_{m,100}$ is the melting enthalpy of 100% crystalline PLLA.

Statistical Methods

Data of the fiber diameter and mechanical properties of the scaffolds were analyzed with one-way ANOVA using Stata/SE 16.1. Data are presented as mean values and error bars corresponding to one standard deviation above and below the corresponding mean value. The histograms shown in the next section were also created with Stata/SE 16.1.

4.3 Results and Discussion

Scaffold Morphology

The porosity of a scaffold material is critical to tissue engineering as it affects cell infiltration, nutrient transport, and cell communication. Therefore, the morphology of the fabricated scaffolds was first characterized in terms of porosity estimations. The average scaffold porosity was found to be ∼90 %, consistent with previous findings (Pu, Komvopoulos 2014). Additionally, the present electrospinning setup has been shown to produce samples having a porosity gradient in the RFL with a quantifiably smaller average porosity (∼78 %) than the AFL (Pu, Komvopoulos 2014). However, while this method has been widely used, there are also other effective techniques (e.g., mercury porosimetry) for measuring the porosity, pore size, and surface-to-volume ratio of fibrous constructs (Lu et al. 2000).

SEM images of as-fabricated AFL and RFL surfaces (Fig. 4.1a and 4.1b, respectively) revealed fiber alignment in the AFL and randomly oriented fibers in the RFL. 2D FFT analysis was used to further study and quantify fiber alignment. The 2D FFT plot of the AFL surface contained a narrow peak at ∼90°, whereas that of the RFL surface was characterized by multiple low-intensity peaks (Fig. 4.1c). This finding is in agreement with previous research (Pu, Komvopoulos 2014) showing the fabrication of a bilayer PLLA scaffold consisting of AFL and RFL, produced under similar electrospinning conditions. Moreover, the overall scaffold thickness (measured from cross-sectional SEM images) was found to be ∼200 µm, with the AFL thickness being equal to ∼50 µm (Fig. 4.1b, top).

Analysis of high-magnification SEM images showed that the average fiber diameter of the scaffolds (including both the AFL and RFL) was (1.4 ± 0.3) µm. Representative SEM images of fiber morphologies and fiber diameter histograms of the AFL and RFL are shown in Fig. 4.2. The as-fabricated RFL and AFL scaffolds (Fig. 4.2a and 4.2b, respectively) showed clear fiber alignment in the AFL and apparent porosity differences between the two layers, the RFL being more porous than the AFL (Pu, Komvopoulos 2014). The images of the degraded samples displayed no fiber breaking, cracking, or voids in the RFL (Fig. 4.2c and 4.2e) and the AFL (Fig. 4.2d and 4.2f). Despite thorough rinsing, salt particles deposited onto some of the degraded samples (e.g., bright spots in Fig. 4.2d), presumably due to the prolonged exposure to the PBS. Moreover, the pore size and porosity in the degraded samples

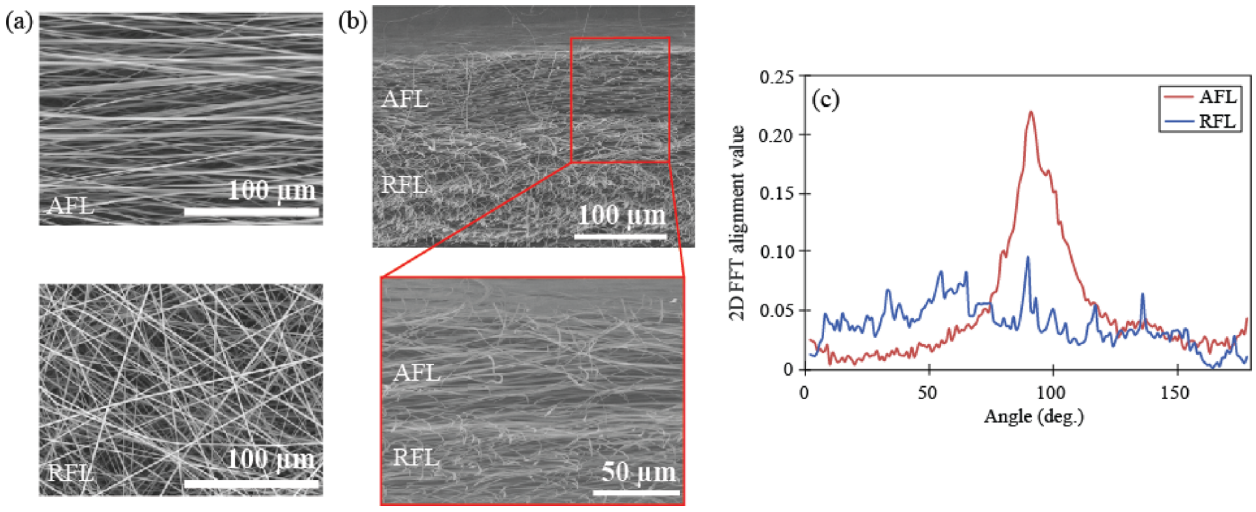

Figure 4.1: (a) Representative SEM images of as-fabricated PLLA scaffold surfaces with aligned fibers (AFL, top) and random fibers (RFL, bottom). (b) Cross-sectional SEM images of a scaffold showing the AFL (top) and RFL (bottom). The inset shows a closer view of the AFL. (c) Representative distributions of fiber alignment (2D FFT plot) on AFL and RFL scaffold surfaces.

appeared to be less than those of the as-fabricated counterparts. This may be attributed to the drying process whereby the fibers came closer to each other as the water was removed from the sample.

Statistical data of the fiber diameter of as-fabricated and degraded AFL and RFL (insets of Fig. 4.2) indicated a slight change in fiber diameter between the two layers and a wider distribution for the RFL fibers. The small change in fiber diameter from the AFL to the RFL may be accredited to variations in the electrostatic force and the needle-to-mandrel distance, which decreased with the progression of electrospinning due to polymer deposition onto the mandrel. This observation is supported by finite element results of the parallel plate electrospinning setup used in this study showing that the underlying reason for the transition from AFL to RFL deposition was the decrease and change in directionality of the electric field intensity with increasing polymer thickness (Echeverria Molina, Komvopoulos 2022). The wider fiber diameter distribution of the RFL may also be associated with the foregoing changes in the electric field intensity. The variation in fiber diameter and distribution between the AFL and RFL of the bilayer scaffolds can also affect the mechanical properties of each layer and, sequentially, the overall mechanical behavior of the scaffolds. The fiber diameter and AFL thickness were influenced by the electrospinning conditions (i.e., voltage, needle-to-mandrel distance, mandrel geometry, flow rate, and material), whereas the RFL thickness was principally controlled by the electrospinning time.

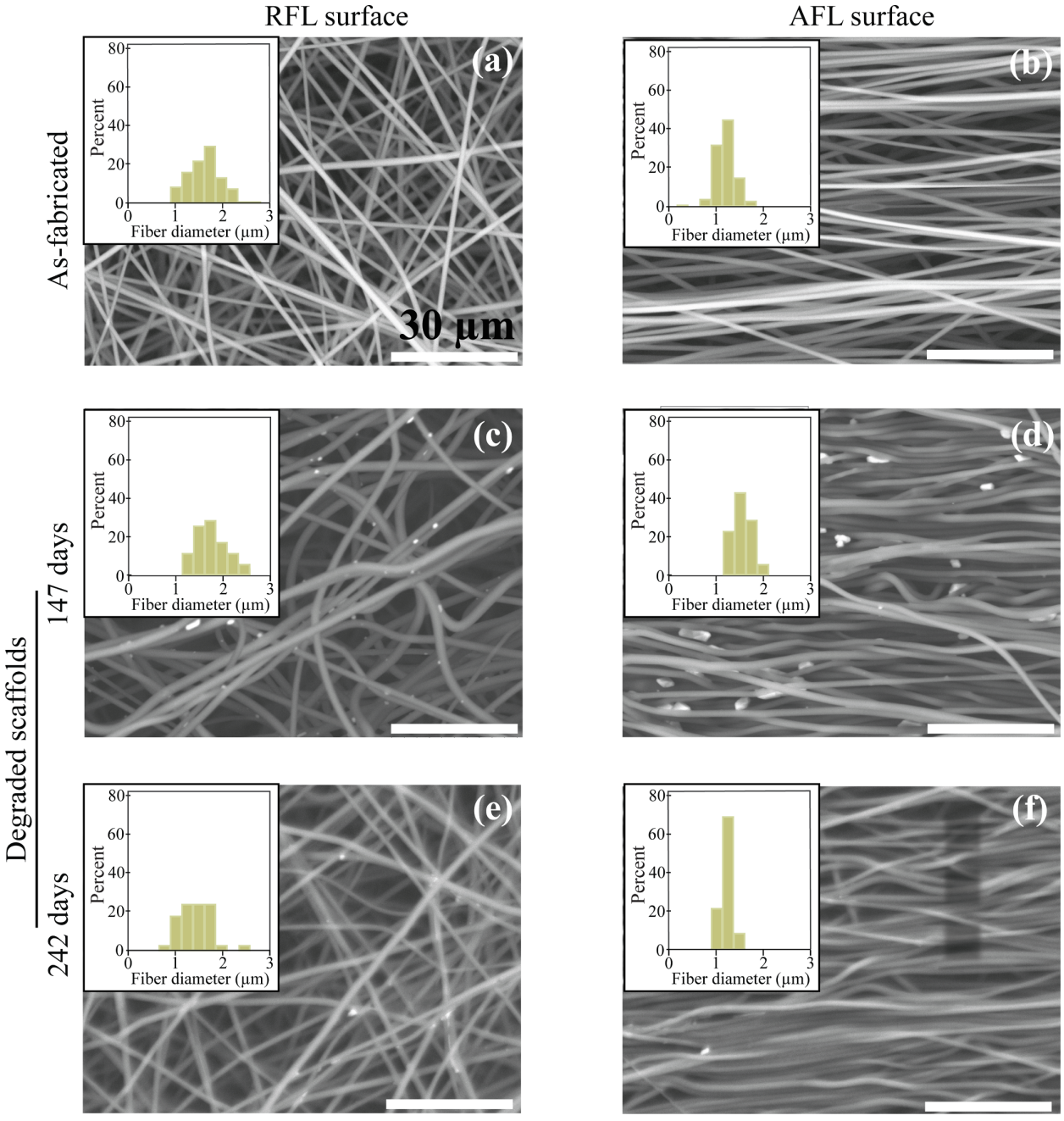

Figure 4.2: Representative SEM images and fiber diameter histograms (insets) of RFL (left column) and AFL (right column) surfaces of (a) and (b) as-fabricated and (c)–(f) degraded PLLA scaffolds. All the magnification scale bars are equal to 30 µm.

In Vitro Degradation

In vitro degradation testing is critical for evaluating the functionality and long-term biomechanical performance of biomaterials. One of the main objectives of this study was to elucidate the mechanism(s) responsible for the morphological modifications (e.g., change in fiber diameter) due to the evolution of material degradation. Fig. 4.3 shows the average fiber diameter of as-fabricated and degraded AFL and RFL samples. The slight increase in fiber diameter after degradation for 147 days in both the RFL and AFL may be attributed to water absorption and fiber swelling due to the prolonged exposure to water in the PBS and the ambient. However, a decrease in average fiber diameter of both RFL and AFL commenced between 147 and 242 days of degradation. This change may be indicative of the inception of aggressive hydrolytic degradation, which became more pronounced with the progression of degradation. Although there was no statistically significant difference between the two sets of degraded fiber diameter in the AFL, the difference in fiber diameter of the RFL between 147 and 242 days was significant. This finding can be attributed to faster water penetration through the more porous structure of the RFL (Fig. 4.2a) compared to that of the AFL (Fig. 4.2b).

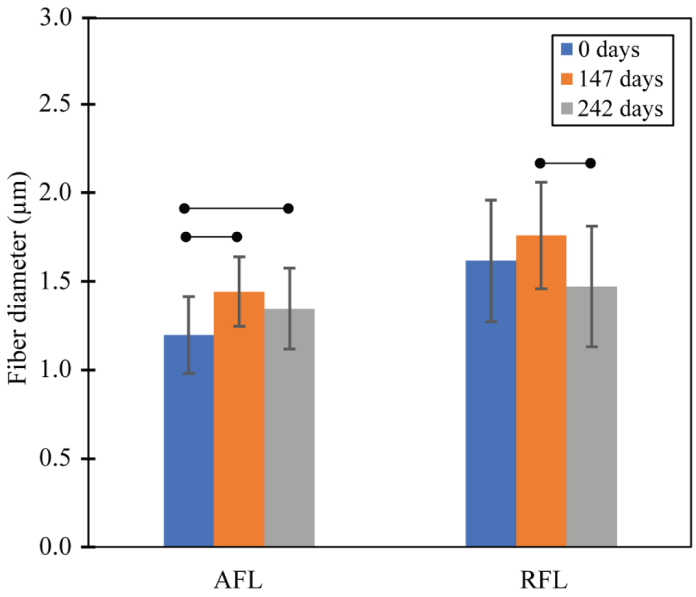

Figure 4.3: Fiber diameter statistics of the AFL and RFL of as-fabricated and degraded PLLA scaffolds. The error bars indicate one standard deviation above and below the corresponding mean value. Lines with end dots represent statistically significant differences between groups ($p < 0.05$).

The fairly insignificant variation in fiber diameter with degradation time and the lack of changes in the fiber morphology, e.g., surface roughening, cracking, or void formation (Fig. 4.2), suggested that degradation occurred at the molecular level without noticeable

alterations in the macroscopic structure of the material, and that the operating hydrolytic degradation mechanism was predominately fiber bulk degradation. It also indicated a fairly slow degradation process that did not affect the fiber diameter even after prolonged degradation. This could be attributed to the effect of several factors, such as the scaffold morphology (i.e., porosity and pore size), the intrinsic properties of the PLLA (i.e., molecular weight, crystallinity, and hydrophobicity), and the prevalent environmental conditions during degradation testing (i.e., temperature and pH), synergistically contributing to the evolution of a low degradation rate.

Measurements of the scaffold mass made before and after degradation and reported as mass loss versus degradation time (Fig. 4.4a) revealed an accelerated scaffold mass loss in the first 30 days reaching almost 7 % of the as-fabricated mass, with a considerable decrease in the rate of mass loss commencing thereafter, yielding a fairly constant mass loss throughout the remaining degradation time (i.e., statistically insignificant difference in mass loss data after 30 days). These results suggested that preferential hydrolysis of the polymer chains in the amorphous phase of the semicrystalline polymer instigated a decrease in molecular weight (Fig. 4.4b), resulting in more water-soluble short chains and less molecular entanglement, which enhanced the chain mobility. The diffusion of the small polymer fragments out of the polymer matrix decreased the scaffold mass (Fig. 4.4a). This process allowed the remaining polymer chains to rearrange in a more orderly structure, leading to the increase of the crystallinity (Fig. 4.4c) and a notable decrease in solubility, consequently limiting the penetration of water causing ester bond cleavage and, in sequence, plateauing of the mass loss.

The apparent increase in crystallinity, calculated from DSC data (Fig. 4.5a), with the degradation time (Fig. 4.4c) can be further interpreted in terms of the hydrolytic degradation process, which preferentially cleaved the amorphous chains into shorter ones. Some of the cleaved chains diffused out of the polymer matrix, increasing the overall volume fraction occupied by the crystalline domains, consequently augmenting the chain mobility and contributing to chain rearrangement. To further quantify degradation-induced changes in the polymer, both the melting temperature T_m and the glass transition temperature T_g were studied as functions of degradation time (Fig. 4.5b). As mentioned previously, hydrolytic cleavage of the amorphous phase of the polymer decreased the molecular weight and reduced the chain entanglement, subsequently enhancing the chain mobility, consistent with the decrease in T_g after 35 days of degradation. With the progression of degradation, T_g increased due to the remaining polymer chains rearranging in a more organized structure. Nevertheless, the insignificant effect of degradation time on T_m, which depends on the crystalline domains, confirmed the existence of an interplay between chain scission and formation of orderly domains during the progression of degradation.

Stress–strain responses of as-fabricated and degraded samples demonstrated a significant change in mechanical behavior (Fig. 4.6a). In view of the strong intermolecular forces inherent to the crystalline domains, the increase in ultimate tensile strength σ_U with the development of degradation (Fig. 4.6a and 4.6b) was associated with the simultaneous increase of the crystallinity (Fig. 4.4c). However, beyond a crystallinity threshold, σ_U decreased due

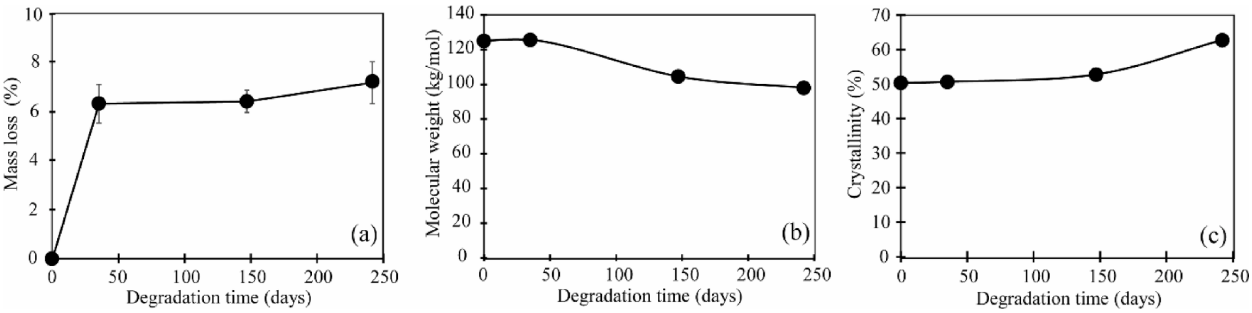

Figure 4.4: Variation of (a) mass loss, (b) weight-average molecular weight, and (c) crystallinity with degradation time of PLLA scaffolds. The error bars indicate one standard deviation above and below the corresponding mean value.

to the formation of structural imperfections, such as voids and interfaces between the crystalline and amorphous regions. This appeared to be the likely reason for the lower σ_U of the scaffolds degraded for 242 days than those degraded for 147 days (Fig. 4.6a and 4.6b). Contrary to the non-monotonic trend demonstrated by σ_U, the yield strength σ_Y remained fairly constant with increasing degradation time (Fig. 4.6c). Yielding was mainly controlled by the deformation in the amorphous regions of the polymer held together by weak intermolecular forces (e.g., van der Waals, dipole–dipole, and hydrogen-bonding forces). The amorphous domains were relatively mobile and could easily slide over each other, especially at a temperature above T_g. However, because the T_g of the PLLA was about 40 °C to 50 °C (Fig. 4.5b), the amorphous chains were not as mobile during the degradation experiments, which were performed at 37 °C, nor under the room-temperature tensile testing conditions. This explains the consistency of σ_Y throughout the duration of degradation (Fig. 4.6c). Importantly, degradation instigated a significant decrease in elastic modulus E by as much as ∼50 % (Fig. 4.6d), suggesting an interplay between the increase in crystallinity, chain mobility, and defect development with the evolution of material degradation, ultimately making the material more compliant and weaker compared to the as-fabricated condition, as evidenced by the decrease in strain to failure with the increase of the degradation time (Fig. 4.6a).

The degradation behavior of the PLLA bilayer scaffolds studied in the present work revealed structural changes gradually commencing over a long period of degradation and a significant decrease in material stiffness. The interaction between the foregoing changes in structure and stiffness is critical for applications where a wound (e.g., skin damage and gum recession) must be protected from bacterial attack over time. This could be accomplished by using the denser AFL upper layer as the protection outer layer and the more porous RFL underlayer as a cell infiltration enhancer. Hence, whereas the structure can remain almost unchanged, the change in stiffness could elicit a cell behavior conducive to the creation of new ECM.

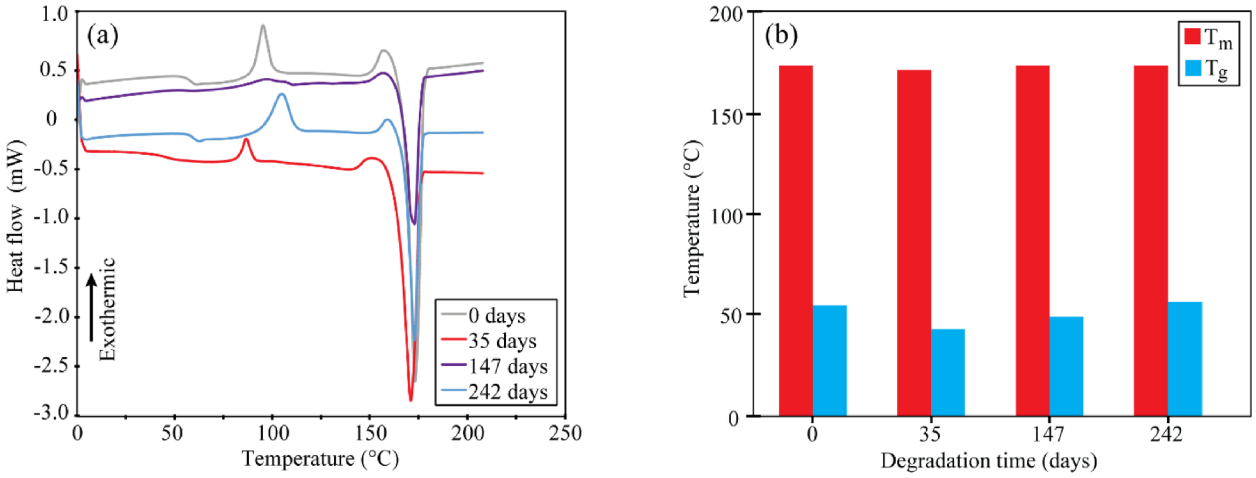

Figure 4.5: (a) DSC thermogram of PLLA with a dominant peak assigned to the melting temperature (173 °C) of the material and (b) melting temperature T_m and glass transition temperature T_g of PLLA determined from DSC thermograms versus degradation time.

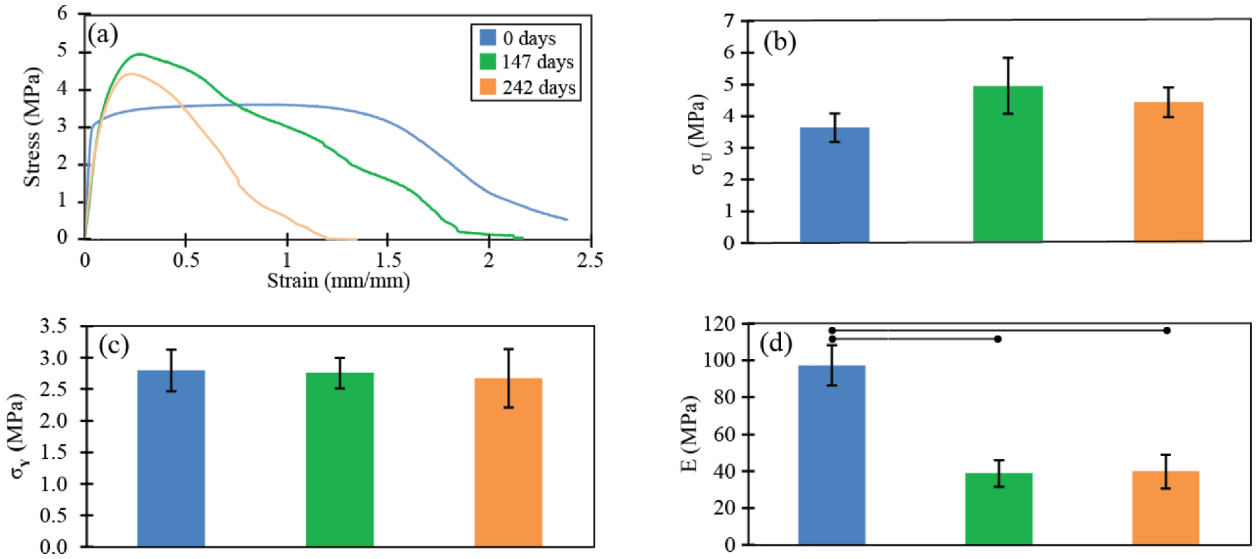

Figure 4.6: (a) Average stress–strain curves for a strain rate equal to 0.017 s^{-1}, (b) ultimate tensile strength σ_U, (c) yield strength σ_Y, and (d) elastic modulus E of as-deposited and degraded electrospun PLLA scaffolds. For all the data presented, the tensile load was applied in the direction of the aligned fibers. Lines with end dots represent statistically significant differences between groups ($p < 0.05$). The error bars indicate one standard deviation above and below the corresponding mean value.

4.4 Conclusions

Electrospun bilayer PLLA scaffolds consisting of a layer with aligned fibers and a layer with randomly oriented fibers were degraded in PBS over an extended period of time. The scaffolds were studied in terms of their thermophysical and mechanical properties. The results suggested hydrolytic degradation with an interplay between chain scission and reorganization, leading to the decrease of the molecular weight, the increase of the crystallinity, ultimate tensile strength, and glass transition temperature, no change in yield strength and melting temperature, and a significant decrease in stiffness compared to as-fabricated scaffolds over a degradation period of 147 days. Despite the considerable decrease in stiffness, the mass loss plateaued and marginal to no changes in fiber diameter and surface morphology were observed over the degradation period. The slow depletion of the scaffold stiffness could be beneficial for cell attachment and migration during tissue regeneration. However, the decrease in stiffness may also influence cell proliferation and differentiation during the degradation process.

This study provided valuable insight into the in vitro evolution of the mechanical properties of electrospun PLLA scaffolds in pH-neutral environment. The obtained results illuminated the potential of these scaffolds for tissue engineering, drug delivery systems, and possible extension to other application areas, such as agriculture, packaging, and disposable products where this set of mechanical properties and morphological changes over time might be desirable. Further mechanical testing in an environment simulating enzymatic degradation conditions should be beneficial to optimizing the scaffold morphology and structure, consequently enabling tuning of the degradation rate of the present fibrous scaffolds according to the requirements of the targeted application.

Chapter 5

Influence of Scaffold Topography and Culture Duration on Fibroblast Morphology in Tissue Engineering

The content of this chapter was published in *Tissue Engineering Part A*, 31(23–24), 1319–1326 (2025), as "Influence of Scaffold Topography and Culture Duration on Fibroblast Morphology in Tissue Engineering" by Maria I. Echeverria Molina and Kyriakos Komvopoulos.

5.1 Introduction

Cell shape is a fundamental aspect of cellular biology, intimately tied to cellular behavior, health, and function. Although cell shape is not merely a structural feature, it often reflects a specialized role in the body, influencing the cell's ability to interact with its surrounding environment. For example, spindled-shaped smooth muscle cells can instinctively perform movements necessary for peristalsis in the intestines and vasoconstriction in blood vessels (Jaslove, Nelson 2018; Hafen, Shook, Burns 2023). Alternatively, epithelial cells display a range of shapes depending on their location and function (Kurn, Daly 2023). Squamous epithelial cells are flat and thin, resembling scales, which facilitate rapid gas exchange in the lungs, whereas columnar epithelial cells in the intestines have a tall structure that maximizes surface area for nutrient absorption. Nerve cells have long, branching structures perfectly suited to transmit chemical and electrical signals over long distances (Cole, Kramer 2016). These examples demonstrate the intricate relationship between cell shape and function, underscoring how cellular morphology is naturally tailored to the specific demands of different tissues.

Furthermore, changes in cell shape may also indicate disease or dysfunction. For instance, cancer cells often exhibit irregular shapes and sizes compared with healthy cells, reflecting disorganized and uncontrolled growth. Similarly, cell shape can change in response to diseases

and external stressors, including mechanical forces (Janmey, Miller 2011; Haftbaradaran Esfahani, Knöll 2020). In tissue engineering, the cell shape is significantly influenced by various scaffold characteristics. Serving as structural frameworks for tissue regeneration, scaffolds offer a variety of physical and biochemical cues that directly impact cell behavior (Pu et al. 2015; Tajima et al. 2008; Cheng et al. 2013a; Klapperich, Pruitt, Komvopoulos 2001; Cheng, Li, Komvopoulos 2009; Cheng, Komvopoulos 2010; Cheng, Komvopoulos, Li 2014). Various key factors, such as pore size and shape, fiber diameter and alignment, porosity, and texture (roughness), influence the cell morphology and affect vital cellular functions, including adhesion, proliferation, infiltration, migration, differentiation, and gene expression (Pu et al. 2015; Echeverria Molina, Malollari, Komvopoulos 2021; Cheng et al. 2013b); see Chapter 2.

Cell–scaffold interactions often occur through mechanotransduction pathways, where cells sense and respond to environmental physical and biochemical cues. For instance, cells seeded on aligned fibrous scaffolds often elongate and align along the fibers, facilitating directional migration and organization, whereas cells attached onto randomly oriented fibrous or porous scaffolds might adopt a more spread shape, enhancing their ability to produce ECM components such as collagen, which are essential for rebuilding tissue structure (Ottosson, Jakobsson, Johansson 2017; Vimal, Ahamad, Katti 2016). In particular, fibroblasts are highly responsive to mechanical signals in their environment, playing central roles in wound healing and tissue repair. Spindle-shaped fibroblasts are typically involved in tissue restoration and can differentiate into myofibroblasts, essential for wound contraction (Li, Wang 2011). In contrast, spreading fibroblasts, while less motile, augment the production of ECM components such as collagen, which are critical for tissue reconstruction. Conversely, rounded fibroblasts often indicate a quiescent state, where the cell is not actively engaged in the repair process (Li, Wang 2011; D'Urso, Kurniawan 2020). Indisputably, understanding how fibroblast morphology influences their function in tissue regeneration is crucial for developing strategies for guiding cell behavior in tissue engineering applications.

Scaffold morphology and mechanical properties also play a key role in modulating immune responses. For instance, it has been reported that macrophage elongation leads to higher levels of cytokines and markers of M2 (prohealing) polarization, while protecting them from M1-inducing (proinflammatory) stimuli cytokines (McWhorter et al. 2013). Scaffold morphology, particularly fiber alignment and the presence of biochemical cues, can therefore modulate the local immune response, influencing tissue regeneration outcomes. Moreover, degradation products of scaffold materials can have additional effects on the immune response. For example, poly-L-lactic acid (PLLA), a commonly used polymer in tissue engineering, valued for its notable mechanical properties, biocompatibility, and resorption capabilities, breaks down through hydrolysis into lactic acid, carbon dioxide, and water. Lactic acid has been shown to regulate macrophage metabolism preventing excessive inflammatory responses (Shi et al. 2024). Given these effects, PLLA and its degradation products may offer unexpected but beneficial immunomodulatory effects in tissue engineering by helping to manage inflammation and promote healing.

In this study, a bilayer fibrous PLLA scaffold consisting of randomly oriented fiber layer

(RFL) and aligned fiber layer (AFL) was used to investigate the shape of fibroblasts F-actin cytoskeleton and nucleus in response to the scaffold morphology and seeding time. The shape was analyzed in terms of shape descriptors, specifically eccentricity, roundness, aspect ratio, and cell-to-nucleus area ratio, as these are closely tied to cellular mechanotransduction. Nucleus deformation is also a key indicator of mechanotransduction, as changes in nuclear shape can signal alterations in chromatin organization and gene regulation in response to external mechanical stimuli (Miroshnikova, Nava, Wickström 2017). It was hypothesized that the effect of topography may be influenced by the seeding time, as cells could gradually adopt a more stable or relaxed morphology over time. The foregoing hypothesis was tested by comparing the nuclear and cellular shape descriptors of fibroblasts adhered to scaffolds with different scaffold topographies (i.e., AFL and RFL) for various cell culture durations (i.e., 1, 3, 6, and 9 days). The cells were then fixed, and actin filaments and nuclei were stained to calculate the shape descriptors for the RFL and AFL scaffold surfaces. Notably, the observed adaptation and subsequent stability in cell morphology on both RFL and AFL surfaces suggest differential mechanobiological pathways influenced by fiber alignment, a distinction that may have critical implications for designing multilayered or bilayer scaffolds.

One particularly promising application of this approach lies in periodontal tissue engineering, where regenerating the cementum–periodontal ligament–alveolar bone complex demands spatially distinct microenvironments to guide diverse cellular behaviors (Costa et al. 2014; Galli et al. 2021). For instance, an AFL could facilitate the organized collagen alignment and fibroblast orientation characteristic of the periodontal ligament, while an RFL could support more isotropic spreading favorable for cementum or alveolar bone formation. Similar design strategies may benefit other multilayered or interface-rich tissues, such as skin (dermis–epidermis) (Girard et al. 2024), osteochondral units (cartilage–bone) (Li et al. 2023; Chen et al. 2023), and vascular grafts (Wang et al. 2021), where region-specific fiber orientation and mechanical cues can direct cell morphology, migration, and differentiation. By revealing how scaffold topography modulates cell behavior over time, this study provides foundational insight for the development of spatially and temporally tailored regenerative platforms across a range of complex tissue systems.

5.2 Materials and Methods

Sample Fabrication

Scaffolds were fabricated by electrospinning using a 19 % w/v solution of PLLA (1.12 dL/g; Evonik–Lactel Absorbable Polymers, Birmingham, AL, USA) in hexafluoroisopropanol (Thermo Fisher Scientific, Waltham, MA, USA).

The solution was sonicated at room temperature overnight and electrospun using an experimental setup described elsewhere (Echeverria Molina, Komvopoulos 2023); see Chapter 4. The produced samples comprised an AFL that gradually transitioned to a thicker RFL.

Cell Culture

All materials were sterilized by immersion in 95 % ethanol (Decon Labs, King of Prussia, PA, USA) for 24 h. Scaffolds cut to a 5 mm width and 15 mm length and sterilized with ethanol were placed on glass slides and air-dried inside a biosafety hood (NV25-600, NuAire, Plymouth, MN, USA). In all the experiments, the RFL of the scaffold was placed facing the bottom of the Petri dish. The top and bottom scaffold areas exposed to the cells were about 15 mm × 4 mm. The tissue culture plates used during scaffold-cell seeding were treated with 1 % w/v Pluronic F108 Prill (BASF, Ludwigshafen, Germany) in deionized water to reduce cell adhesion on the culture plates. The solution was left sitting for 1 h, then removed, and the plates were air dried.

In vitro testing was performed using primary cells such as *Mus musculus musculus* (PWK) tail fibroblasts (PWK-F). The cells were isolated and prepared using a methodology described elsewhere (Kang et al. 2023) and cultured in an expansion medium consisting of Dulbecco's modified Eagle's medium, with calcium and sodium pyruvate (Sigma-Aldrich, Hamburg, Germany) including 10 % fetal bovine serum. The cells were grown and maintained in the media in a humidified incubator with 5 % carbon dioxide atmosphere at 37 °C. The cells were seeded onto scaffolds at passages 16–18 with a density of 50,000 cells per mL in 1 mL of media while the AFL scaffold surface was facing up. During cell seeding, scaffolds were left floating in the media (i.e., without holding by any means) and the medium was supplemented with 1 % penicillin-streptomycin solution (Thermo Fisher Scientific, Pittsburgh, PA, USA).

Microscopy

Before cell seeding onto the fabricated bilayer scaffolds, images of the fibrous topographies of the AFL and RFL surfaces were obtained with a scanning electron microscope (SEM) (Zeiss Crossbeam 550, Oberkochen, Germany). Subsequently, fibroblasts attached to the scaffolds and incubated for 1, 3, 6, or 9 days were fixed, permeabilized, and blocked using protocols developed by Life Sciences (ThermoFisher Scientific 2014) (Thermo Fisher Scientific, Waltham, MA, USA). The cellular shapes attained by the fibroblasts attached to the PLLA bilayer scaffold surfaces were stained according to the manufacturer's protocols with fluorescent dyes, such as Hoechst 33342 (NucBlue Live ReadyProbe Reagent, Invitrogen, Waltham, MA, USA) for visualizing the nucleus and AlexaFluor 488 phalloidin (ReadyProbe Reagent, Invitrogen, Waltham, MA, USA) for visualizing F-actin filaments. The fibroblasts were subsequently imaged with a LionHeart FX cellular imaging system (Agilent/Biotek, Santa Clara, CA, USA), using DAPI and GFP filter cubes for imaging blue and green fluorescent stains, respectively, at magnifications 4×, 10×, and 20× using identical cell populations.

Cell and Nucleus Shape Descriptors

Cellular morphometric analysis was performed using Gen5 Image Prime (v3.14, BioTek Instruments, Santa Clara, CA, USA) under the "Cellular Analysis" module within the Analyze

tab. Fluorescence images were acquired as Z-stacks and their projection was processed with Gen5. Prior to analysis, rolling ball background subtraction was applied using Gen5's built-in preprocessing tools to reduce background noise and enhance object segmentation. Object masks for nuclei and actin-defined cell bodies were generated using channel-specific intensity thresholds and object size filters. From these masks, area, length, and width measurements were extracted for both nuclei and entire cells. The data were exported directly from Gen5 for downstream statistical evaluation. Cell and nuclear shape descriptors were obtained from the software-generated measurements for each individual cell. Data points in which the cell area was smaller than the corresponding nuclear area were excluded from the analysis, as this was interpreted as evidence of compromised cells, potentially undergoing apoptosis or exhibiting cytoplasmic/actin fragmentation.

Cell and nucleus roundness, eccentricity, aspect ratio, and area ratio were used as shape descriptors to analyze cell morphology. The roundness ($4A/\pi l^2$, where A is the projected area and l is the length or major axis of the oval cell) quantified how closely a cell or cell nucleus resembled a perfect circle, with higher values indicating a more circular shape. The eccentricity ($[1-(w/l)^2]^{1/2}$, where w is the width or minor axis of the cell) reflected the degree to which the cell shape deviated from a circle, with values closer to 1 signifying a more elongated (elliptical) cell. The aspect ratio (l/w) representing the cell length-to-width ratio increased with elongation, whereas the area ratio (A/A_n, where A is the total cell area and A_n is the nucleus area) provided a relative comparison between cell size and its nucleus.

Statistical Methods

The data sets were initially analyzed using MATLAB R2023b for one-way analysis of variance test assumptions at 20× magnification. Nucleus and cell shape descriptor data obtained at 4× and 10× magnifications were also analyzed. These data can be found in the Supplementary Data section (Section 5.4). However, in all cases, either the homogeneity of variances among the groups or the normality of the groups within each variable was violated. Therefore, the Kruskal–Wallis test with Dunn–Sidák post hoc correction was used to evaluate group differences based on median or distribution differences. Boxplots were created using the MATLAB R2023b boxplot function and algorithms. A total of 80–100 cells per condition were included in the nuclear and cytoskeletal morphology analysis.

5.3 Results and Discussion

Scaffold Characterization

SEM images of the fiber topographies of the fabricated bilayer scaffolds revealed fiber alignment in the AFL (Fig. 5.1a) and randomly oriented fibers in the RFL (Fig. 5.1b), consistent with previous studies (Echeverria Molina, Komvopoulos 2023; Pu, Komvopoulos 2014) showing that PLLA electrospinning under similar conditions yields bilayer scaffolds consist-

ing of a thin layer with aligned fibers and a relatively thicker and more porous layer with randomly dispersed fibers. The fiber diameter of these bilayer membranes, including AFL and RFL, was measured at (1.2 ± 0.3) µm, in agreement with previously reported values. The fiber alignment distribution has also been previously characterized (Echeverria Molina, Komvopoulos 2023).

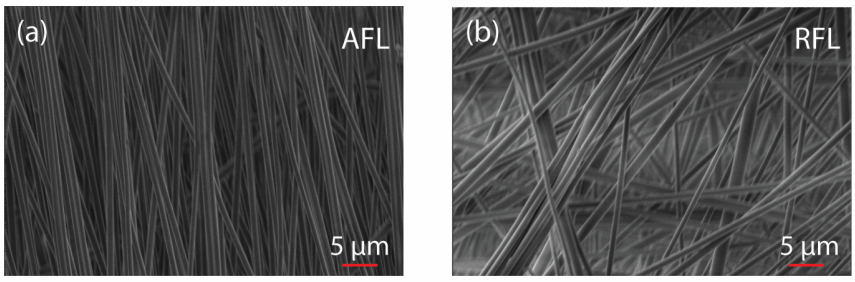

Figure 5.1: Representative scanning electron microscopy (SEM) images of the fibrous layers in the bilayer scaffolds: (a) aligned fiber layer (AFL) and (b) randomly oriented fiber layer (RFL).

Representative fluorescent images of stained PWK-F cells attached to the AFL and RFL scaffold surfaces obtained at 20× magnification after 1, 3, 6, and 9 days of cell culture (Fig. 5.2) elucidated the multiscale dynamics of cellular morphology and adhesion behavior in response to scaffold topography. The images displayed the progression of cell elongation, spreading, and infiltration over time and across surface types, offering qualitative support for trends observed with shape descriptors. Specifically, Figure 5.2 shows that cells on AFL scaffolds exhibited continuing elongation and alignment along the fiber axis, particularly visible at days 3 and 6, while those on RFL surfaces demonstrated more isotropic, branched morphologies. By day 9, cell infiltration through both surfaces became apparent, indicating adaptation to and interaction with the scaffold microarchitecture. Together with the quantitative shape description metrics, these images highlight the role of scaffold architecture and culture duration in driving cytoskeletal organization and mechanobiological adaptation. Data sets of nuclear and cell shape descriptors are presented next in the form of boxplots, offering a statistical overview of shape descriptor variation across conditions.

Analysis of Shape Descriptors

For both nuclear and cellular morphologies, the data were initially grouped by scaffold surface topography (AFL and RFL), culture duration (1, 3, 6, and 9 days), and magnification (4×, 10×, and 20×). Lower magnifications resulted in reduced image resolution and broader distributions of the calculated shape descriptors. Accordingly, the subsequent analysis is focused on the relationships between scaffold topography and cellular or nuclear morphol-

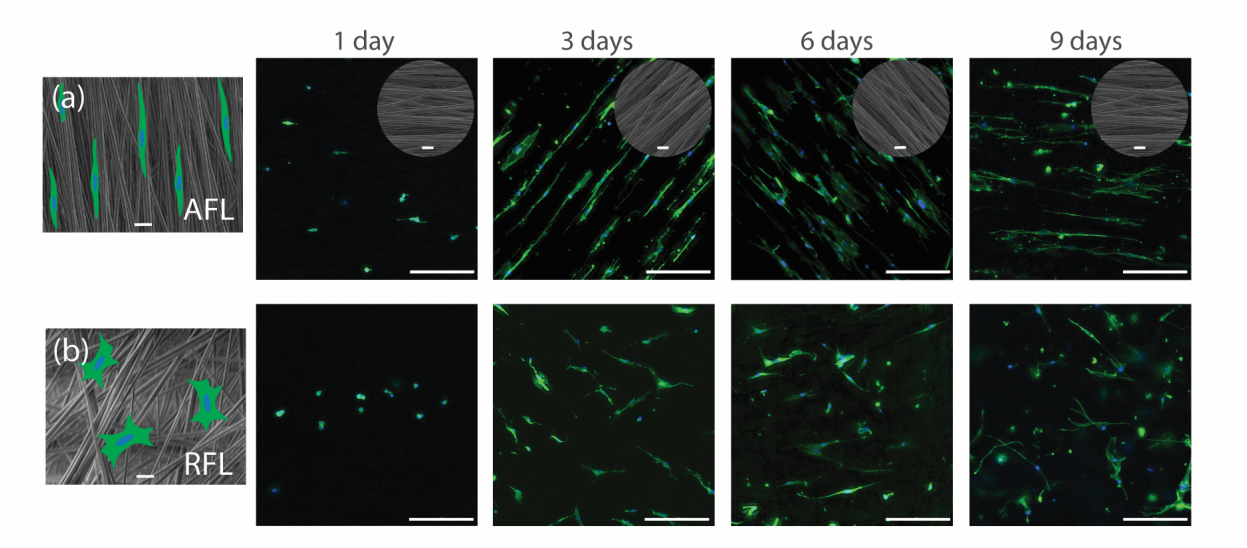

Figure 5.2: Representative fluorescent images of PWK-F cells stained for F-actin filaments (green, AlexaFluor 488 phalloidin) and nuclei (blue, Hoechst 33342) attached to AFL (first-row images) and RFL (second-row images) scaffold surfaces obtained after 1, 3, 6, and 9 days of cell culture (20× magnification). Subparts (a) and (b) show composite images of overlaid SEM (grayscale) and fluorescent (actin/nucleus) images. The SEM images within the upper right circles show corresponding fiber morphologies. Scale bars: 200 µm (fluorescence images), 5 µm (SEM inserts).

ogy, emphasizing shape descriptors derived from 20× magnification micrographs for optimal accuracy and consistency. Complementary results obtained at 4× and 10× magnifications demonstrating broader spatial trends in cell distribution and alignment are shown in the Supplementary Data section (Section 5.4). These results highlight macroscale morphological patterns not captured at a higher magnification.

Nucleus Shape Descriptors

After 1 day since cell seeding, nuclear shape descriptors, including roundness, eccentricity, and aspect ratio, differed significantly from those at all other time points, with both AFL and RFL surfaces exhibiting higher roundness and lower elongation metrics (Fig. 5.3). These findings suggest that, at early stages, nuclear morphology was not yet sensitive to scaffold topography. Rather, the high roundness and compact nuclear shape likely reflect a transient, nonspreading cellular state associated with initial substrate contact, low cytoskeletal tension, and limited mechanotransduction.

After 3 days of cell culture, however, nuclear shape became more responsive to scaffold surface characteristics. At this time point, statistically significant changes relative to day

1 were observed for both AFL and RFL scaffold surfaces. In particular, the AFL showed a decreased median roundness and a downward-shifted boxplot, indicating a possible effect of fiber alignment on nuclear morphology (Fig. 5.3). These shape changes imply an early mechanobiological response to topography via nucleus–cytoskeleton coupling, potentially mediated by the LINC complex (Skinner, Johnson 2017; Uzer, Rubin, Rubin 2016), highlighting the ability of the AFL surface to promote anisotropic cell behavior. Such behavior is particularly valuable in tissue engineering scenarios where directional alignment and migration are essential, such as the periodontal ligament, tendon, and vascular smooth muscle layers.

After 6 days of cell culture, nuclear shape descriptors showed similar median values and IQR across both scaffold surfaces with statistically insignificant differences in roundness (Fig. 5.3a), eccentricity (Fig. 5.3b), and aspect ratio (Fig. 5.3c). Nevertheless, extending the cell culture duration to 6 and 9 days produced an overall trend of increasing median roundness and decreasing median eccentricity and aspect ratio for both AFL and RFL. These shifts suggest a transition from an elongated, potentially migratory state to a more spread and stable phenotype. Interestingly, by day 6, nuclear shape descriptors stabilized with no significant differences between AFL and RFL surfaces, suggesting that the cells had adapted to their microenvironment, reaching mechanical and morphological homeostasis.

Nuclei rounding over time may reflect increased cell–cell interactions, matrix deposition, or cellular maturation, all of which reduce cytoskeletal tension and limit nuclear deformation. In biological terms, this morphological stabilization may correspond to a transition from dynamic migration to tissue integration or early differentiation. Such behavior could be particularly advantageous in bilayer scaffolds designed for periodontal interfaces (Galli et al. 2021), where fibroblasts in the AFL region initially migrate and align directionally, while cells in the RFL region adopt more isotropic, matrix-producing configurations to support cementum or bone regeneration.

Cellular Shape Descriptors

The analysis of the PWK-F cell shape descriptors (Fig. 5.4) revealed a similar pattern of response to scaffold surface type and culture duration. After 1 day of cell culture, cell body shape descriptors, including roundness, eccentricity, and aspect ratio, revealed minimal sensitivity to scaffold topography, with both AFL and RFL surfaces showing similarly high roundness and low elongation metrics (Fig. 5.4), and cells on both scaffold surfaces predominantly exhibiting a balled-up shape, characterized by a higher median roundness and lower median eccentricity and aspect ratio than those observed at 3, 6, and 9 days of cell culture. This likely reflects an early stage where cells had not yet fully adhered to or responded to the fiber topography. This behavior is consistent with previous reports indicating that cell attachment requires sustained actin fiber engagement and integrin-based adhesion (Cavalcanti-Adam et al. 2007), both of which appear to require more than 24 h to mature following cell seeding in this case. Nonetheless, as shown in Figure 5.2, some cells on the AFL surface already appeared to initiate elongation along the aligned fibers at day

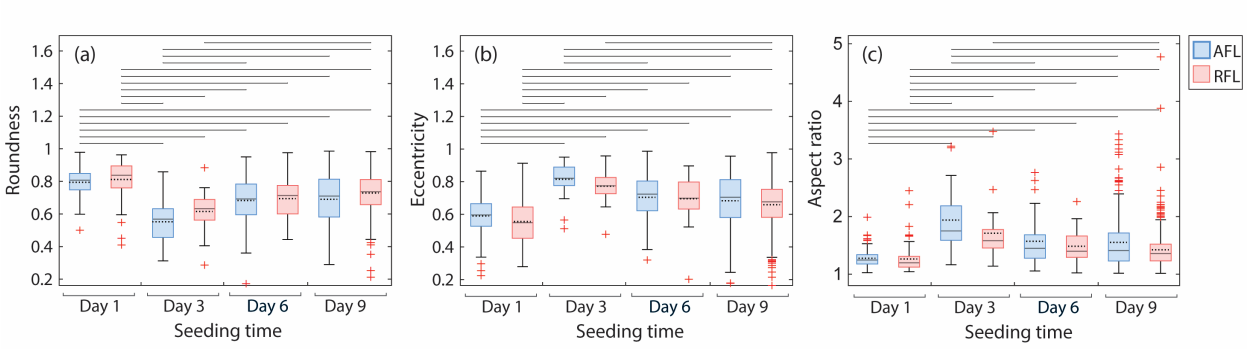

Figure 5.3: Effects of scaffold topography and culture duration on nuclear shape descriptors of PWK-F cells on AFL and RFL scaffold surfaces: (a) roundness, (b) eccentricity, and (c) aspect ratio. The horizontal solid and dashed lines inside each box symbol represent the median and mean values, respectively, of the particular dataset, while the horizontal solid lines above the box symbols indicate statistically significant differences for $p < 0.05$. The red + symbols represent boxplot outliers.

1. Statistically, all cell shape descriptors at day 1 differed appreciably from the data at 3, 6, and 9 days of cell culture.

After 3 days of cell culture, cells attached to the AFL surface exhibited significantly lower roundness (Fig. 5.4a) and higher eccentricity (Fig. 5.4b) and aspect ratio (Fig. 5.4c) than those on the RFL surface. These differences reflected a narrower distribution in roundness and eccentricity and a marked upward shift in aspect ratio, suggesting an increased elongation and alignment of cells in response to the directional cues presented by the aligned fibers on the AFL surface. This finding is consistent with the nuclear data, where initial nucleus elongation was more pronounced for the cells on the AFL surface at this time point. The elongated morphology and cytoskeletal polarization of the cells on AFL scaffolds suggest that these structures provided directional cues that promoted cell alignment and migration (Echeverria Molina, Malollari, Komvopoulos 2021; Chi et al. 2022), a phenomenon beneficial in regenerating tissues where anisotropic organization is critical for function. For instance, in tendon and ligament tissue engineering, aligned scaffolds have been proven to facilitate the alignment of fibroblasts, leading to the formation of organized collagen fibers that mimic native tissue architecture (Ruiz-Alonso et al. 2021; Govindaraju et al. 2023). Similarly, in neural tissue engineering, aligned nanofibers support the directional growth of neurons and glial cells, which is essential for effective nerve regeneration (Shi, Ou, Cheng 2023). In contrast, cells on the RFL surface displayed a more isotropic spread, with a broader distribution of shape descriptors, consistent with their interaction with a randomly organized environment (Echeverria Molina, Malollari, Komvopoulos 2021; Chi et al. 2022). This characteristic is advantageous in regenerating tissues that require a more homogeneous cell organization. For example, in skin tissue engineering, random-fiber scaffolds can promote a uniform ker-

atinocyte distribution, facilitating the formation of stratified epidermal layers (Wu et al. 2025).

Nevertheless, statistically significant differences in roundness, eccentricity, and aspect ratio of the cells attached to the AFL surfaces were found when going from 3 to 6 days and from 3 to 9 days of cell culture (Fig. 5.4a–c). Still, there was no significant difference from 6 to 9 days, indicating that the effect of scaffold alignment on cell elongation became stable as soon as day 6, as the cells adapted to the topographical features of the scaffold. While cells on the RFL surface showed an increase in distribution spread across shape descriptors without statistically significant temporal changes, those on the AFL surface exhibited both a broader distribution and a significant twofold decrease in median aspect ratio between days 3 and 6 (Fig. 5.4c). From 6 to 9 days, a slight decrease in median roundness and an increase in eccentricity and aspect ratio were observed for both scaffold surfaces, though these changes were not statistically significant. These results indicate that cells on both surfaces underwent a unique dynamic adaptation to their topographic environment, as evidenced by their physical configuration in Figure 5.2.

Additional evidence of the differential impact of scaffold topography on cell behavior was derived from the results of the area ratio (Fig. 5.4d). At day 1, cells on both AFL and RFL surfaces displayed area ratios close to 1, confirming that they were not well spread. For the RFL surface, the area ratio remained consistent across 3, 6, and 9 days with no statistical difference, suggesting a stable cell morphology relative to the nucleus of the cells attached to the RFL surface. Conversely, the cells on the AFL surface demonstrated a significant decrease in area ratio from day 3 to day 6, with the median value decreasing by more than half and the data clustering more tightly around the median. This drop in elongation may reflect the onset of a more stable, spread phenotype as fibroblasts transitioned from an exploratory, migratory state to one associated with increased cell–cell contact and differentiation, as also supported by prior studies linking reduced aspect ratios with enhanced substrate attachment and lineage commitment. A slight increase in median area ratio was observed between days 6 and 9, accompanied by a wider IQR and distribution, although the difference was not statistically significant. This suggests that while scaffold topography initially guided cell shape and alignment, other factors such as cell–cell interactions or matrix remodeling could have overridden topographical influence over time. Nonetheless, the dynamic changes in shape observed particularly on the AFL surfaces underscore the time-dependent responsiveness of fibroblasts to aligned fiber architecture and reinforce the importance of considering culture duration in scaffold-based tissue engineering applications. These patterns are visually supported by the physical morphology of the cells shown in Figure 5.2.

At early time points, particularly on the AFL scaffold surface, fibroblasts displayed elongation along the aligned fibers (Fig. 5.2), indicating that directional topographic cues promoted cytoskeletal polarization and migratory behavior. By day 3, this elongated morphology was accompanied by changes in nuclear shape, suggesting early responsiveness to scaffold features. However, by day 6 and day 9, both nuclear and cellular shape descriptors stabilized across surfaces (Figs. 5.3 and 5.4), indicating a shift toward more rounded, spread morphologies. These transitions reflect a dynamic remodeling process in which cells initially

respond to surface alignment but gradually adjust through cell–matrix and cell–cell interactions. The increase in roundness and the decrease in elongation and aspect ratio over time likely represent a transition from an exploratory to a more integrated and stable phenotype. This behavior is in agreement with prior reports linking rounded cell shapes to reduced motility, increased cell–cell contact, and enhanced viability and lineage commitment (Yao, Peng, Ding 2013; Rabel et al. 2020; Li et al. 2024; Papageorgiou et al. 2024; Sheets et al. 2013).

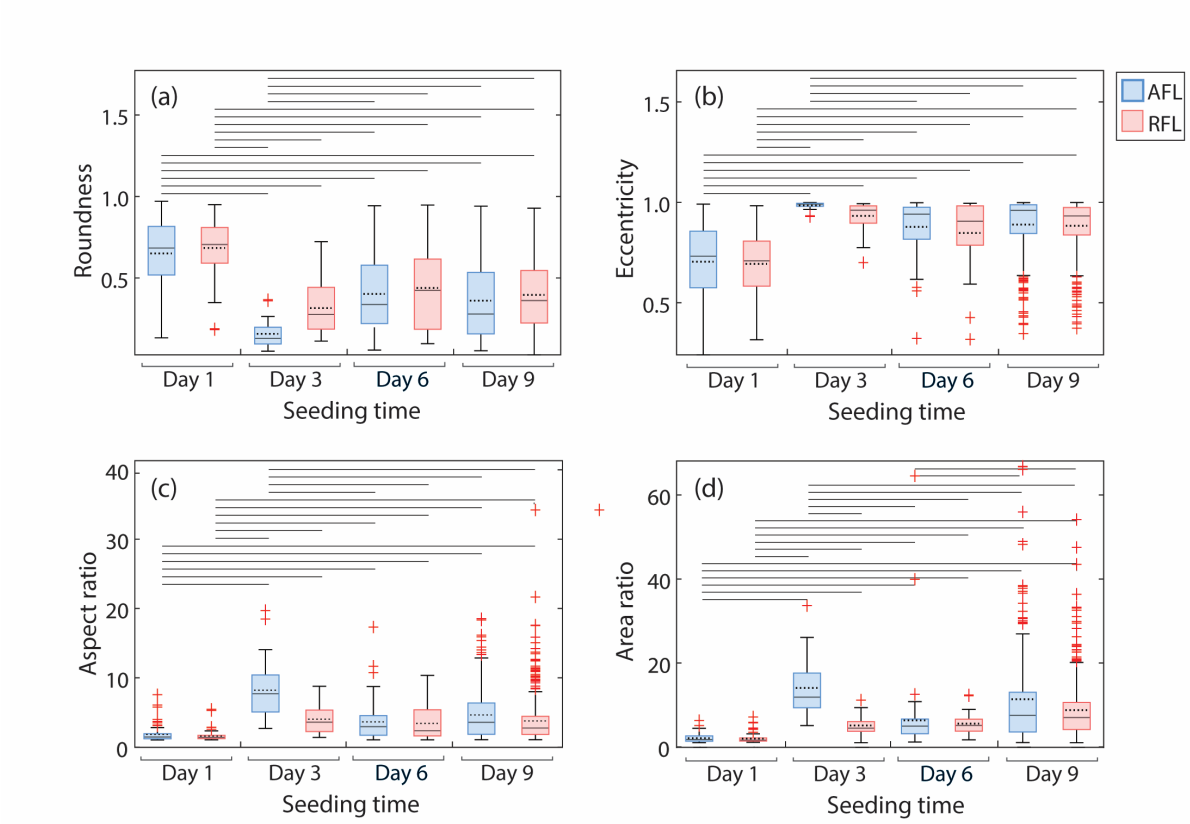

Figure 5.4: Effects of scaffold topography and culture duration on cell shape descriptors of PWK-F cells on AFL and RFL scaffold surfaces: (a) roundness, (b) eccentricity, (c) aspect ratio, and (d) area ratio. The horizontal solid and dashed lines inside each box symbol represent the median and mean values, respectively, of the particular dataset, while the horizontal solid lines above the box symbols indicate statistically significant differences for $p < 0.05$. The red + symbols represent boxplot outliers.

Overall, the findings of this study underscore the morphological plasticity of cells and their ability to remodel cytoskeletal and nuclear architecture in response to topographical and temporal cues. Notably, the results suggest that scaffold design should not only con-

sider static topography but also the timing of cellular responses to these cues. By aligning scaffold architecture with the temporal stages of cellular adaptation, it may be possible to sequentially direct cell morphology and function, depending on tissue application. It is also important to note that while these morphological adaptations appeared to stabilize by day 6, this period may also coincide with transcriptional changes. Therefore, further studies integrating gene expression profiling alongside morphological analyses will be essential to delineate whether these changes are solely structural or involve broader shifts in cell phenotype and function. Such studies may significantly contribute to functional outcomes in tissue-engineered constructs.

Although the standard shape descriptors (i.e., roundness, eccentricity, aspect ratio, and area ratio) capture global morphological trends, they may overlook other structural features. For instance, the morphological differences between cells on RFL and AFL surfaces (Fig. 5.2) suggest that additional descriptors, such as tortuosity, a measure of how much a shape deviates from a straight path, could provide added insight. Cells on AFL surfaces appeared relatively straight and aligned with the fiber axis, likely exhibiting low tortuosity. In contrast, those on RFL surfaces branched and curved along randomly oriented fibers without fully polarizing their cytoskeleton, possibly exhibiting higher tortuosity. Including tortuosity in future analyses may help distinguish between mechanically relevant subtypes of elongated morphology, such as directed migration versus matrix remodeling behavior.

The distinct morphologies observed with AFL and RFL scaffolds offer valuable design principles for tissue engineering. In particular, the time-dependent morphological adaptation of fibroblasts to scaffold alignment indicates that incorporating time as a design parameter may be essential when creating biomimetic scaffolds. Scaffold layers could be designed to first promote elongation and alignment (e.g., through AFL structures) followed by transition into regions that support stabilization and integration (e.g., through RFL patterns), consequently aligning with the different phases of tissue regeneration. The aligned cell elongation promoted by AFL surfaces may benefit uniaxial organization of tissues such as tendons, ligaments, peripheral nerves, and cardiac muscle, where directional cellular orientation supports mechanical strength, signaling, or contractility. In contrast, the more branched and spatially adaptive morphologies seen on RFL surfaces resemble fibroblast behavior in dermal, stromal, or connective tissues, where multidirectional interactions facilitate wound healing and extracellular matrix remodeling. These findings also support the use of bilayer or multilayer scaffolds to recapitulate tissue interfaces. For instance, in periodontal tissue engineering, an AFL layer could promote the aligned collagen structure of the periodontal ligament, while an RFL layer supports isotropic spreading for cementum or bone regeneration. Similar strategies could be applied to skin (dermis–epidermis), osteochondral units (cartilage–bone), and vascular interfaces, where regional fiber alignments and mechanical cues are key to function. Altogether, the ability of fibroblasts to remodel in response to topography supports a modular scaffold design approach tailored to the needs of complex, stratified tissues.

5.4 Supplementary Data

Effect of Imaging Magnification on Shape Descriptors

Compared to the cytoskeletal structures, nuclei, and overall cell morphology obtained at 20× magnification, image analysis at lower imaging resolutions, i.e., 4× and 10×, demonstrated broader distributions in shape descriptors. For comparison, shape descriptor data obtained at 4× and 10× magnifications were plotted together with data obtained at 20× magnification for 3 and 6 days of cell culture time.

Figures 5.5 and 5.6 show statistical results revealing the effects of scaffold topography, cell culture duration, and imaging magnification on nuclear and cell shape descriptors, respectively, of cells cultured on AFL and RFL scaffold surfaces for 3 and 6 days.

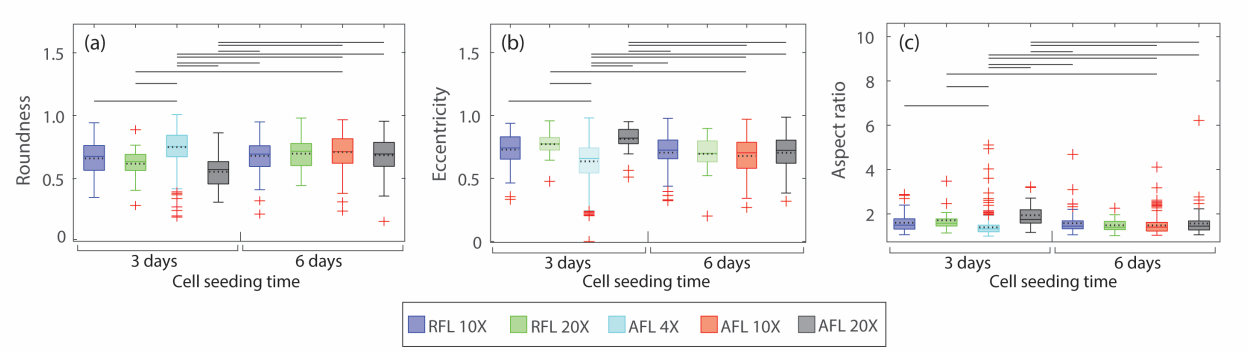

Figure 5.5: Effects of scaffold topography, cell culture duration, and imaging magnification on nuclear shape descriptors of cells seeded on AFL and RFL scaffold surfaces: (a) roundness, (b) eccentricity, and (c) aspect ratio. The horizontal solid and dashed lines inside each box symbol represent the median and mean values, respectively, of the particular dataset, while the horizontal solid lines above the box symbols indicate statistically significant differences for $p < 0.05$. The red + symbols represent boxplot outliers.

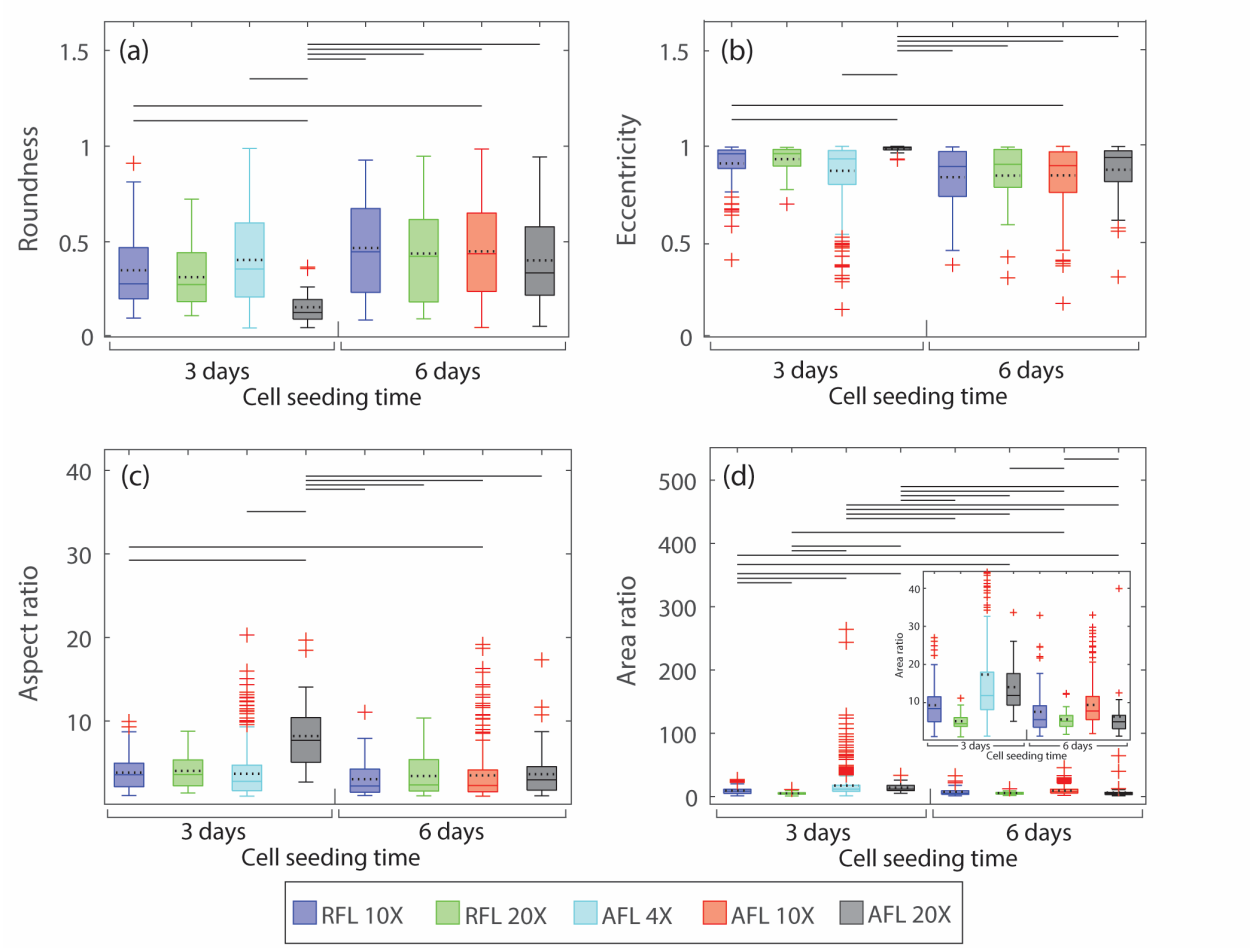

Figure 5.6: Effects of scaffold topography, cell culture duration, and imaging magnification on shape descriptors of cells seeded on AFL and RFL scaffold surfaces: (a) roundness, (b) eccentricity, (c) aspect ratio, and (d) area ratio. The horizontal solid and dashed lines inside each box symbol represent the median and mean values, respectively, of the particular dataset, while the horizontal solid lines above the box symbols indicate statistically significant differences for $p < 0.05$. The red + symbols represent boxplot outliers.

Chapter 6

Scaffold Fiber Architecture and Uniaxial Stretch Differentially Regulate Cell and Nuclear Morphology in Human Dermal Fibroblasts

The content of this chapter was published in *Tissue Engineering Part A* (2026), as "Scaffold Fiber Architecture and Uniaxial Stretch Differentially Regulate Cell and Nuclear Morphology in Human Dermal Fibroblasts" by Maria Echeverria Molina and Kyriakos Komvopoulos.

6.1 Introduction

Fibrous connective tissues, including tendons, ligaments, and dermal tissue, possess highly organized and anisotropic ECMs that are essential for their mechanical function. Successful regeneration of these tissues requires scaffolds capable of recapitulating both their aligned microstructure and mechanically active microenvironment (Baldwin et al. 2022; Stender et al. 2018; Ní Annaidh et al. 2012). Despite their structural similarities, fibrous tissues generally exhibit limited intrinsic healing capacity, often resulting in scar formation or mechanically inferior tissue repair following injury (Voleti, Buckley, Soslowsky 2012; Frank 2004; Gurtner et al. 2008). This limitation is particularly pronounced in poorly vascularized tissues such as tendons and ligaments. Consequently, tissue engineering approaches have emerged as promising alternatives to conventional graft-based reconstruction strategies, with the goal of restoring both tissue structure and function.

Mechanical cues play a fundamental role in the development, homeostasis, and remodeling of fibrous tissues. Cells residing within tendons, ligaments, and skin are continuously

exposed to tensile forces generated by physiological loading, growth, and daily movement. Although these tissues experience complex mechanical environments that may also include compressive and shear stresses, uniaxial tensile loading represents one of the dominant and most ubiquitous stimuli across fibrous connective tissues (Galli et al. 2021; Wang, Thampatty 2006). Accordingly, mechanical stretching has been widely incorporated into tissue-engineered constructs to better reproduce native biomechanical environments in vitro.

Both static and dynamic loading regimens have been shown to regulate cellular behavior through mechanotransductive pathways that convert external mechanical stimuli into intracellular biochemical signals. Dynamic loading has most commonly been associated with modulation of lineage-specific gene expression, whereas static uniaxial stretching has frequently been linked to changes in cell morphology, alignment, and ECM organization (Juncosa-Melvin et al. 2007; Reichenbach, Reimann, Reuter 2014; Riehl et al. 2012; Martyts et al. 2026). However, these effects are not mutually exclusive. Gene expression changes have also been reported under static loading conditions, while dynamic stretching has been shown to influence matrix deposition, structural organization, and cytokine-related signaling pathways (Espinoza-Álvarez et al. 2024; Kaiser et al. 2024; Yang et al. 2025). In skin and other fibrous soft tissues, mechanical stimulation regulates the proliferation, migration, and differentiation of multiple cell types, including keratinocytes, fibroblasts, and mesenchymal stem cells (Guo et al. 2022; Jiang et al. 2016). Dermal fibroblasts, in particular, are the primary matrix-producing cells responsible for collagen I synthesis and ECM maintenance. However, excessive or dysregulated mechanical stimulation can promote aberrant fibroblast activation and excessive matrix accumulation, processes associated with pathological remodeling and hypertrophic scar formation (He et al. 2021; Ma et al. 2023). Collectively, these responses are highly dependent on strain magnitude, loading mode, frequency, and duration.

The magnitude of applied strain is a particularly important design parameter. Physiological tendon strains are generally reported to remain below approximately 2 % during normal elastic deformation and may approach 4 % during the onset of microscopic damage, with strains approaching 10 % leading to progressive tissue failure (Wang 2006). However, elastic strains as high as 14 % have also been reported in certain tendon types and loading conditions (Devkota, Weinhold 2003). In vitro studies have investigated a broader range of tensile strains, often reaching 15 % (Bramson, Van Houten, Corr 2021), with moderate strains of up to 10 % frequently applied to examine the mechanoregulation of fibrous tissue-related cellular responses (Riehl et al. 2012). These observations support the use of uniaxial strains in the range of approximately 1 % to 10 % as physiologically relevant conditions for modeling fibrous tissue environments in vitro.

Cellular orientation is another critical determinant of tissue functionality and mechanical integrity. Consequently, scaffold design strategies for fibrous tissues frequently incorporate physical guidance cues that promote cell elongation and alignment. Electrospun scaffolds with aligned fibers have consistently been shown to direct the orientation of fibroblasts, Schwann cells, and other stromal cell populations along the fiber axis, while providing anisotropic topographical cues that further support tendon- and ligament-like ECM organization and deposition (Chew et al. 2008; Yang et al. 2022; Abbasian et al. 2025; Chen et al.

2017a; Lee et al. 2005). The combined effects of aligned fiber architectures and mechanical stimulation have also been extensively investigated, with fiber alignment and applied strain acting to enhance fibroblast differentiation, matrix organization, and ECM deposition in ligament and periodontal tissue models (Lee et al. 2005; Tang et al. 2021; Kim et al. 2016).

Previous studies have demonstrated that scaffold microarchitecture, including fiber alignment and bilayer organization, regulates cell morphology, cytoskeletal organization, and tissue-specific cellular behavior (Chi et al. 2022). It was further demonstrated that scaffold topography and culture duration jointly modulate fibroblast nuclear and cytoskeletal morphology in bilayer electrospun membranes containing regions of aligned and randomly oriented fibers (Echeverria Molina, Komvopoulos 2025); see Chapter 5. Mechanical stretching has also been reported to influence cell orientation, focal adhesion organization, and gene expression associated with matrix remodeling (Juncosa-Melvin et al. 2007; Espinoza-Álvarez et al. 2024; Sun et al. 2016). Importantly, the directional response of cells to applied strain depends strongly on the loading regime and substrate properties. Under cyclic strain, adherent cells, including fibroblasts, endothelial cells, smooth muscle cells, and mesenchymal stem cells, typically exhibit a strain-avoidance response, reorienting their actin cytoskeleton perpendicular to or at oblique angles (approximately 45° to 90°) relative to the stretching direction. The precise orientation depends on loading frequency, strain amplitude, substrate stiffness, and other material properties (Giverso et al. 2023; Huang et al. 2013). When topographical guidance cues are present, however, cells often maintain alignment along the underlying fiber direction despite cyclic loading, indicating that geometric constraints can override strain-avoidance reorientation (Wang, Grood 2000). In contrast, under static or quasistatic loading conditions and in the absence of competing topographical cues, cells generally align parallel to the direction of applied stretch (Tondon, Kaunas 2014; Rens, Merks 2017). Because fibrous tissue regeneration is governed by the interplay of structural and mechanical cues, understanding how scaffold-induced contact guidance and externally applied strain jointly regulate cellular organization remains an important challenge, particularly in fibrous scaffold systems where stretching can itself alter scaffold topography through fiber reorientation.

In this context, the present study investigates how static mechanical stretching influences fibroblast morphology and orientation on electrospun bilayer scaffolds consisting of an aligned-fiber layer (AFL) that gradually transforms to a random-fiber layer (RFL). It was hypothesized that static uniaxial stretching would enhance scaffold morphology-guided cellular organization in aligned fiber architectures, and that, in the absence of structural guidance cues, applied strain would become the dominant directional stimulus through strain-induced fiber realignment. Using a custom stretching device, scaffolds were subjected to 0 % and 10 % elongation, and adult human dermal fibroblast morphology was quantitatively evaluated using shape descriptors and qualitatively assessed through cell orientation analysis. This approach enabled direct assessment of the relative contributions of scaffold anisotropy and mechanical deformation to fibroblast organization. The results demonstrate that static stretching promotes cellular alignment along the stretching direction even in the absence of pre-existing structural anisotropy. More broadly, the findings suggest that scaffolds with

both aligned and random fiber regions can achieve consistent and controlled cellular organization when combined with appropriate mechanical stimulation, providing a versatile platform for engineering functional fibrous tissues, such as tendons, ligaments, and related connective tissue interfaces.

6.2 Materials and Methods

Sample fabrication

Fibrous scaffolds were fabricated by electrospinning a 19 % (w/v) solution of poly(L-lactic acid) (PLLA; 1.12 dL/g intrinsic viscosity; Evonik–Lactel Absorbable Polymers, Birmingham, AL, USA) dissolved in hexafluoroisopropanol (Thermo Fisher Scientific, Waltham, MA, USA). The polymer solution was sonicated overnight at room temperature and subsequently processed using a custom electrospinning system described elsewhere (Echeverria Molina, Komvopoulos 2023); see Chapter 4. The resulting bilayer membranes consisted of an AFL that gradually transitioned to a thicker RFL.

Scaffold characterization

Scaffold morphology, with particular emphasis on fiber alignment, was characterized using scanning electron microscopy (SEM) and two-dimensional fast Fourier transform (FFT) analysis. SEM images acquired at 2000× magnification were analyzed using ImageJ software (version 1.53e, National Institutes of Health, Bethesda, MD, USA) for scaffolds subjected to 0 %, 10 %, and 20 % elongation. Details of the image processing methodology have been reported previously (Echeverria Molina, Komvopoulos 2023; Ayres et al. 2008). The physicochemical characterization of the scaffolds, including their mechanical properties and biodegradation characteristics, has also been described elsewhere (Echeverria Molina, Komvopoulos 2023).

Stretching device

Controlled uniaxial elongation was applied with a custom-designed stretching device (Fig. 6.1) consisting of two stainless-steel components connected by screws and springs. The apparatus was equipped with a precision micrometer head for displacement control. Elongation was applied manually, and the strain rate was determined from the time required to achieve the prescribed extension.

Cell culture

Electrospun membranes were cut into strips measuring 5 mm × 15 mm, sterilized in ethanol, mounted on glass slides, and air-dried in a biosafety cabinet (NV25-600, NuAire, Plymouth,

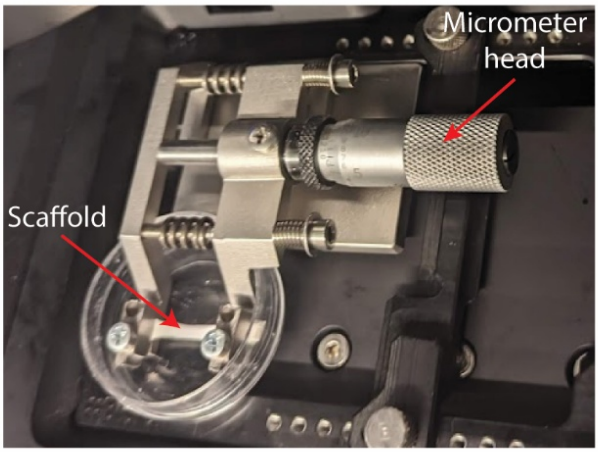

Figure 6.1: Custom uniaxial stretching device showing an electrospun scaffold maintained under elongation within a 35-mm-diameter cell culture dish.

MN, USA). During all experiments, the RFL side of the scaffold faced the bottom of the culture dish, leaving an exposed surface area of approximately 15 mm × 4 mm for cell attachment. To minimize nonspecific cell attachment to the culture plates, the plates were pretreated with 1 % (w/v) Pluronic F108 Prill (BASF, Ludwigshafen, Germany) in deionized water for 1 h, after which the solution was removed and the plates were allowed to air-dry. Surgical instruments used during sample preparation were sterilized by immersion in 95 % ethanol (Decon Labs, King of Prussia, PA, USA) for 24 h.

Primary adult human dermal fibroblasts (HDFa; PCS-201-012, ATCC, Manassas, VA, USA) were used for all in vitro experiments. Cells were cultured in Dulbecco's modified Eagle's medium containing calcium and sodium pyruvate (Sigma-Aldrich, Hamburg, Germany), supplemented with 10 % fetal bovine serum, and maintained at 37 °C in a humidified atmosphere containing 5 % CO_2. At passage 2, cells were seeded onto bilayer scaffolds submerged in culture media, with the AFL side facing upward, at a density of 70,000 cells per mL in 1 mL of medium supplemented with 1 % penicillin-streptomycin (Thermo Fisher Scientific, Pittsburgh, PA, USA). Scaffolds were cultured for either 3 or 5 days. For the stretched condition, scaffolds were initially cultured for 3 days, after which one scaffold was subjected to 10 % uniaxial elongation using the stretching device and subsequently cultured for an additional 2 days under sustained strain, resulting in a total culture duration of 5 days.

Microscopic analysis

The topographies of AFL and RFL scaffold surfaces maintained at 0 %, 10 %, and 20 % elongation were examined using field-emission SEM (Zeiss Crossbeam 550, Oberkochen, Germany). Following 3 or 5 days of culture, cell-seeded scaffolds, including those maintained under 10 % elongation, were fixed, permeabilized, and blocked according to the manufacturer's protocols (Life Science, Thermo Fisher Scientific, Waltham, MA, USA). Cellular morphology was evaluated by fluorescence staining. Cell nuclei were labelled with Hoechst 33342 (NucBlue Live ReadyProbe Reagent, Invitrogen, Waltham, MA, USA), whereas F-actin filaments were stained using Alexa Fluor 488 phalloidin (ReadyProbe Reagent, Invitrogen, Waltham, MA, USA). Fluorescence images were acquired using a LionHeart FX cellular imaging system (Agilent/BioTek, Santa Clara, CA, USA) equipped with DAPI and GFP filter cubes at 10× and 20× magnifications.

Cell and nucleus shape analysis

Cellular and nuclear morphologies were quantified from fluorescence z-stack images processed using Gen5 Image Prime software (version 3.14, BioTek Instruments, Santa Clara, CA, USA) with the Cellular Analysis module. Z-stack images were projected into two-dimensional representations, and background correction was performed using a rolling-ball algorithm to improve segmentation accuracy. Individual fluorescence channels were processed independently to generate binary masks corresponding to nuclear and cytoskeletal regions.

Morphometric parameters for each cell, including projected area, major-axis length, and minor-axis length, were extracted and used to calculate morphological descriptors. Cells exhibiting projected areas smaller than their corresponding nuclear areas were excluded from the analysis, as these cases were indicative of apoptotic or structurally compromised cells.

Cellular and nuclear morphology were characterized using four shape descriptors: roundness, eccentricity, aspect ratio, and area ratio. Roundness, $4A/(\pi l^2)$, where A is the projected area and l is the major-axis length, quantifies similarity to a perfect circle and ranges from 0 to 1, with values approaching unity indicating increasingly circular shapes. Eccentricity, $[1-(w/l)^2]^{1/2}$, where w is the minor-axis length, measures deviation from circularity, with values approaching unity indicating increasingly elongated geometries. Aspect ratio, l/w, provides a direct measure of elongation. The area ratio, A/A_n, where A_n is the nuclear area, quantifies the relative size relationship between the cell and nucleus. These descriptors were subsequently used for statistical comparisons among experimental groups.

Statistical analysis

All statistical analyses were performed in MATLAB R2023b (MathWorks, Natick, MA, USA) using data obtained from images captured at 10× magnification. The experimental dataset consisted of five independent scaffold samples for the 3-day unstretched condition and six

independent scaffold samples for the 5-day unstretched condition, each providing measurements from both AFL and RFL surfaces. Individual cells were treated as the unit of analysis. A total of 443 cells were analyzed for the 3-day unstretched condition and 866 cells for the 5-day unstretched condition. For the stretched condition, a single scaffold maintained under static strain of 10 % for 2 days following an initial 3-day culture period was analyzed, yielding measurements from 524 cells across AFL and RFL regions. Because violations of normality and/or homogeneity of variance were observed for all measured variables, statistical comparisons were performed using the nonparametric Kruskal-Wallis test followed by Dunn–Šidák post-hoc correction. Box plots were generated using MATLAB's built-in boxplot function and associated algorithms. Statistical comparisons were conducted using individual-cell measurements. Biological replication was provided by five and six independent scaffolds for the 3-day and 5-day unstretched conditions, respectively. Because only a single scaffold was available for the stretched condition, results obtained under mechanical loading should be interpreted accordingly and viewed primarily as evidence of mechanobiological trends rather than estimates of inter-sample variability.

6.3 Results

Scaffold morphology

SEM micrographs of the as-fabricated electrospun scaffolds confirmed the intended microstructural architectures prior to mechanical loading. The RFL surfaces exhibited an isotropic fiber distribution (Fig. 6.2a), whereas the AFL surfaces displayed a high degree of uniaxial fiber alignment (Fig. 6.2g). These qualitative observations were corroborated by two-dimensional FFT analysis. RFL surfaces produced multiple low-intensity peaks without a dominant orientation (Fig. 6.2b), whereas AFL surfaces exhibited a narrow, high-intensity peak centered at approximately 90° (Fig. 6.2h), indicative of strong uniaxial alignment. Distinct responses to uniaxial stretching were observed for the two scaffold architectures. At 10 % and 20 % elongation, RFL surfaces developed a pronounced alignment peak oriented along the stretch direction (Fig. 6.2d,f), consistent with the fiber reorientation evident in the corresponding SEM images (Fig. 6.2c,e). In contrast, AFL surfaces retained their original alignment at all elongation levels (Fig. 6.2i,k), and the corresponding FFT profiles remained largely unchanged (Fig. 6.2j,l). SEM imaging indicated that the fibers within the AFL primarily accommodated deformation through axial elongation along their pre-existing orientation rather than through rotational reorganization. At 20 % elongation, localized necking was observed in some AFL fibers, suggesting the onset of fiber-level deformation without disruption of the overall aligned architecture.

These findings demonstrate that uniaxial stretching up to 20 % elongation along the preferred fiber direction preserves the pre-existing fiber alignment while inducing substantial anisotropy in initially random fiber networks. The contrasting responses reflect fundamental differences in load redistribution mechanisms. In RFL scaffolds, deformation promotes fiber

rotation and recruitment toward the loading direction, whereas in AFL scaffolds the applied strain is accommodated predominantly through elongation of already aligned fibers. This mechanically induced alignment of RFL scaffolds highlights the potential for dynamically modifying scaffold anisotropy after fabrication, an attractive feature for applications in which isotropic architectures facilitate handling or implantation but aligned cellular organization is ultimately desired in situ.

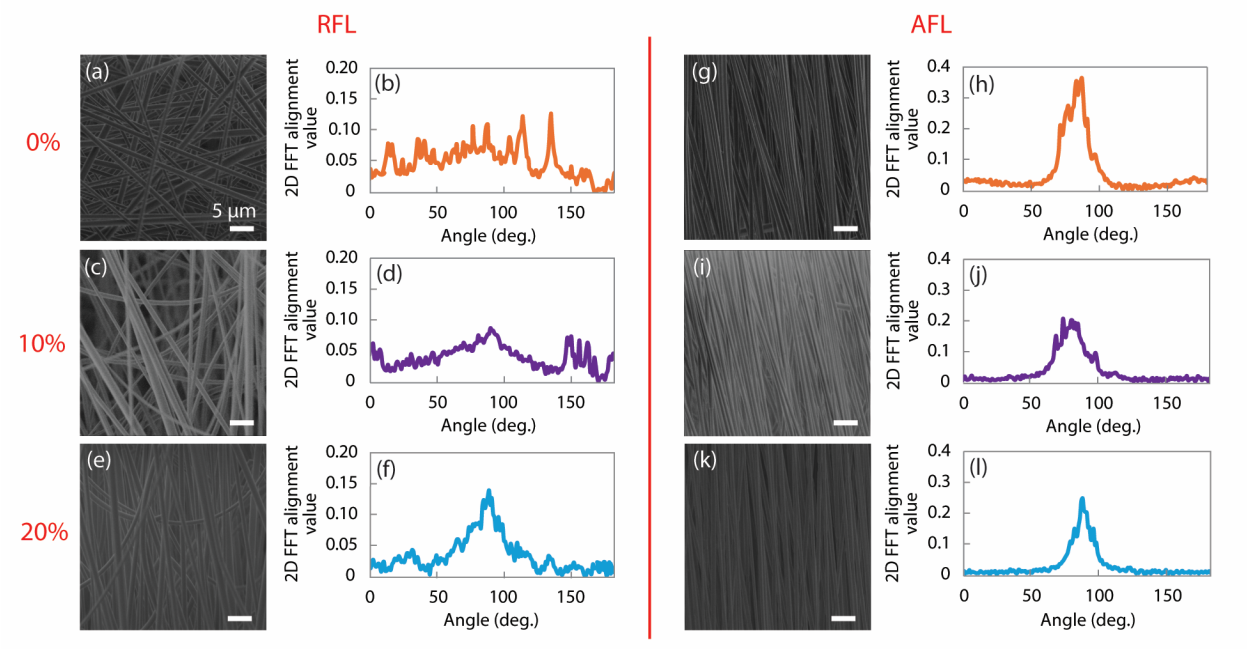

Figure 6.2: Scaffold topography and fiber alignment analysis. Representative SEM micrographs of RFL scaffold surfaces (a, c, e) and AFL scaffold surfaces (g, i, and k) together with the corresponding two-dimensional FFT-derived fiber orientation distributions for elongation (b, h) 0 %, (d, j) 10 %, and (f, l) 20 %. Uniaxial stretching was applied in the vertical direction of the SEM images. The RFL scaffolds exhibited progressive fiber realignment with increasing elongation, whereas the AFL scaffolds maintained their pre-existing alignment throughout the deformation range examined. Scale bars = 5 µm.

Nuclear morphology

To assess the influence of scaffold architecture and mechanical deformation on nuclear organization, nuclear shape descriptors were quantified for HDFa cells cultured on AFL and RFL surfaces under unstretched and stretched conditions (Fig. 6.3). For cells cultured on AFL scaffolds, no significant differences in nuclear shape descriptors were observed between days 3 and 5 under unstretched conditions. This finding is consistent with previous ob-

servations for murine fibroblasts cultured on electrospun scaffolds under static conditions (Echeverria Molina, Komvopoulos 2025). In the present study, these earlier observations were extended to adult human dermal fibroblasts cultured on mechanically deformed bilayer scaffolds, enabling direct evaluation of the combined effects of structural and mechanical cues on nuclear morphology. Application of 10 % static strain, however, produced substantial changes in nuclear morphology on AFL surfaces. Relative to unstretched day-5 controls, nuclear roundness decreased by approximately 17 %, whereas eccentricity and aspect ratio increased by approximately 9 % and 15 %, respectively. These changes were reflected in clear shifts of the corresponding descriptor distributions (Fig. 6.3). A similar response was observed on RFL surfaces. Although nuclear morphology remained unchanged between days 3 and 5 under unstretched conditions, stretched scaffolds exhibited reduced nuclear roundness (∼9 %) together with increased eccentricity (∼8 %) and aspect ratio (∼10 %) relative to unstretched day-5 controls. Corresponding distribution shifts further support these trends (Fig. 6.3). These observations suggest that nuclear morphology responds strongly to mechanical stretching, largely independent of the initial fiber organization of the scaffold.

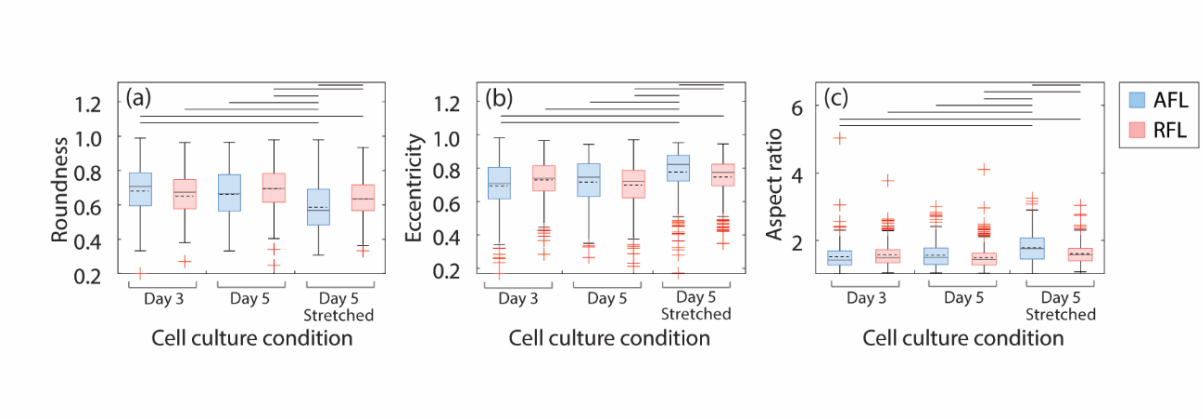

Figure 6.3: Effects of scaffold topography and 10 % uniaxial elongation on the nuclear shape descriptors of HDFa cells cultured on AFL and RFL scaffold surfaces, quantified in terms of (a) roundness, (b) eccentricity, and (c) aspect ratio. The solid and dashed horizontal lines within each box symbol denote the median and mean values, respectively. Horizontal lines above the boxplots indicate statistically significant differences ($p < 0.05$). Red "+" symbols represent outliers identified by the boxplot analysis.

The absence of significant differences in nuclear shape descriptors between AFL and RFL scaffolds under unstretched conditions suggests that scaffold architecture alone was insufficient to induce distinguishable alterations in nuclear morphology at the examined time points. This observation agrees with previous reports indicating that nuclear morphology is often less sensitive to substrate architecture in differentiated fibroblast-like cell populations than in stem cells (Nathan et al. 2011). In contrast, mechanical loading induced nuclear

elongation on both scaffold surfaces and revealed architecture-dependent differences that were not evident under static conditions (Nathan et al. 2011). Similar findings have been reported for murine fibroblasts cultured on bilayer electrospun scaffolds, where nuclear morphology exhibited temporal adaptation but limited sensitivity to scaffold architecture alone (Echeverria Molina, Komvopoulos 2025).

The foregoing results suggest that mechanical strain acts as a primary driver of nuclear deformation, while scaffold architecture modulates the magnitude and nature of the response once tensile loading is applied. The lack of differences between days 3 and 5 under unstretched conditions further suggests that fibroblasts may have largely adapted to scaffold-derived morphological cues by day 3. Similar temporal adaptation has been reported for meniscal fibrochondrocytes subjected to 10 % scaffold strain for 2 hours, where nuclear aspect ratio exhibited a decrease over time (Nathan et al. 2011). Time-dependent nuclear remodeling has also been observed in gingival keratinocytes cultured on aligned and randomly oriented fibrous substrates, although the specific trends differed between scaffold architectures – nuclei became progressively more elongated over time on scaffolds with aligned fibers, while the aspect ratio decreased on scaffolds with randomly oriented fibers at culture days 3 and 7 (Ramminger et al. 2026).

Nuclear elongation under uniaxial strain is consistent with force transmission through the cytoskeletal and linker of nucleoskeleton and cytoskeleton complexes (Janota, Calero-Cuenca, Gomes 2020), highlighting the integrated nature of cellular mechanotransduction. Collectively, these findings demonstrate that nuclear morphology is influenced by both scaffold architecture and applied mechanical strain, with loading conditions revealing architecture-dependent responses that are not apparent under static culture conditions over the timeframes examined.

Cell morphology

In contrast to the pronounced strain-induced changes observed at the nuclear level, whole-cell morphology was influenced primarily by scaffold architecture rather than mechanical loading. Quantification of cell roundness, eccentricity, and aspect ratio revealed no statistically significant differences among culture conditions (day 3 unstretched, day 5 unstretched, and day 5 stretched) for either scaffold architecture (Fig. 6.4). For cells cultured on RFL surfaces, median values of all shape descriptors varied by only approximately 0–3 % across conditions. Similarly, cells cultured on AFL surfaces exhibited only modest variations in roundness and aspect ratio ($\sim$2–12 %), while eccentricity remained nearly unchanged. The consistency of the descriptor shape distributions across all conditions suggests that 10 % static strain did not substantially alter the overall cell shape during the experimental period. This apparent decoupling between nuclear deformation and alteration of the global cell morphology has been reported in other mechanically stimulated systems and may reflect differences in the sensitivity and temporal dynamics of nuclear and cytoplasmic remodeling. Previous studies have shown that changes in cell spreading do not necessarily produce proportional changes in nuclear area and that nuclear deformation can occur independently of alterations

in overall cell morphology (Gilbert et al. 2019). It has also been reported that for some cell types, nuclear elongation can be encountered as a result of structural confinement, while in others it remains relatively constant, illustrating that nuclear morphology can be regulated independently of overall cell morphology (Doolin, Ornstein, Stroka 2019). In contrast to the limited influence of strain, scaffold architecture exerted a pronounced effect on cellular morphology. At all time points and loading conditions, cells cultured on AFL surfaces exhibited significantly lower roundness (Fig. 6.4a) and markedly higher eccentricity (Fig. 6.4b) and aspect ratio (Fig. 6.4c) than cells cultured on RFL surfaces. Moreover, the distributions of eccentricity values were narrower for AFL-cultured cells, indicating a more uniform and consistently elongated cell population. These findings reinforce the dominant role of topographical contact guidance in directing cell morphology on aligned fibrous substrates (Jenkins, Little 2019; Echeverria Molina, Malollari, Komvopoulos 2021); see Chapter 2.

Although static stretching did not produce significant quantitative changes in cell shape descriptors, fluorescence microscopy revealed notable qualitative changes in cell orientation, particularly on RFL surfaces (Fig. 6.5). On AFL surfaces, fibroblasts attached and spread preferentially along the direction of the aligned fibers after 3 days in culture (Fig. 6.5a), demonstrating the strong contact guidance imposed by the ordered fiber architecture. By day 5, cell density had stabilized and the cells retained their elongated morphology, with well-developed actin filaments predominantly aligned with the underlying fibers (Fig. 6.5c). When uniaxial stretching was applied from day 3 to day 5, cellular alignment along the loading direction appeared more pronounced (Fig. 6.5e), suggesting a cooperative effect of scaffold anisotropy and mechanical stimulation on cytoskeletal organization and directional cell growth. In contrast, fibroblasts cultured on RFL surfaces exhibited a markedly different response due to the absence of a dominant structural orientation. After 3 days in culture, cells attached and spread in multiple directions (Fig. 6.5b), reflecting the isotropic nature of the randomly oriented fiber network. By day 5 under unstretched conditions, fibroblasts had proliferated while maintaining a broad distribution of orientations (Fig. 6.5d). However, application of uniaxial stretching from day 3 to day 5 induced realignment of the initially random fiber network along the loading direction, resulting in a corresponding preferential orientation of the fibroblasts (Fig. 6.5f). This apparent cellular reorganization is consistent with the strain-induced fiber alignment observed at the scaffold level (Fig. 6.2a–f) and suggests that stretching can promote directional cellular organization even in the absence of pre-existing topographical guidance cues. Consequently, fibroblasts cultured on stretched RFL surfaces exhibited a degree of directional alignment along the stretch axis (Fig. 6.5e,f) comparable to that for cells cultured on unstretched AFL surfaces (Fig. 6.5g–j). Collectively, these observations highlight the distinct yet complementary roles of scaffold architecture and mechanical loading in regulating cellular organization. Whereas scaffold anisotropy primarily directs cell morphology and alignment through contact guidance, mechanical stretching can induce similar organizational outcomes indirectly through strain-induced fiber realignment, thereby providing an additional mechanism for controlling cellular orientation and cytoskeletal development.

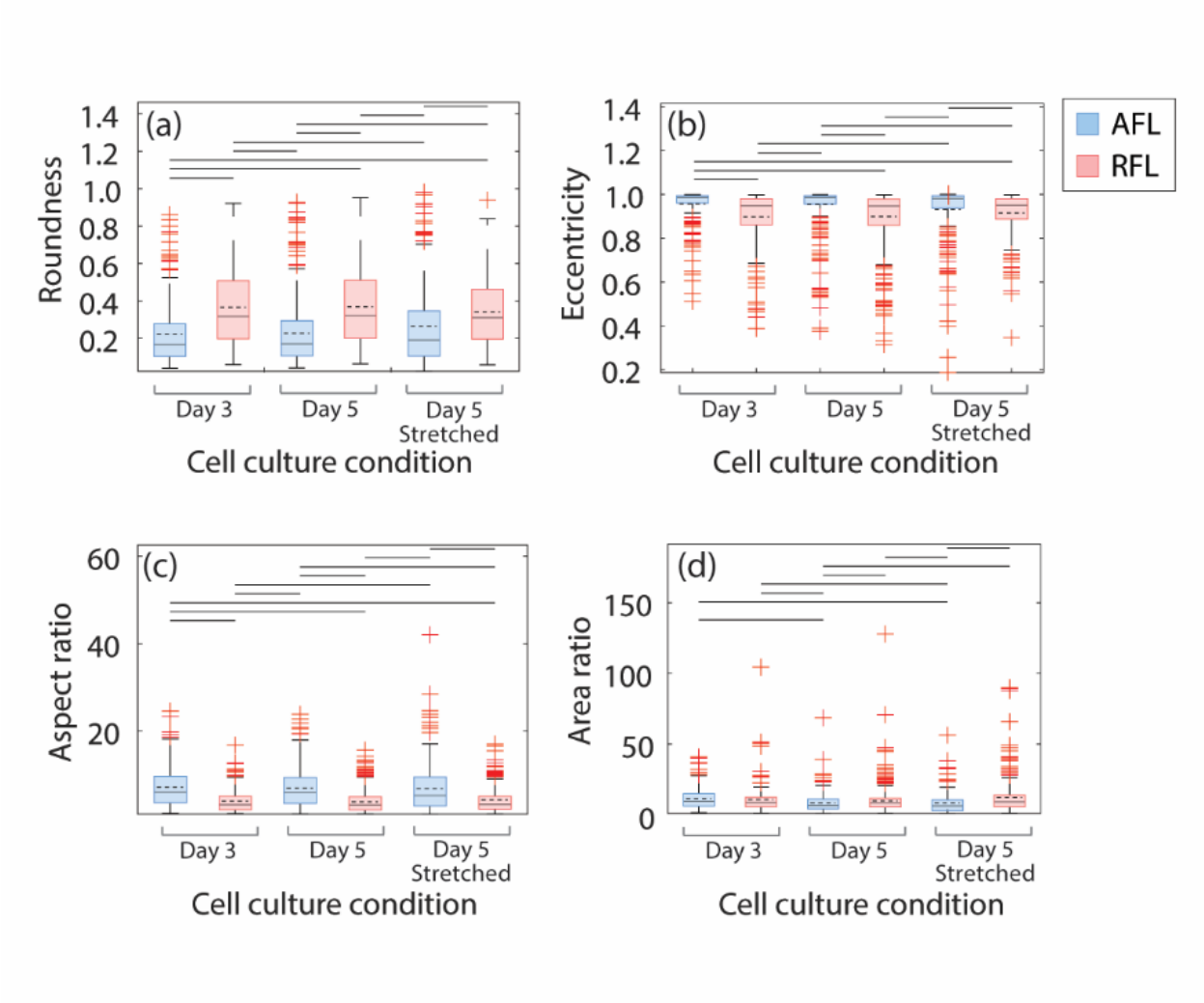

Figure 6.4: Effects of scaffold topography and 10 % uniaxial elongation on the cell shape descriptors of HDFa cells cultured on AFL and RFL scaffold surfaces, quantified in terms of (a) roundness, (b) eccentricity, (c) aspect ratio, and (d) area ratio. The solid and dashed horizontal lines within each box symbol denote the median and mean values, respectively. Horizontal lines above the boxplots indicate statistically significant differences ($p < 0.05$). Red "+" symbols represent outliers identified by the boxplot analysis.

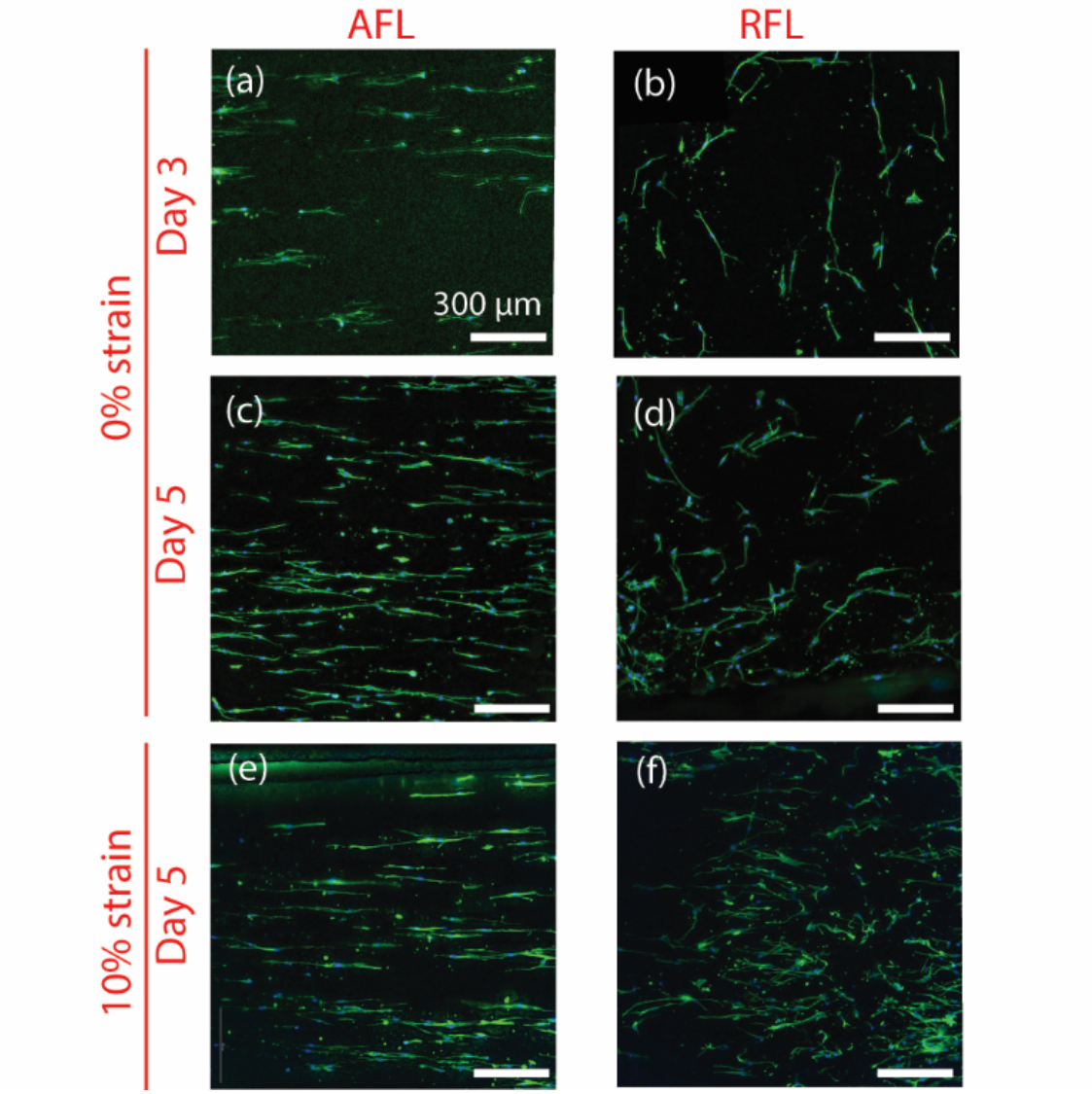

Figure 6.5: Representative fluorescence micrographs of HDFa cells stained for F-actin filaments (green; Alexa Fluor 488 phalloidin) and nuclei (blue; Hoechst 33342) cultured on AFL (left column) and RFL (right column) scaffold surfaces. Cells were cultured on unstretched scaffolds for (a, b) 3 days and (c, d) 5 days. Panels (e) and (f) show cells cultured for 3 days followed by an additional 2 days under 10 % uniaxial elongation (i.e., 5 days of total culture duration). The direction of uniaxial stretching is horizontal in the fluorescence images and corresponds to the aligned fiber direction in the AFL scaffolds. Scale bars = 300 µm.

6.4 Discussion

Cells respond to both topographical and mechanical cues through mechanotransductive processes, although these stimuli regulate cellular organization through distinct yet complementary mechanisms. As illustrated in Figure 6.6, topographical cues, such as aligned versus randomly oriented scaffold fibers, primarily influence cell behavior through contact guidance, whereby cells sense and respond to the physical features of their substrate. Following attachment to a fibrous scaffold, fibroblasts establish integrin-mediated focal adhesions that mechanically couple the ECM to the actin cytoskeleton. On AFL scaffold surfaces, these adhesion sites preferentially form along the fiber axis, directing the organization of actin stress fibers in the same orientation. Because aligned fibers impose anisotropic geometric constraints, they promote cellular extension along the fiber direction while restricting spreading in the transverse direction. Consequently, cells adopt elongated morphologies accompanied by increased nuclear elongation and reduced roundness, as illustrated in Figure 6.6. This behavior is consistent with the well-established role of aligned fibrous topographies in promoting cell elongation, migration, and tissue-specific organization in fibrous scaffold systems (Feng et al. 2026).

Cells continuously probe their surroundings through filopodia and lamellipodia, which preferentially extend and stabilize along continuous topographic features. As these protrusions establish new adhesion sites, cytoskeleton tension is redistributed along the fiber axis, reinforcing cell elongation and orientation. In contrast, RFL scaffold surfaces provide isotropic topographical cues that permit cell attachment and spreading in multiple directions. Consequently, focal adhesion formation, cytoskeletal organization, and cell orientation are more heterogeneous, resulting in broader distributions of cell morphology characterized by greater spreading, higher roundness, and lower elongation of the cells.

Mechanical stretching influences cell behavior through a fundamentally different mechanism. Rather than providing geometric guidance, it introduces externally imposed tensile forces that are transmitted to adherent cells through focal adhesions and the cytoskeletal network (Sun, Guo, Fässler 2016). This loading increases intracellular tension and activates mechanotransduction pathways that promote actin polymerization and stress-fiber assembly along the direction of maximum tensile stress. Because static stretching generates a persistent anisotropic force field, cells reorganize their focal adhesions and cytoskeletal architecture to achieve efficient force distribution and maintain equilibrium, ultimately favoring alignment parallel to the stretching direction (Giverso et al. 2023). Importantly, this response differs from the strain-avoidance behavior commonly observed under cyclic loading. Fibroblasts and other adherent cell types subjected to cyclic strain often reorient perpendicular or oblique to the stretch axis as a mechanism for minimizing repetitive deformation (Giverso et al. 2023; Huang et al. 2013). In contrast, static and quasistatic loading generally promote alignment parallel to the applied strain (Giverso et al. 2023; Tondon, Kaunas 2014; Rens, Merks 2017). Because a 10 % static strain sustained over a 2-day period was used in the present study, strain avoidance is not expected to occur. Rather, the applied loading appears to provide a dominant directional cue, particularly when structural guidance is initially weak. For

example, fibroblasts cultured on stretched RFL scaffolds exhibited a narrower eccentricity distribution together with preferential orientation along the stretch direction, suggesting cytoskeletal and focal-adhesion reorganization in response to sustained tensile loading.

When topographical and mechanical cues co-exist, the cellular response reflects their sequential and mutually reinforcing stimuli effects. On AFL scaffolds, where topographical contact guidance already promotes cellular elongation and cytoskeletal organization, static stretching reinforces the existing preferential orientation, consistent with the observed enhancement of cellular alignment. In contrast, the cellular response on RFL scaffolds involves an additional intermediate step. The initially isotropic fiber network undergoes passive realignment under tensile loading, rapidly generating an anisotropic topography aligned with the loading direction. Cells subsequently experience both sustained tensile stress and a newly organized substrate architecture. Because these cues are collinear, contact guidance arising from fiber realignment reinforces the mechanical stimulus, resulting in progressive cellular organization along the stretch axis during the loading period.

A notable finding of this study is that nuclear morphology appeared to be more sensitive to tensile loading (stretching) than whole-cell morphology. Whereas cell shape was primarily governed by scaffold architecture, nuclear morphology exhibited measurable changes following stretching on both scaffold surfaces. This differential response suggests a hierarchical regulation of cellular organization, wherein nuclear deformation serves as a sensitive indicator of externally applied mechanical forces, while overall cell morphology remains constrained by substrate-derived contact-guidance cues. The apparent decoupling between nuclear and cellular responses under static uniaxial strain may reflect either cellular adaptation to sustained mechanical loading or differences in the temporal scales of cytoplasmic and nuclear remodeling. Although nuclear shape exhibited an architecture-modulated response under applied strain, global cell morphology remained comparatively stable over the 2-day loading period. One possible explanation is that transient cytoplasmic remodeling occurred shortly after the onset of loading and subsequently stabilized, rendering these changes undetectable at the later observation time point. Future studies incorporating shorter observation intervals may therefore provide additional insight into the early stages of cell adaptation to sustained mechanical stimulation.

The greater sensitivity of nuclear morphology to tensile loading may also reflect the increasingly recognized role of the nucleus as an active mechanosensory organelle rather than a passive structural component. Through physical coupling of the cytoskeleton to the nuclear envelope via the linker of nucleoskeleton and cytoskeleton complex, externally applied forces can be transmitted directly to the nucleus, altering nuclear shape, chromatin organization, and potentially gene regulatory activity. Although gene expression was not examined in the present study, the observed strain-induced nuclear elongation suggests that mechanical loading may influence downstream transcriptional processes associated with matrix synthesis and tissue remodeling. Future studies combining morphological analyses with mechanosensitive gene expression profiling would help establish direct links between nuclear deformation and functional cellular responses.

Beyond mechanistic considerations, the present findings have direct implications for scaf-

fold design. Mechanical loading appears capable of promoting directional cellular organization across structurally heterogeneous scaffolds, effectively reducing differences arising from local architectural variations. In this context, randomly oriented fiber regions provide an initially isotropic environment, whereas externally applied strain induces both directional cellular organization and structural remodeling through fiber reorientation. Although the present study used adult human dermal fibroblasts, similar strain-responsive alignment behaviors have been reported for other mesenchymal cell populations in constrained environments (Walters et al. 2017; Kurpinski et al. 2006), suggesting that this response may represent a broadly conserved mechanobiological phenomenon rather than a fibroblast-specific effect.

An important observation is that mechanical stretching not only influenced cell organization directly but also altered the scaffold microenvironment itself through fiber realignment. This dual action highlights a dynamic feedback mechanism between scaffold mechanics and cellular behavior. Unlike conventional scaffold systems in which architecture is considered fixed after fabrication, the present results demonstrate that scaffold anisotropy can evolve during mechanical stimulation. Consequently, the structural cues experienced by cells may change over time as a function of loading history, providing opportunities to design adaptive biomaterial systems whose topographical characteristics evolve in concert with tissue maturation.

The results also highlight certain methodological considerations. Conventional shape descriptors effectively quantify global cellular morphology but may not fully capture changes in cell orientation, cytoskeletal organization, or collective cellular behavior. Although significant differences in cellular alignment were evident qualitatively in fluorescence micrographs, particularly following stretching of RFL scaffolds, these changes were not fully reflected by the selected morphometric descriptors. Future studies could therefore incorporate quantitative orientation analyses, angular dispersion measurements, cytoskeletal anisotropy indices, and automated image-based alignment metrics to provide a more comprehensive assessment of mechanically induced cellular organization. Such approaches may be particularly valuable for distinguishing subtle mechanobiological responses that are not reflected in traditional morphometric parameters. From a translational perspective, the conceptual framework summarized in Figure 6.6 suggests strategies for designing multifunctional scaffolds that integrate both isotropic and anisotropic regions while implementing physiological loading to achieve coordinated cellular organization. Recent advances in tendon-bone interface engineering have emphasized multiphasic and gradient scaffold architectures, which better replicate native transitions between soft and hard tissues than discrete layered constructs as a key strategy for spatially coordinated tissue regeneration (Feng et al. 2026). The bilayer electrospun scaffold investigated in this study, consisting of a layer with aligned fibers that transitions gradually to a layer with randomly oriented fibers, follows this design philosophy. The present findings further suggest that mechanical loading can extend directional cellular organization across structurally distinct scaffold zones, potentially enhancing tissue integration and functional maturation. Such strategies are directly relevant to the engineering of load-bearing fibrous tissues, including tendons, ligaments, and graded tissue interfaces where

region-specific architecture and mechanobiological regulation are both required.

Several limitations should be considered when interpreting the present findings. First, the mechanically stretched condition was evaluated using a single scaffold specimen, limiting assessment of biological and inter-sample variability under loading. Consequently, the stretched-condition results should be interpreted primarily as evidence of mechanobiological trends rather than definitive estimates of population-level behavior. Second, only one strain magnitude (10 %) and one loading duration (2 days) were investigated. Different strain magnitudes, durations, and dynamic loading regimens may produce distinct cellular and nuclear responses. Third, the study focused primarily on morphological outcomes and did not evaluate gene expression, ECM production, focal adhesion maturation, or long-term tissue remodeling. Therefore, although the observed structural responses provide important mechanistic insights, additional studies are required to establish how these morphological adaptations influence functional tissue regeneration outcomes.

Overall, the results indicate that scaffold microarchitecture and externally applied mechanical strain act as independent yet interacting regulators of cellular organization in fibrous tissue systems. Scaffold fiber architecture establishes baseline patterns of cellular morphology and orientation through contact guidance, whereas mechanical loading provides an additional organizational stimulus that modifies both scaffold structure and cellular behavior. Notably, initially isotropic fiber networks can acquire anisotropic organization under tensile loading, suggesting that mechanical stimulation alone may generate aligned structural and cellular patterns even in the absence of pre-aligned fiber architectures. More broadly, these findings provide design principles for mechanically active biomaterial systems in which scaffold architecture, cellular organization, and the mechanical environment are co-engineered to promote functional tissue regeneration. Importantly, the present findings suggest that scaffold architecture should not necessarily be viewed as a static design variable. Rather, scaffold microstructure, mechanical loading, and cellular organization may evolve together as an integrated mechanobiological system. Designing scaffolds whose structural anisotropy can be actively modulated through physiological loading may therefore represent a powerful strategy for achieving spatiotemporal control of tissue formation and maturation. This framework aligns closely with the emerging structure–signal–function paradigm proposed for next-generation scaffold designs (Feng et al. 2026; Lv et al. 2024).

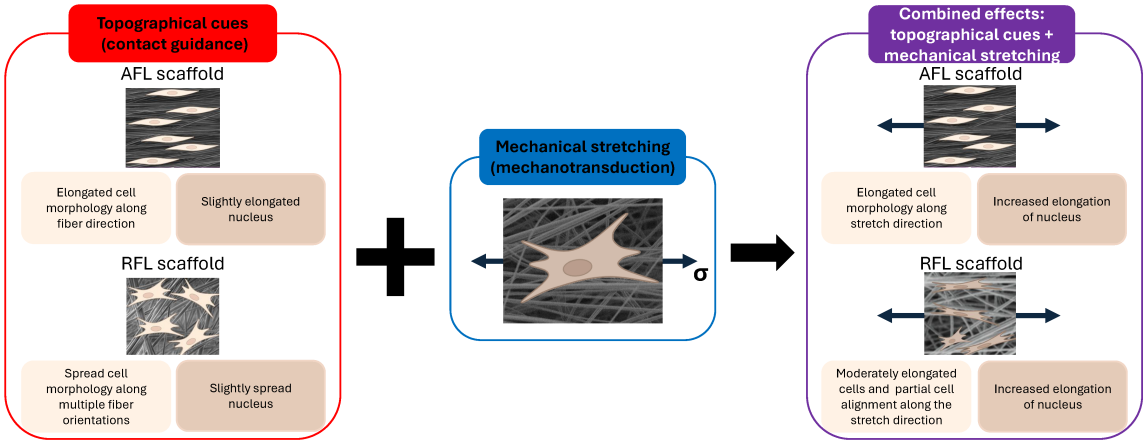

Figure 6.6: Schematic illustration of the influence of scaffold topography and mechanical stretching on cellular and nuclear morphology. The left panel depicts the effect of topographical cues (contact guidance), whereby AFL scaffolds promote elongated cell and nuclear morphologies, whereas RFL scaffolds support more spread cellular morphologies and nuclei with greater roundness after 5 days of culture. The right panel illustrates the combined effects of topographical cues and mechanical stimulation (mechanotransduction). Application of uniaxial tensile strain induces directional organization even on initially random fiber networks, resulting in modestly increased cellular and nuclear elongation along the stretch direction. This combined action of aligned fiber topography and mechanical loading produces the most pronounced response, characterized by highly elongated and aligned cells and nuclei exhibiting the highest aspect ratio and lowest roundness among all experimental conditions.

6.5 Conclusions

In conclusion, this study investigated the coupled effects of scaffold fiber architecture and static uniaxial stretching on scaffold organization and the morphology of adult human dermal fibroblasts cultured on bilayer electrospun PLLA scaffolds. Mechanical stretching induced substantial realignment of initially random fiber networks while preserving the alignment of pre-oriented fibers. Cellular morphology was governed predominantly by scaffold topography, with aligned fibers promoting elongated cell shapes and randomly oriented fibers supporting more isotropic morphologies. In contrast, nuclear morphology exhibited greater sensitivity to externally applied strain, demonstrating significant elongation under sustained tensile loading regardless of the initial scaffold architecture. Fluorescence imaging further revealed that stretching promoted directional cellular organization, particularly on initially random fiber

surfaces through strain-induced fiber reorientation. These findings demonstrate that scaffold architecture and mechanical loading regulate cellular organization through distinct yet complementary mechanisms operating across multiple length scales. More broadly, the results establish design principles for mechanically active fibrous scaffolds in which structural anisotropy can be generated or enhanced through applied loading, providing a promising strategy for engineering tendons, ligaments, and complex tissue interfaces requiring coordinated spatial organization and mechanical functionality.

Chapter 7

Conclusions and Future Directions

7.1 Conclusions

The engineering of fibrous connective tissues requires scaffolds that reproduce the chemical environment of their native extracellular matrix, its structural organization, and mechanical behavior. This dissertation followed a bilayer electrospun PLLA scaffold across its full development cycle. The work spanned computational modeling of the fabrication process, physicochemical and degradation characterization, and the morphological response of fibroblasts under topographical, temporal, and mechanical cues. The polymer was used unmodified, without biochemical additives or surface functionalization, so that the effect of these cues could be isolated from any confounding chemical signal. The principal findings are summarized below. First, an electrostatic finite element analysis established how the parallel-plate collector geometry produces the bilayer architecture. Simulations revealed that the directionality of the electric field controls fiber alignment between the plates, and that the progressive decrease in field intensity and loss of directionality, in conjunction with the increasing polymer thickness, leads to the deposition of randomly oriented fibers. The depositing polymer itself was shown to produce a local electric effect, altering the field intensity in its vicinity and driving an asymptotic approach toward the air-dielectric condition. Next, the degradation behavior of the bilayer scaffold was characterized in phosphate-buffered saline over an extended period. The results showed that degradation occurred hydrolytically through an interplay between chain scission and chain reorganization, producing a decrease in molecular weight together with increases in crystallinity, ultimate tensile strength, and glass transition temperature, while yield strength, melting temperature, and surface morphology showed marginal to no change, and fiber diameter showed relatively limited changes overall. Conversely, stiffness decreased substantially. A reduction in stiffness over this period is favorable for tissue engineering, supporting cell attachment and migration while the scaffold transfers load to the developing tissue, although it may equally influence proliferation and differentiation as degradation advances. Importantly, the relatively limited changes in fiber diameter and surface morphology establish that the architectural cues presented to cells remained

stable over timescales relevant to in vitro culture. The influence of scaffold topography and culture duration on fibroblast morphology was then quantified using shape descriptors. Fiber alignment proved to be a strong determinant of cell shape, with cells on aligned fibers adopting elongated, oriented morphologies while those on randomly oriented fibers spread in a branched, multidirectional manner. Culture duration emerged as a second governing factor, with cells on both surfaces converging toward rounder, stabilized morphologies by day 6. This time-dependent adaptation indicates that culture duration must be treated as a design parameter rather than as an incidental experimental variable. Finally, the combined effects of scaffold architecture and applied mechanical loading were examined. Static uniaxial stretching realigned initially random fibers along the loading direction while preserving the orientation of pre-aligned regions. At the cellular level, nuclear morphology exhibited little dependence on scaffold architecture under unstretched conditions but responded markedly to applied strain, whereas cell morphology was governed primarily by fiber alignment and showed limited sensitivity to sustained loading. Fluorescence imaging further revealed that stretching promoted directional cellular organization on initially isotropic surfaces, mediated by strain-induced fiber reorientation instead of strain avoidance. Taken together, scaffold architecture, culture duration, and applied strain each contribute to that organization. As argued in Chapter 2, no universal design criteria exist across tissue types, and these properties must be considered together rather than in isolation. A further implication is that scaffold architecture is a parameter that may change over time. Applied strain reorganizes the fiber network, and the reorganized network then guides the cells, so the structural cues a cell experiences evolve with loading history. This points toward adaptive biomaterial systems whose topography develops alongside tissue maturation. Several limitations of the present work, discussed in the individual chapters, motivate the future directions outlined below.

7.2 Future Directions

The findings and limitations of this dissertation suggest several directions for further work.

- **Temporal response.** Culture duration and loading duration both shaped the responses reported here, but these were not varied independently under loading. Chapter 5 established that fibroblast morphology continues to adapt over the culture period, converging toward stabilized shapes by day 6, while Chapter 6 applied a single 2-day loading window following an initial 3-day culture period. The decoupling observed between nuclear and cellular responses may therefore reflect differences in the temporal scales of nuclear and cytoplasmic remodeling, where transient cytoplasmic reorganization may have occurred shortly after the onset of loading and stabilized before the observation time point. Shorter observation intervals during the early stages of loading would test this directly. Varying the pre-loading culture period and the loading duration (i.e., culture for 1, 3, or 5 days then apply strain for 2 days; culture for 3

days then apply strain for 1, 2, or 3 days) would further establish whether the timing of load application relative to the cells' adaptation to the scaffold affects the response.

- **Functional readouts.** Connecting morphology to tissue function requires measures beyond cell shape. Extracellular matrix deposition and organization, mechanotransduction and focal adhesion markers, and mechanosensitive gene expression profiling would establish whether the morphological responses observed here translate into transcriptional and matrix-synthetic outcomes that determine functional tissue regeneration.
- **Quantitative orientation analysis.** Shape descriptors capture global morphology but do not fully resolve cellular alignment. Orientation histograms, angular dispersion measurements, cytoskeletal anisotropy indices, and automated alignment metrics would allow the qualitative orientation changes observed under stretching to be quantified, and would be particularly valuable for detecting responses not reflected in conventional morphometric parameters.

Bibliography

Abagnale, G., Steger, M., Nguyen, V. H., Hersch, N., Sechi, A., Joussen, S., Denecke, B., Merkel, R., Hoffmann, B., Dreser, A., Schnakenberg, U., Gillner, A., Wagner, W., 2015. "Surface topography enhances differentiation of mesenchymal stem cells towards osteogenic and adipogenic lineages". *Biomaterials* 61, 316–326.

Abarzúa-Illanes, P. N., Padilla, C., Ramos, A., Isaacs, M., Ramos-Grez, J., Olguín, H. C., Valenzuela, L. M., 2017. "Improving myoblast differentiation on electrospun poly(ϵ-caprolactone) scaffolds." *Journal of Biomedical Materials Research Part A* 105(8), 2241–2251.

Abbasian, S., Shafaei, N., Daraeinejad, Z., Rajabi, M., Shabani, I., 2025. "Investigating the effect of alignment on electrospun nanofiber properties and regulating cellular behaviors". *Polymer Reviews* 66(1), 109–158.

Allen, L. T., Tosetto, M., Miller, I. S., O'Connor, D. P., Penney, S. C., Lynch, I., Keenan, A. K., Pennington, S. R., Dawson, K. A., Gallagher, W. M., 2006. "Surface-induced changes in protein adsorption and implications for cellular phenotypic responses to surface interaction". *Biomaterials* 27(16), 3096–3108.

Anderson, J. M., Jiang, S., 2017. "Implications of the acute and chronic inflammatory response and the foreign body reaction to the immune response of implanted biomaterials". In: *The Immune Response to Implanted Materials and Devices: The Impact of the Immune System on the Success of an Implant*. Ed. by Corradetti, B. Cham: Springer International Publishing, 15–36.

Anderson, J. M., Rodriguez, A., Chang, D. T., 2008. "Foreign body reaction to biomaterials". *Seminars in Immunology* 20(2), 86–100.

Andorko, J. I., Jewell, C. M., 2017. "Designing biomaterials with immunomodulatory properties for tissue engineering and regenerative medicine". *Bioengineering & Translational Medicine* 2(2), 139–155.

Annor, A. H., Tang, M. E., Pui, C. L., Ebersole, G. C., Frisella, M. M., Matthews, B. D., Deeken, C. R., 2012. "Effect of enzymatic degradation on the mechanical properties of biological scaffold materials". *Surgical Endoscopy* 26(10), 2767–2778.

Auger, F. A., Gibot, L., Lacroix, D., 2013. "The pivotal role of vascularization in tissue engineering". *Annual Review of Biomedical Engineering* 15, 177–200.

Ayres, C. E., Jha, B. S., Meredith, H., Bowman, J. R., Bowlin, G. L., Henderson, S. C., Simpson, D. G., 2008. "Measuring fiber alignment in electrospun scaffolds: A user's guide

to the 2D fast Fourier transform approach". *Journal of Biomaterials Science, Polymer Edition* 19(5), 603–621.

Azagarsamy, M. A., Anseth, K. S., 2013. "Bioorthogonal click chemistry: an indispensable tool to create multifaceted cell culture scaffolds". *ACS Macro Letters* 2(1), 5–9.

Badami, A. S., Kreke, M. R., Thompson, M. S., Riffle, J. S., Goldstein, A. S., 2006. "Effect of fiber diameter on spreading, proliferation, and differentiation of osteoblastic cells on electrospun poly (lactic acid) substrates". *Biomaterials* 27(4), 596–606.

Baji, A., Mai, Y.-W., Wong, S.-C., Abtahi, M., Chen, P., 2010. "Electrospinning of polymer nanofibers: Effects on oriented morphology, structures and tensile properties". *Composites Science and Technology* 70, 703–718.

Baker, B. M., Nerurkar, N. L., Burdick, J. A., Elliott, D. M., Mauck, R. L., 2009. "Fabrication and modeling of dynamic multipolymer nanofibrous scaffolds". *Journal of Biomechanical Engineering* 131(10), 101012.

Baker, B. M., Trappmann, B., Wang, W. Y., Sakar, M. S., Kim, I. L., Shenoy, V. B., Burdick, J. A., Chen, C. S., 2015. "Cell-mediated fibre recruitment drives extracellular matrix mechanosensing in engineered fibrillar microenvironments". *Nature Materials* 14(12), 1262–1268.

Baldwin, M. J., Mimpen, J. Y., Cribbs, A. P., Stace, E., Philpott, M., Dakin, S. G., Carr, A. J., Snelling, S. J., 2022. "Electrospun Scaffold Micro-Architecture Induces an Activated Transcriptional Phenotype within Tendon Fibroblasts". *Frontiers in Bioengineering and Biotechnology* 9, 795748.

Balguid, A., Mol, A., Van Marion, M. H., Bank, R. A., Bouten, C. V., Baaijens, F. P., 2009. "Tailoring fiber diameter in electrospun poly(ϵ-Caprolactone) scaffolds for optimal cellular infiltration in cardiovascular tissue engineering". *Tissue Engineering Part A* 15(2), 437–444.

Bashur, C. A., Shaffer, R. D., Dahlgren, L. A., Guelcher, S. A., Goldstein, A. S., 2009. "Effect of fiber diameter and alignment of electrospun polyurethane meshes on mesenchymal progenitor cells." *Tissue Engineering Part A* 15(9), 2435–2445.

Bean, A. C., Tuan, R. S., 2015. "Fiber diameter and seeding density influence chondrogenic differentiation of mesenchymal stem cells seeded on electrospun poly(ϵ-caprolactone) scaffolds". *Biomedical Materials (Bristol)* 10(1).

Bi, L., Cao, Z., Hu, Y., Song, Y., Yu, L., Yang, B., Mu, J., Huang, Z., Han, Y., 2011. "Effects of different cross-linking conditions on the properties of genipin-cross-linked chitosan/collagen scaffolds for cartilage tissue engineering". *Journal of Materials Science: Materials in Medicine* 22(1), 51–62.

Binder, C., Milleret, V., Hall, H., Eberli, D., Lühmann, T., 2013. "Influence of micro and submicro poly(lactic-glycolic acid) fibers on sensory neural cell locomotion and neurite growth". *Journal of Biomedical Materials Research Part B: Applied Biomaterials* 101(7), 1200–1208.

Bittner, S. M., Guo, J. L., Melchiorri, A., Mikos, A. G., 2018. "Three-dimensional printing of multilayered tissue engineering scaffolds". *Materials Today* 21(8), 861–874.

Bolbasov, E. N., Maryin, P. V., Stankevich, K. S., Kozelskaya, A. I., Shesterikov, E. V., Khodyrevskaya, Y. I., Nasonova, M. V., Shishkova, D. K., Kudryavtseva, Y. A., Anissimov, Y. G., Tverdokhlebov, S. I., 2018. "Surface modification of electrospun poly-(l-lactic) acid scaffolds by reactive magnetron sputtering". *Colloids and Surfaces B: Biointerfaces* 162, 43–51.

Bramson, M. T. K., Van Houten, S. K., Corr, D. T., 2021. "Mechanobiology in tendon, ligament, and skeletal muscle tissue engineering". *Journal of Biomechanical Engineering* 143(7), 070801.

Brannigan, R. P., Dove, A. P., 2017. "Synthesis, properties and biomedical applications of hydrolytically degradable materials based on aliphatic polyesters and polycarbonates". *Biomaterials Science* 5(1), 9–21.

Brown, B. N., Londono, R., Tottey, S., Zhang, L., Kukla, K. A., Wolf, M. T., Daly, K. A., Reing, J. E., Badylak, S. F., 2012. "Macrophage phenotype as a predictor of constructive remodeling following the implantation of biologically derived surgical mesh materials". *Acta Biomaterialia* 8(3), 978–987.

Cai, Y., Li, J., Poh, C. K., Tan, H. C., San Thian, E., Fuh, J. Y. H., Sun, J., Tay, B. Y., Wang, W., 2013. "Collagen grafted 3D polycaprolactone scaffolds for enhanced cartilage regeneration". *Journal of Materials Chemistry B* 1(43), 5971–5976.

Cajori, F. A., Crouter, C. Y., Pemberton, R., 1924. "The alleged role of lactic acid in arthritis and rheumatoid conditions". *Archives of Internal Medicine* 34(4), 566–572.

Cavalcanti-Adam, E. A., Volberg, T., Micoulet, A., Kessler, H., Geiger, B., Spatz, J. P., 2007. "Cell spreading and focal adhesion dynamics are regulated by spacing of integrin ligands". *Biophysical Journal* 92(8), 2964–2974.

Chen, C.-H., Chen, S.-H., Kuo, C.-Y., Li, M.-L., Chen, J.-P., 2017a. "Response of dermal fibroblasts to biochemical and physical cues in aligned polycaprolactone/silk fibroin nanofiber scaffolds for application in tendon tissue engineering". *Nanomaterials* 7(8), 219.

Chen, H., Cheng, R., Zhao, X., Zhang, Y., Tam, A., Yan, Y., Shen, H., Zhang, Y. S., Qi, J., Feng, Y., Liu, L., Pan, G., Cui, W., Deng, L., 2019. "An injectable self-healing coordinative hydrogel with antibacterial and angiogenic properties for diabetic skin wound repair". *NPG Asia Materials* 11(1), 3.

Chen, H., Huang, X., Zhang, M., Damanik, F., Baker, M. B., Leferink, A., Yuan, H., Truckenmüller, R., Blitterswijk, C. van, Moroni, L., 2017b. "Tailoring surface nanoroughness of electrospun scaffolds for skeletal tissue engineering". *Acta Biomaterialia* 59, 82–93.

Chen, R., Pye, J. S., Li, J., Little, C. B., Li, J. J., 2023. "Multiphasic scaffolds for the repair of osteochondral defects: Outcomes of preclinical studies". *Bioactive Materials* 27, 505–545.

Chen, S., Sun, L., Zhou, X., Guo, Y., Song, J., Qian, S., Liu, Z., Guan, Q., Meade Jeffries, E., Liu, W., Wang, Y., He, C., You, Z., 2020. "Mechanically and biologically skin-like elastomers for bio-integrated electronics". *Nature Communications* 11(1), 1107.

Cheng, L., Cai, Z., Ye, T., Yu, X., Chen, Z., Yan, Y., Qi, J., Wang, L., Liu, Z., Cui, W., Deng, L., 2020. "Injectable polypeptide-protein hydrogels for promoting infected wound healing". *Advanced Functional Materials* 30(25), 2001196.

Cheng, Q., Komvopoulos, K., 2010. "Integration of plasma-assisted surface chemical modification, soft lithography, and protein surface activation for single-cell patterning". *Applied Physics Letters* 97(4), 043705.

Cheng, Q., Komvopoulos, K., Li, S., 2014. "Plasma-assisted heparin conjugation on electrospun poly(l-lactide) fibrous scaffolds". *Journal of Biomedical Materials Research Part A* 102(5), 1408–1414.

Cheng, Q., Lee, B. L.-P., Komvopoulos, K., Li, S., 2013a. "Engineering the microstructure of electrospun fibrous scaffolds by microtopography". *Biomacromolecules* 14(5), 1349–1360.

Cheng, Q., Lee, B. L.-P., Komvopoulos, K., Yan, Z., Li, S., 2013b. "Plasma surface chemical treatment of electrospun poly(l-lactide) microfibrous scaffolds for enhanced cell adhesion, growth, and infiltration". *Tissue Engineering Part A* 19(9-10), 1188–1198.

Cheng, Q., Li, S., Komvopoulos, K., 2009. "Plasma-assisted surface chemical patterning for single-cell culture". *Biomaterials* 30(25), 4203–4210.

Cheng, W., Zeng, X., Chen, H., Li, Z., Zeng, W., Mei, L., Zhao, Y., 2019. "Versatile polydopamine platforms: synthesis and promising applications for surface modification and advanced nanomedicine". *ACS Nano* 13(8), 8537–8565.

Chew, S. Y., Mi, R., Hoke, A., Leong, K. W., 2008. "The effect of the alignment of electrospun fibrous scaffolds on Schwann cell maturation". *Biomaterials* 29(6), 653–661.

Chi, J., Wang, M., Chen, J., Hu, L., Chen, Z., Backman, L. J., Zhang, W., 2022. "Topographic orientation of scaffolds for tissue regeneration: Recent advances in biomaterial design and applications". *Biomimetics* 7(3), 131.

Christopherson, G. T., Song, H., Mao, H.-Q., 2009. "The influence of fiber diameter of electrospun substrates on neural stem cell differentiation and proliferation". *Biomaterials* 30(4), 556–564.

Cole, L., Kramer, P. R., 2016. "Chapter 3.4 - Brain and nervous system". In: *Human Physiology, Biochemistry and Basic Medicine*. Ed. by Cole, L., Kramer, P. R. Boston: Academic Press, 93–99.

Cooke, S. L., Whittington, A. R., 2016. "Influence of therapeutic radiation on polycaprolactone and polyurethane biomaterials". *Materials Science and Engineering: C* 60, 78–83.

Costa, P. F., Vaquette, C., Zhang, Q., Reis, R. L., Ivanovski, S., Hutmacher, D. W., 2014. "Advanced tissue engineering scaffold design for regeneration of the complex hierarchical periodontal structure". *Journal of Clinical Periodontology* 41(3), 283–294.

Costantini, M., Barbetta, A., 2018. "Gas foaming technologies for 3D scaffold engineering". In: *Functional 3D Tissue Engineering Scaffolds*. Ed. by Deng, Y., Kuiper, J. Woodhead Publishing. Chap. 6, 127–149.

Crescenzi, V., Cornelio, L., Di Meo, C., Nardecchia, S., Lamanna, R., 2007. "Novel hydrogels via click chemistry: synthesis and potential biomedical applications". *Biomacromolecules* 8(6), 1844–1850.

Cui, W., Li, X., Zhou, S., Weng, J., 2008. "Degradation patterns and surface wettability of electrospun fibrous mats". *Polymer Degradation and Stability* 93(3), 731–738.

Cui, W., Li, X., Zhu, X., Yu, G., Zhou, S., Weng, J., 2006. "Investigation of drug release and matrix degradation of electrospun poly(dl-lactide) fibers with paracetanol inoculation". *Biomacromolecules* 7(5), 1623–1629.

D'Urso, M., Kurniawan, N. A., 2020. "Mechanical and physical regulation of fibroblast–myofibroblast transition: From cellular mechanoresponse to tissue pathology". *Frontiers in Bioengineering and Biotechnology* 8, 609653.

Dado, D., Levenberg, S., 2009. "Cell–scaffold mechanical interplay within engineered tissue". *Seminars in Cell & Developmental Biology* 20(6), 656–664.

Daniele, M. A., Adams, A. A., Naciri, J., North, S. H., Ligler, F. S., 2014. "Interpenetrating networks based on gelatin methacrylamide and PEG formed using concurrent thiol click chemistries for hydrogel tissue engineering scaffolds". *Biomaterials* 35(6), 1845–1856.

Daud, M. F. B., Pawar, K. C., Claeyssens, F., Ryan, A. J., Haycock, J. W., 2012. "An aligned 3D neuronal-glial co-culture model for peripheral nerve studies". *Biomaterials* 33(25), 5901–5913.

DeForest, C. A., Anseth, K. S., 2011. "Cytocompatible click-based hydrogels with dynamically tunable properties through orthogonal photoconjugation and photocleavage reactions". *Nature Chemistry* 3(12), 925.

DeForest, C. A., Anseth, K. S., 2012. "Photoreversible patterning of biomolecules within click-based hydrogels". *Angewandte Chemie International Edition* 51(8), 1816–1819.

DeForest, C. A., Polizzotti, B. D., Anseth, K. S., 2009. "Sequential click reactions for synthesizing and patterning three-dimensional cell microenvironments". *Nature Materials* 8(8), 659–664.

DeForest, C. A., Tirrell, D. A., 2015. "A photoreversible protein-patterning approach for guiding stem cell fate in three-dimensional gels". *Nature Materials* 14(5), 523–531.

Dellacherie, M. O., Seo, B. R., Mooney, D. J., 2019. "Macroscale biomaterials strategies for local immunomodulation". *Nature Reviews Materials* 4(6), 379–397.

Devkota, A. C., Weinhold, P. S., 2003. "Mechanical response of tendon subsequent to ramp loading to varying strain limits". *Clinical Biomechanics* 18(10), 969–974.

Di Luca, A., Longoni, A., Criscenti, G., Mota, C., Van Blitterswijk, C., Moroni, L., 2016a. "Toward mimicking the bone structure: Design of novel hierarchical scaffolds with a tailored radial porosity gradient". *Biofabrication* 8(4), 045007.

Di Luca, A., Lorenzo-Moldero, I., Mota, C., Lepedda, A., Auhl, D., Van Blitterswijk, C., Moroni, L., 2016b. "Tuning Cell Differentiation into a 3D Scaffold Presenting a Pore Shape Gradient for Osteochondral Regeneration". *Advanced Healthcare Materials* 5(14), 1753–1763.

Di Luca, A., Ostrowska, B., Lorenzo-Moldero, I., Lepedda, A., Swieszkowski, W., Van Blitterswijk, C., Moroni, L., 2016c. "Gradients in pore size enhance the osteogenic differentiation of human mesenchymal stromal cells in three-dimensional scaffolds." *Scientific Reports* 6, 22898.

Di Luca, A., Szlazak, K., Lorenzo-Moldero, I., Ghebes, C. A., Lepedda, A., Swieszkowski, W., Van Blitterswijk, C., Moroni, L., 2016d. "Influencing chondrogenic differentiation of

human mesenchymal stromal cells in scaffolds displaying a structural gradient in pore size." *Acta Biomaterialia* 36, 210–219.

Do, A. V., Khorsand, B., Geary, S. M., Salem, A. K., 2015. "3D printing of scaffolds for tissue regeneration applications". *Advanced Healthcare Materials* 4(12), 1742–1762.

Doolin, M. T., Ornstein, T. S., Stroka, K. M., 2019. "Nuclear deformation in response to mechanical confinement is cell type dependent". *Cells* 8(5), 427.

Doyle, A. D., Carvajal, N., Jin, A., Matsumoto, K., Yamada, K. M., 2015. "Local 3D matrix microenvironment regulates cell migration through spatiotemporal dynamics of contractility-dependent adhesions". *Nature Communications* 6, 8720.

Drury, J. L., Mooney, D. J., 2003. "Hydrogels for tissue engineering: Scaffold design variables and applications". *Biomaterials* 24(24), 4337–4351.

Dutta, R. C., Dey, M., Dutta, A. K., Basu, B., 2017. "Competent processing techniques for scaffolds in tissue engineering". *Biotechnology Advances* 35(2), 240–250.

Dvir, T., Timko, B. P., Kohane, D. S., Langer, R., 2011. "Nanotechnological strategies for engineering complex tissues". *Nature Nanotechnology* 6(1), 13.

Dziki, J. L., Badylak, S. F., 2018. "Immunomodulatory biomaterials". *Current Opinion in Biomedical Engineering* 6, 51–57.

Dziki, J. L., Wang, D. S., Pineda, C., Sicari, B. M., Rausch, T., Badylak, S. F., 2017. "Solubilized extracellular matrix bioscaffolds derived from diverse source tissues differentially influence macrophage phenotype". *Journal of Biomedical Materials Research Part A* 105(1), 138–147.

Echeverria Molina, M. I., Komvopoulos, K., 2023. "In vitro degradation of fibrous bilayer poly-L-lactic acid scaffolds". *Journal of Biomechanics* 161, 111823.

Echeverria Molina, M. I., Komvopoulos, K., 2025. "Influence of scaffold topography and culture duration on fibroblast morphology in tissue engineering". *Tissue Engineering Part A* 31(23-24), 1319–1326.

Echeverria Molina, M. I., Komvopoulos, K., 2026. "Scaffold fiber architecture and uniaxial stretch differentially regulate cell and nuclear morphology in human dermal fibroblasts". *Tissue Engineering Part A*.

Echeverria Molina, M. I., Malollari, K. G., Komvopoulos, K., 2021. "Design challenges in polymeric scaffolds for tissue engineering". *Frontiers in Bioengineering and Biotechnology* 9, 617141.

Echeverria Molina, M. I., Komvopoulos, K., 2022. "An electrostatic finite element analysis of the electrospinning process of bilayer constructs using a parallel-plate collector". *Materials Letters* 313, 131649.

Elkasaby, M., Hegab, H. A., Mohany, A., Rizvi, G. M., 2018. "Modeling and optimization of electrospinning of polyvinyl alcohol (PVA)". *Advances in Polymer Technology* 37(6), 2114–2122.

Entekhabi, E., Haghbin Nazarpak, M., Moztarzadeh, F., Sadeghi, A., 2016. "Design and manufacture of neural tissue engineering scaffolds using hyaluronic acid and polycaprolactone nanofibers with controlled porosity". *Materials Science and Engineering: C* 69, 380–387.

Erisken, C., Zhang, X., Moffat, K. L., Levine, W. N., Lu, H. H., 2013. "Scaffold fiber diameter regulates human tendon fibroblast growth and differentiation". *Tissue Engineering Part A* 19(3-4), 519–528.

Espinoza-Álvarez, M. L., Rojas-Rojas, L., Morales-Sánchez, J., Guillén-Girón, T., 2024. "Impact of uniaxial static strain on myoblast differentiation in collagen-coated PCL microfilament scaffolds: Role of onset time of mechanical stimulation". *Bioengineering* 11(9), 919.

Estabridis, H. M., Jana, A., Nain, A., Odde, D. J., 2018. "Cell Migration in 1D and 2D Nanofiber Microenvironments". *Annals of Biomedical Engineering* 46(3), 392–403.

Faia-Torres, A. B., Charnley, M., Goren, T., Guimond-Lischer, S., Rottmar, M., Maniura-Weber, K., Spencer, N. D., Reis, R. L., Textor, M., Neves, N. M., 2015. "Osteogenic differentiation of human mesenchymal stem cells in the absence of osteogenic supplements: A surface-roughness gradient study". *Acta Biomaterialia* 28, 64–75.

Fan, Y., Xiu, K., Duan, H., Zhang, M., 2008. "Biomechanical and histological evaluation of the application of biodegradable poly-L-lactic cushion to the plate internal fixation for bone fracture healing". *Clinical Biomechanics* 23 Suppl 1, S7–S16.

Feng, H., Yu, X., Zhang, G., Yuan, Z., Al-Enizi, A. M., Qin, C. X., EL-Newehy, M., Mo, X., 2026. "Advanced engineering strategies for biomaterial scaffolds application in tendon–bone interface regeneration". *Burns & Trauma* 14, tkaf078.

Ferrari, P. F., Aliakbarian, B., Lagazzo, A., Tamayol, A., Palombo, D., Perego, P., 2017. "Tailored electrospun small-diameter graft for vascular prosthesis". *International Journal of Polymeric Materials and Polymeric Biomaterials* 66(12), 635–643.

Ferreira, C. L., Valente, C. A., Zanini, M. L., Sgarioni, B., Ferreira Tondo, P. H., Chagastelles, P. C., Braga, J., Campos, M. M., Malmonge, J. A., Souza Basso, N. R. de, 2019. "Biocompatible PCL/PLGA/Polypyrrole composites for regenerating nerves". *Macromolecular Symposia* 383(1), 1800028.

Fischer, E. W., Sterzel, H. J., Wegner, G., 1973. "Investigation of the structure of solution grown crystals of lactide copolymers by means of chemical reactions". *Kolloid-Zeitschrift und Zeitschrift für Polymere* 251(11), 980–990.

Folkman, J., Hochberg, M., 1973. "Self-regulation of growth in three dimensions". *The Journal of Experimental Medicine* 138(4), 745–753.

Frank, C. B., 2004. "Ligament structure, physiology and function". *Journal of Musculoskeletal & Neuronal Interactions* 4(2), 199–201.

Fu, W., Liu, Z., Feng, B., Hu, R., He, X., Wang, H., Yin, M., Huang, H., Zhang, H., Wang, W., 2014. "Electrospun gelatin/PCL and collagen/PLCL scaffolds for vascular tissue engineering". *International Journal of Nanomedicine* 9, 2335–2344.

Galli, M., Yao, Y., Giannobile, W. V., Wang, H. L., 2021. "Current and future trends in periodontal tissue engineering and bone regeneration". *Plastic and Aesthetic Research* 8, 3.

Gao, X., Han, S., Zhang, R., Liu, G., Wu, J., 2019. "Progress in electrospun composite nanofibers: Composition, performance and applications for tissue engineering". *Journal of Materials Chemistry B* 7(45), 7075–7089.

Garg, K., Pullen, N. A., Oskeritzian, C. A., Ryan, J. J., Bowlin, G. L., 2013. "Macrophage functional polarization (M1/M2) in response to varying fiber and pore dimensions of electrospun scaffolds". *Biomaterials* 34(18), 4439–4451.

Ge, Z., Tian, X., Heng, B. C., Fan, V., Yeo, J. F., Cao, T., 2009. "Histological evaluation of osteogenesis of 3D-printed poly-lactic-co-glycolic acid (PLGA) scaffolds in a rabbit model." *Biomedical Materials (Bristol, England)* 4(2), 21001.

Ghanian, M. H., Farzaneh, Z., Barzin, J., Zandi, M., Kazemi-Ashtiani, M., Alikhani, M., Ehsani, M., Baharvand, H., 2015. "Nanotopographical control of human embryonic stem cell differentiation into definitive endoderm". *Journal of Biomedical Materials Research Part A* 103(11), 3539–3553.

Gilbert, H. T. J., Mallikarjun, V., Dobre, O., Jackson, M. R., Pedley, R., Gilmore, A. P., Richardson, S. M., Swift, J., 2019. "Nuclear decoupling is part of a rapid protein-level cellular response to high-intensity mechanical loading". *Nature Communications* 10(1), 4149.

Girard, F., Lajoye, C., Camman, M., Tissot, N., Berthelot Pedurand, F., Tandon, B., Moedder, D., Liashenko, I., Salameh, S., Dalton, P. D., Rielland, M., 2024. "First advanced bilayer scaffolds for tailored skin tissue engineering produced via electrospinning and melt electrowriting". *Advanced Functional Materials* 34(27), 2314757.

Giverso, C., Loy, N., Lucci, G., Preziosi, L., 2023. "Cell orientation under stretch: A review of experimental findings and mathematical modelling". *Journal of Theoretical Biology* 572, 111564.

Gonçalves de Pinho, A. R., Odila, I., Leferink, A., Blitterswijk, C. van, Camarero-Espinosa, S., Moroni, L., 2019. "Hybrid polyester-hydrogel electrospun scaffolds for tissue engineering applications". *Frontiers in Bioengineering and Biotechnology* 7, 1–13.

Gopinathan, J., Noh, I., 2018. "Click chemistry-based injectable hydrogels and bioprinting inks for tissue engineering applications". *Tissue Engineering and Regenerative Medicine* 15(5), 531–546.

Govindaraju, D. T., Chen, C. H., Shalumon, K. T., Kao, H. H., Chen, J. P., 2023. "Bioactive nanostructured scaffold-based approach for tendon and ligament tissue engineering". *Nanomaterials* 13(12), 1847.

Grand View Research, 2020. *Tissue engineering market size, share & trends analysis report by application (Cord blood & cell banking, cancer, GI & gynecology, dental, orthopedics, musculoskeletal, & spine), by region, and segment forecasts, 2020 - 2027*. Tech. rep. Grand View Research.

Greener, B., Hughes, A. A., Bannister, N. P., Douglass, J., 2005. "Proteases and pH in chronic wounds." *Journal of Wound Care* 14(2), 59–61.

Greenwood, J. E., Wagstaff, M. J. D., 2016. "The use of biodegradable polyurethane in the development of dermal scaffolds". In: *Advances in Polyurethane Biomaterials*. Ed. by Cooper, S. L., Guan, J. Woodhead Publishing. Chap. 22, 631–662.

Guo, Y., Song, Y., Xiong, S., Wang, T., Liu, W., Yu, Z., Ma, X., 2022. "Mechanical stretch induced skin regeneration: Molecular and cellular mechanism in skin soft tissue expansion". *International Journal of Molecular Sciences* 23(17), 9622.

Gurtner, G. C., Werner, S., Barrandon, Y., Longaker, M. T., 2008. "Wound repair and regeneration". *Nature* 453, 314–321.

Guvendiren, M., Burdick, J. A., 2012. "Stiffening hydrogels to probe short-and long-term cellular responses to dynamic mechanics". *Nature Communications* 3(1), 1–9.

Guvendiren, M., Perepelyuk, M., Wells, R. G., Burdick, J. A., 2014. "Hydrogels with differential and patterned mechanics to study stiffness-mediated myofibroblastic differentiation of hepatic stellate cells". *Journal of the Mechanical Behavior of Biomedical Materials* 38, 198–208.

Hafeman, A. E., Zienkiewicz, K. J., Zachman, A. L., Sung, H.-J., Nanney, L. B., Davidson, J. M., Guelcher, S. A., 2011. "Characterization of the degradation mechanisms of lysine-derived aliphatic poly(ester urethane) scaffolds". *Biomaterials* 32(2), 419–429.

Hafen, B. B., Shook, M., Burns, B., 2023. *Anatomy, smooth muscle*. Treasure Island, FL: StatPearls Publishing.

Haftbaradaran Esfahani, P., Knöll, R., 2020. "Cell shape: Effects on gene expression and signaling". *Biophysical Reviews* 12(4), 895–901.

Han, F., Dong, Y., Su, Z., Yin, R., Song, A., Li, S., 2014. "Preparation, characteristics and assessment of a novel gelatin-chitosan sponge scaffold as skin tissue engineering material". *International Journal of Pharmaceutics* 476(1), 124–133.

Han, Y., Jia, B., Lian, M., Sun, B., Wu, Q., Sun, B., Qiao, Z., Dai, K., 2021. "High-precision, gelatin-based, hybrid, bilayer scaffolds using melt electro-writing to repair cartilage injury". *Bioactive Materials* 6(7), 2173–2186.

He, J., Fang, B., Shan, S., Xie, Y., Wang, C., Zhang, Y., Zhang, X., Li, Q., 2021. "Mechanical stretch promotes hypertrophic scar formation through mechanically activated cation channel Piezo1". *Cell Death & Disease* 12(3), 226.

He, L., Liao, S., Quan, D., Ma, K., Chan, C., Ramakrishna, S., Lu, J., 2010. "Synergistic effects of electrospun PLLA fiber dimension and pattern on neonatal mouse cerebellum C17. 2 stem cells". *Acta Biomaterialia* 6(8), 2960–2969.

Holloway, J. L., Ma, H., Rai, R., Burdick, J. A., 2014. "Modulating hydrogel crosslink density and degradation to control bone morphogenetic protein delivery and in vivo bone formation". *Journal of Controlled Release* 191, 63–70.

Hong, J., Yeo, M., Yang, G. H., Kim, G., 2019. "Cell-electrospinning and its application for tissue engineering". *International Journal of Molecular Sciences* 20(24).

Hong, S., Yang, K., Kang, B., Lee, C., Song, I. T., Byun, E., Park, K. I., Cho, S.-W., Lee, H., 2013. "Hyaluronic acid catechol: a biopolymer exhibiting a pH-dependent adhesive or cohesive property for human neural stem cell engineering". *Advanced Functional Materials* 23(14), 1774–1780.

Hoyle, C. E., Lowe, A. B., Bowman, C. N., 2010. "Thiol-click chemistry: a multifaceted toolbox for small molecule and polymer synthesis". *Chemical Society Reviews* 39(4), 1355–1387.

Hsia, H. C., Nair, M. R., Mintz, R. C., Corbett, S. A., 2011. "The fiber diameter of synthetic bioresorbable extracellular matrix influences human fibroblast morphology and fibronectin matrix assembly." *Plastic and Reconstructive Surgery* 127(6), 2312–2320.

Hsieh, F.-Y., Tao, L., Wei, Y., Hsu, S.-h., 2017. "A novel biodegradable self-healing hydrogel to induce blood capillary formation". *NPG Asia Materials* 9(3), e363.

Huaga, H. S., Choub, S. H., Don, T. M., Lai, W. C., Cheng, L. P., 2009. "Formation of microporous poly(hydroxybutyric acid) membranes for culture of osteoblast and fibroblast". *Polymers for Advanced Technologies* 20(12), 1082–1090.

Huang, C., Miyazaki, K., Akaishi, S., Watanabe, A., Hyakusoku, H., Ogawa, R., 2013. "Biological effects of cellular stretch on human dermal fibroblasts". *Journal of Plastic, Reconstructive and Aesthetic Surgery* 66(12), e351–e361.

Huber, E., Mirzaee, M., Bjorgaard, J., Hoyack, M., Noghanian, S., Chang, I., 2016. "Dielectric property measurement of PLA". *2016 IEEE International Conference on Electro Information Technology (EIT)*, 788–792.

Idaszek, J., Zinn, M., Obarzanek-Fojt, M., Zell, V., Swieszkowski, W., Bruinink, A., 2013. "Tailored degradation of biocompatible poly(3-hydroxybutyrate-co-3- hydroxyvalerate)/calcium silicate/poly(lactide-co-glycolide) ternary composites: An in vitro study". *Materials Science and Engineering: C* 33(7), 4352–4360.

Israni, A. K., Zaun, D., Hadley, N., Rosendale, J. D., Schaffhausen, C., McKinney, W., Snyder, J. J., Kasiske, B. L., 2020. "OPTN/SRTR 2018 Annual data report: Deceased organ donation". *American Journal of Transplantation* 20, 509–541.

Iwasaki, A., Medzhitov, R., 2010. "Regulation of adaptive immunity by the innate immune system". *Science* 327(5963), 291–295.

Janmey, P. A., Miller, R. T., 2011. "Mechanisms of mechanical signaling in development and disease". *Journal of Cell Science* 124(1), 9–18.

Janota, C. S., Calero-Cuenca, F. J., Gomes, E. R., 2020. "The role of the cell nucleus in mechanotransduction". *Current Opinion in Cell Biology* 63, 204–211.

Jaslove, J. M., Nelson, C. M., 2018. "Smooth muscle: A stiff sculptor of epithelial shapes". *Philosophical Transactions of the Royal Society B: Biological Sciences* 373(1759), 20170318.

Jenkins, T. L., Little, D., 2019. "Synthetic scaffolds for musculoskeletal tissue engineering: Cellular responses to fiber parameters". *npj Regenerative Medicine* 4(1), 15.

Jiang, M., Qiu, J., Zhang, L., Lü, D., Long, M., Chen, L., Luo, X., 2016. "Changes in tension regulates proliferation and migration of fibroblasts by remodeling expression of ECM proteins". *Experimental and Therapeutic Medicine* 12(3), 1542–1550.

Jiang, Y., Chen, J., Deng, C., Suuronen, E. J., Zhong, Z., 2014. "Click hydrogels, microgels and nanogels: emerging platforms for drug delivery and tissue engineering". *Biomaterials* 35(18), 4969–4985.

Jones, E. M., Cochrane, C. A., Percival, S. L., 2015. "The effect of pH on the extracellular matrix and biofilms". *Advances in Wound Care* 4(7), 431–439.

Juncosa-Melvin, N., Matlin, K. S., Holdcraft, R. W., Nirmalanandhan, V. S., Butler, D. L., 2007. "Mechanical stimulation increases collagen type I and collagen type III gene expression of stem cell-collagen sponge constructs for patellar tendon repair." *Tissue Engineering* 13(6), 1219–1226.

Kaiser, K., Bendixen, S. M., Sørensen, J. A., Brewer, J. R., 2024. "From static to dynamic: The influence of mechanotransduction on skin equivalents analyzed by bioimaging and RNAseq". *Materials Today Bio* 25, 101010.

Kalia, J., Raines, R. T., 2008. "Hydrolytic stability of hydrazones and oximes". *Angewandte Chemie International Edition* 47(39), 7523–7526.

Kang, T., Moore, E. C., Kopania, E. E. K., King, C. D., Schilling, B., Campisi, J., Good, J. M., Brem, R. B., 2023. "A natural variation-based screen in mouse cells reveals USF2 as a regulator of the DNA damage response and cellular senescence." *G3 (Bethesda, Md.)* 13(7), jkad091.

Karpov, T. E., Peltek, O. O., Muslimov, A. R., Tarakanchikova, Y. V., Grunina, T. M., Poponova, M. S., Karyagina, A. S., Chernozem, R. V., Pariy, I. O., Mukhortova, Y. R., Zhukov, M. V., Surmeneva, M. A., Zyuzin, M. V., Timin, A. S., Surmenev, R. A., 2020. "Development of optimized strategies for growth factor incorporation onto electrospun fibrous scaffolds To promote prolonged release". *ACS Applied Materials & Interfaces* 12(5), 5578–5592.

Keirouz, A., Chung, M., Kwon, J., Fortunato, G., Radacsi, N., 2020. "2D and 3D electrospinning technologies for the fabrication of nanofibrous scaffolds for skin tissue engineering: A review". *WIREs Nanomedicine and Nanobiotechnology* 12(4), e1626.

Kennedy, K. M., Bhaw-Luximon, A., Jhurry, D., 2017. "Cell-matrix mechanical interaction in electrospun polymeric scaffolds for tissue engineering: Implications for scaffold design and performance". *Acta Biomaterialia* 50, 41–55.

Khetan, S., Guvendiren, M., Legant, W. R., Cohen, D. M., Chen, C. S., Burdick, J. A., 2013. "Degradation-mediated cellular traction directs stem cell fate in covalently crosslinked three-dimensional hydrogels". *Nature Materials* 12(5), 458–465.

Kianpour, G., Bagheri, R., Pourjavadi, A., Ghanbari, H., 2020. "In situ synthesized TiO2-polyurethane nanocomposite for bypass graft application: In vitro endothelialization and degradation". *Materials Science and Engineering: C* 114, 111043.

Kievit, F. M., Cooper, A., Jana, S., Leung, M. C., Wang, K., Edmondson, D., Wood, D., Lee, J. S. H., Ellenbogen, R. G., Zhang, M., 2013. "Aligned chitosan-polycaprolactone polyblend nanofibers promote the migration of glioblastoma cells". *Advanced Healthcare Materials* 2(12), 1651–1659.

Kim, J.-H., Kang, M. S., Eltohamy, M., Kim, T.-H., Kim, H.-W., 2016. "Dynamic mechanical and nanofibrous topological combinatory cues designed for periodontal ligament engineering". *PLOS ONE* 11(3), e0149967.

Kishan, A. P., Nezarati, R. M., Radzicki, C. M., Renfro, A. L., Robinson, J. L., Whitely, M. E., Cosgriff-Hernandez, E. M., 2015. "In situ crosslinking of electrospun gelatin for improved fiber morphology retention and tunable degradation". *Journal of Materials Chemistry B* 3(40), 7930–7938.

Klapperich, C., Pruitt, L., Komvopoulos, K., 2001. "Chemical and biological characteristics of low-temperature plasma treated ultra-high molecular weight polyethylene for biomedical applications". *Journal of Materials Science: Materials in Medicine* 12(6), 549–556.

Kolb, H. C., Finn, M. G., Sharpless, K. B., 2001. "Click chemistry: diverse chemical function from a few good reactions". *Angewandte Chemie International Edition* 40(11), 2004–2021.

Korcari, A., Buckley, M. R., Loiselle, A. E., 2022. "Characterization of scar tissue biomechanics during adult murine flexor tendon healing". *Journal of the Mechanical Behavior of Biomedical Materials* 130, 105192.

Ku, S. H., Park, C. B., 2010. "Human endothelial cell growth on mussel-inspired nanofiber scaffold for vascular tissue engineering". *Biomaterials* 31(36), 9431–9437.

Kuppan, P., Sethuraman, S., Krishnan, U. M., 2015. "Interaction of human smooth muscle cells with nanofibrous scaffolds: Effect of fiber orientation on cell adhesion, proliferation, and functional gene expression". *Journal of Biomedical Materials Research Part A* 103(7), 2236–2250.

Kurn, H., Daly, D. T., 2023. *Histology, epithelial cell.* Treasure Island, FL: StatPearls Publishing.

Kurosaki, T., Kometani, K., Ise, W., 2015. "Memory B cells". *Nature Reviews Immunology* 15(3), 149–159.

Kurpinski, K., Chu, J., Hashi, C., Li, S., 2006. "Anisotropic mechanosensing by mesenchymal stem cells". *Proceedings of the National Academy of Sciences* 103(44), 16095–16100.

Lam, C. X. F., Hutmacher, D. W., Schantz, J.-T., Woodruff, M. A., Teoh, S. H., 2009. "Evaluation of polycaprolactone scaffold degradation for 6 months in vitro and in vivo". *Journal of Biomedical Materials Research Part A* 90A(3), 906–919.

Lancuški, A., Bossard, F., Fort, S., 2013. "Carbohydrate-decorated PCL fibers for specific protein adhesion". *Biomacromolecules* 14(6), 1877–1884.

Lancuški, A., Fort, S., Bossard, F., 2012. "Electrospun azido-PCL nanofibers for enhanced surface functionalization by click chemistry". *ACS Applied Materials & Interfaces* 4(12), 6499–6504.

Lanza, R., Langer, R., Vacanti, J. P., Atala, A., 2020. *Principles of tissue engineering.* Academic Press.

Laughlin, S. T., Baskin, J. M., Amacher, S. L., Bertozzi, C. R., 2008. "In vivo imaging of membrane-associated glycans in developing zebrafish". *Science* 320(5876), 664–667.

Lee, C. H., Shin, H. J., Cho, I. H., Kang, Y.-M., Kim, I. A., Park, K.-D., Shin, J.-W., 2005. "Nanofiber alignment and direction of mechanical strain affect the ECM production of human ACL fibroblast". *Biomaterials* 26(11), 1261–1270.

Lee, H., Dellatore, S. M., Miller, W. M., Messersmith, P. B., 2007. "Mussel-inspired surface chemistry for multifunctional coatings". *Science* 318(5849), 426–430.

Lee, N. M., Erisken, C., Iskratsch, T., Sheetz, M., Levine, W. N., Lu, H. H., 2017. "Polymer fiber-based models of connective tissue repair and healing". *Biomaterials* 112, 303–312.

Lee, Y. B., Shin, Y. M., Lee, J.-h., Jun, I., Kang, J. K., Park, J.-C., Shin, H., 2012. "Polydopamine-mediated immobilization of multiple bioactive molecules for the development of functional vascular graft materials". *Biomaterials* 33(33), 8343–8352.

Leijten, J., Seo, J., Yue, K., Trujillo-de Santiago, G., Tamayol, A., Ruiz-Esparza, G. U., Shin, S. R., Sharifi, R., Noshadi, I., Álvarez, M. M., 2017. "Spatially and temporally controlled

hydrogels for tissue engineering". *Materials Science and Engineering: R: Reports* 119, 1–35.

Leong, N. L., Kator, J. L., Clemens, T. L., James, A., Enamoto-Iwamoto, M., Jiang, J., 2020. "Tendon and Ligament Healing and Current Approaches to Tendon and Ligament Regeneration." *Journal of Orthopaedic Research* 38(1), 7–12.

Li, B., Wang, J. H.-C., 2011. "Fibroblasts and myofibroblasts in wound healing: Force generation and measurement". *Journal of Tissue Viability* 20(4), 108–120.

Li, J., Wang, T., Kirtane, A. R., Shi, Y., Jones, A., Moussa, Z., Lopes, A., Collins, J., Tamang, S. M., Hess, K., Shakur, R., Karandikar, P., Lee, J. S., Huang, H.-W., Hayward, A., Traverso, G., 2020. "Gastrointestinal synthetic epithelial linings". *Science Translational Medicine* 12(558), eabc0441.

Li, K., Ling, H., Huang, W., Luo, W., Gu, C., Tao, B., Xie, Q., Qiu, P., 2024. "Single-cell RNA-sequencing analysis reveals α-syn induced astrocyte-neuron crosstalk-mediated neurotoxicity". *International Immunopharmacology* 139, 112676.

Li, X., Sun, S., Wang, X., Dong, W., 2023. "Polyester polymer scaffold-based therapeutics for osteochondral repair". *Journal of Drug Delivery Science and Technology* 90, 105116.

Liang, R., Gu, Y., Wu, Y., Bunpetch, V., Zhang, S., 2021. "Lithography-based 3D bioprinting and bioinks for bone repair and regeneration". *ACS Biomaterials Science & Engineering* 7(3), 806–816.

Lim, S. H., Liu, X. Y., Song, H., Yarema, K. J., Mao, H.-Q., 2010. "The effect of nanofiber-guided cell alignment on the preferential differentiation of neural stem cells". *Biomaterials* 31(34), 9031–9039.

Lim, W. L., Liau, L. L., Ng, M. H., Chowdhury, S. R., Law, J. X., 2019. "Current progress in tendon and ligament tissue engineering". *Tissue Engineering and Regenerative Medicine* 16(6), 549–571.

Lins, L. C., Wianny, F., Livi, S., Dehay, C., Duchet-Rumeau, J., Gérard, J.-F., 2017. "Effect of polyvinylidene fluoride electrospun fiber orientation on neural stem cell differentiation". *Journal of Biomedical Materials Research Part B: Applied Biomaterials* 105(8), 2376–2393.

Liu, H., Wang, S., Qi, N., 2012. "Controllable structure, properties, and degradation of the electrospun PLGA/PLA-blended nanofibrous scaffolds". *Journal of Applied Polymer Science* 125(S2), E468–E476.

Liu, S., Qin, S., He, M., Zhou, D., Qin, Q., Wang, H., 2020. "Current applications of poly(lactic acid) composites in tissue engineering and drug delivery". *Composites Part B: Engineering* 199, 108238.

Lokmic, Z., Mitchell, G. M., 2008. "Engineering the microcirculation". *Tissue Engineering Part B: Reviews* 14(1), 87–103.

Lowe, A. B., 2010. "Thiol-ene "click" reactions and recent applications in polymer and materials synthesis". *Polymer Chemistry* 1(1), 17–36.

Lowery, J. L., Datta, N., Rutledge, G. C., 2010. "Effect of fiber diameter, pore size and seeding method on growth of human dermal fibroblasts in electrospun poly(ε-caprolactone) fibrous mats". *Biomaterials* 31(3), 491–504.

Lu, L., Peter, S. J., Lyman, M. D., Lai, H.-L., Leite, S. M., Tamada, J. A., Vacanti, J. P., Langer, R., Mikos, A. G., 2000. "In vitro degradation of porous poly(l-lactic acid) foams". *Biomaterials* 21(15), 1595–1605.

Lv, Z., Ji, Y., Wen, G., Liang, X., Zhang, K., Zhang, W., 2024. "Structure-optimized and microenvironment-inspired nanocomposite biomaterials in bone tissue engineering". *Burns & Trauma* 12, tkae036.

Ma, C. H., Zhang, H. B., Yang, S. M., Yin, R. X., Yao, X. J., Zhang, W. J., 2018. "Comparison of the degradation behavior of PLGA scaffolds in micro-channel, shaking, and static conditions". *Biomicrofluidics* 12(3), 1–11.

Ma, Y., Liu, Z., Miao, L., Jiang, X., Ruan, H., Xuan, R., Xu, S., 2023. "Mechanisms underlying pathological scarring by fibroblasts during wound healing." *International Wound Journal* 20(6), 2190–2206.

Ma, Z., He, W., Yong, T., Ramakrishna, S., 2005. "Grafting of gelatin on electrospun poly (caprolactone) nanofibers to improve endothelial cell spreading and proliferation and to control cell orientation". *Tissue Engineering* 11(7-8), 1149–1158.

Mabry, K. M., Lawrence, R. L., Anseth, K. S., 2015. "Dynamic stiffening of poly (ethylene glycol)-based hydrogels to direct valvular interstitial cell phenotype in a three-dimensional environment". *Biomaterials* 49, 47–56.

Madhurakkat Perikamana, S. K., Lee, J., Lee, Y. B., Shin, Y. M., Lee, E. J., Mikos, A. G., Shin, H., 2015. "Materials from mussel-inspired chemistry for cell and tissue engineering applications". *Biomacromolecules* 16(9), 2541–2555.

Malollari, K. G., Delparastan, P., Sobek, C., Vachhani, S. J., Fink, T. D., Zha, R. H., Messersmith, P. B., 2019. "Mechanical enhancement of bioinspired polydopamine nanocoatings". *ACS Applied Materials & Interfaces* 11(46), 43599–43607.

Mandal, B. B., Kundu, S. C., 2009. "Cell proliferation and migration in silk fibroin 3D scaffolds". *Biomaterials* 30(15), 2956–2965.

Martyts, A., Sachs, D., Stracuzzi, A., Kromer, D., Al-Nuaimi, D., Pramotton, F. M., Robmann, S., Kourouklis, A., Hopf, R., Ehret, A. E., Tibbitt, M. W., Werner, S., Giampietro, C., Mazza, E., 2026. "Quantification of stretch-induced stimuli altering the mechanome of dermal fibroblasts". *Journal of Investigative Dermatology* 146(1), 116–129.e15.

Marumo, K., Sato, Y., Suzuki, H., Kurosaka, D., 2006. "MRI study of bioabsorbable poly-l-lactic acid devices used for fixation of fracture and osteotomies". *Journal of Orthopaedic Science* 11(2), 154–158.

McWhorter, F. Y., Wang, T., Nguyen, P., Chung, T., Liu, W. F., 2013. "Modulation of macrophage phenotype by cell shape". *Proceedings of the National Academy of Sciences* 110(43), 17253–17258.

Medzhitov, R., 2008. "Origin and physiological roles of inflammation". *Nature* 454(7203), 428–435.

Meehan, S., Nain, A. S., 2014. "Role of suspended fiber structural stiffness and curvature on single-cell migration, nucleus shape, and focal-adhesion-cluster length". *Biophysical Journal* 107(11), 2604–2611.

Mehrasa, M., Asadollahi, M. A., Nasri-Nasrabadi, B., Ghaedi, K., Salehi, H., Dolatshahi-Pirouz, A., Arpanaei, A., 2016. "Incorporation of mesoporous silica nanoparticles into random electrospun PLGA and PLGA/gelatin nanofibrous scaffolds enhances mechanical and cell proliferation properties". *Materials Science and Engineering: C* 66, 25–32.

Meldal, M., Tornøe, C. W., 2008. "Cu-catalyzed azide–alkyne cycloaddition". *Chemical Reviews* 108(8), 2952–3015.

Mestas, J., Hughes, C. C. W., 2004. "Of mice and not men: differences between mouse and human immunology". *The Journal of Immunology* 172(5), 2731–2738.

Mienaltowski, M. J., Haddox, N. L., Beall, J. M., Pechanec, M. Y., 2021. "Basic structure, physiology, and biochemistry of connective tissues and extracellular matrix collagens". In: *Progress in Heritable Soft Connective Tissue Diseases*. Ed. by Halper, J. Cham: Springer International Publishing, 5–43.

Milleret, V., Hefti, T., Hall, H., Vogel, V., Eberli, D., 2012. "Influence of the fiber diameter and surface roughness of electrospun vascular grafts on blood activation". *Acta Biomaterialia* 8(12), 4349–4356.

Milošev, I., Levašič, V., Vidmar, J., Kovač, S., Trebše, R., 2017. "pH and metal concentration of synovial fluid of osteoarthritic joints and joints with metal replacements". *Journal of Biomedical Materials Research Part B: Applied Biomaterials* 105(8), 2507–2515.

Miroshnikova, Y. A., Nava, M. M., Wickström, S. A., 2017. "Emerging roles of mechanical forces in chromatin regulation". *Journal of Cell Science* 130(14), 2243–2250.

Narayanan, N., Jiang, C., Wang, C., Uzunalli, G., Whittern, N., Chen, D., Jones, O. G., Kuang, S., Deng, M., 2020. "Harnessing fiber diameter-dependent effects of myoblasts toward biomimetic scaffold-based skeletal muscle regeneration". *Frontiers in Bioengineering and Biotechnology* 8, 1–12.

Nathan, A. S., Baker, B. M., Nerurkar, N. L., Mauck, R. L., 2011. "Mechano-topographic modulation of stem cell nuclear shape on nanofibrous scaffolds." *Acta Biomaterialia* 7(1), 57–66.

Nathan, C., 2006. "Neutrophils and immunity: challenges and opportunities". *Nature Reviews Immunology* 6(3), 173–182.

Neisiany, R. E., Enayati, M. S., Kazemi-Beydokhti, A., Das, O., Ramakrishna, S., 2020. "Multilayered Bio-Based Electrospun Membranes: A Potential Porous Media for Filtration Applications". *Frontiers in Materials* 7, 67.

Ng, W. L., Goh, M. H., Yeong, W. Y., Naing, M. W., 2018. "Applying macromolecular crowding to 3D bioprinting: Fabrication of 3D hierarchical porous collagen-based hydrogel constructs". *Biomaterials Science* 6(3), 562–574.

Nguyen, A. T., Sathe, S. R., Yim, E. K., 2016. "From nano to micro: Topographical scale and its impact on cell adhesion, morphology and contact guidance". *Journal of Physics Condensed Matter* 28(18), 183001.

Ní Annaidh, A., Bruyère, K., Destrade, M., Gilchrist, M. D., Otténio, M., 2012. "Characterization of the anisotropic mechanical properties of excised human skin". *Journal of the Mechanical Behavior of Biomedical Materials* 5(1), 139–148.

Nimmo, C. M., Owen, S. C., Shoichet, M. S., 2011. "Diels–Alder click cross-linked hyaluronic acid hydrogels for tissue engineering". *Biomacromolecules* 12(3), 824–830.

Noriega, S. E., Hasanova, G. I., Schneider, M. J., Larsen, G. F., Subramanian, A., 2012. "Effect of fiber diameter on the spreading, proliferation and differentiation of chondrocytes on electrospun chitosan matrices." *Cells Tissues Organs* 195(3), 207–221.

Nunes-Pereira, J., Ribeiro, S., Ribeiro, C., Gombek, C. J., Gama, F. M., Gomes, A. C., Patterson, D. A., Lanceros-Méndez, S., 2015. "Poly(vinylidene fluoride) and copolymers as porous membranes for tissue engineering applications". *Polymer Testing* 44, 234–241.

O'Connell, B., 2012. *OVAL Profile Plot: ImageJ Plugin*.

Oh, S. H., Park, I. K., Kim, J. M., Lee, J. H., 2007. "In vitro and in vivo characteristics of PCL scaffolds with pore size gradient fabricated by a centrifugation method". *Biomaterials* 28(9), 1664–1671.

Ottosson, M., Jakobsson, A., Johansson, F., 2017. "Accelerated wound closure - Differently organized nanofibers affect cell migration and hence the closure of artificial wounds in a cell based in vitro model". *PLOS ONE* 12(1), e0169419.

Owen, S. C., Shoichet, M. S., 2010. "Design of three-dimensional biomimetic scaffolds". *Journal of Biomedical Materials Research Part A* 94(4), 1321–1331.

Papageorgiou, S., Pashley, S. L., O'Regan, L., Straatman, K. R., Fry, A. M., 2024. "Microtubule association of EML4–ALK V3 is key for the elongated cell morphology and enhanced migration observed in V3 cells". *Cells* 13(23), 1954.

Park, K.-S., Kim, B.-J., Lih, E., Park, W., Lee, S.-H., Joung, Y. K., Han, D. K., 2018. "Versatile effects of magnesium hydroxide nanoparticles in PLGA scaffold–mediated chondrogenesis". *Acta Biomaterialia* 73, 204–216.

Park, S.-H., Gil, E. S., Kim, H. J., Lee, K., Kaplan, D. L., 2010. "Relationships between degradability of silk scaffolds and osteogenesis". *Biomaterials* 31(24), 6162–6172.

Peppas, N. A., Hoffman, A. S., 2020. "Hydrogels". In: *Biomaterials Science: An Introduction to Materials in Medicine. 4th ed.* Ed. by Wagner, W. R., Sakiyama-Elbert, S. E., Zhang, G., Yaszemski, M. J. 4th ed. Academic Press, 153–166.

Prescher, J. A., Dube, D. H., Bertozzi, C. R., 2004. "Chemical remodelling of cell surfaces in living animals". *Nature* 430(7002), 873–877.

Pruitt, L. A., Chakravartula, A. M., 2011. *Mechanics of biomaterials: Fundamental principles for implant design*. Cambridge Texts in Biomedical Engineering. Cambridge University Press.

Pu, J., Komvopoulos, K., 2014. "Mechanical properties of electrospun bilayer fibrous membranes as potential scaffolds for tissue engineering". *Acta Biomaterialia* 10(6), 2718–2726.

Pu, J., Yuan, F., Li, S., Komvopoulos, K., 2015. "Electrospun bilayer fibrous scaffolds for enhanced cell infiltration and vascularization in vivo". *Acta Biomaterialia* 13, 131–141.

Pucino, V., Certo, M., Bulusu, V., Cucchi, D., Goldmann, K., Pontarini, E., Haas, R., Smith, J., Headland, S. E., Blighe, K., Ruscica, M., Humby, F., Lewis, M. J., Kamphorst, J. J., Bombardieri, M., Pitzalis, C., Mauro, C., 2019. "Lactate buildup at the site of chronic inflammation promotes disease by inducing CD4+ T cell metabolic rewiring". *Cell Metabolism* 30(6), 1055–1074.

Rabel, K., Kohal, R.-J., Steinberg, T., Tomakidi, P., Rolauffs, B., Adolfsson, E., Palmero, P., Fürderer, T., Altmann, B., 2020. "Controlling osteoblast morphology and proliferation via surface micro-topographies of implant biomaterials". *Scientific Reports* 10(1), 12810.

Radwan-Pragłowska, J., Janus, Ł., Piątkowski, M., Bogdał, D., Matýsek, D., 2020. "Hybrid bilayer PLA/chitosan nanofibrous scaffolds doped with ZnO, Fe3O4, and Au nanoparticles with bioactive properties for skin tissue engineering". *Polymers* 12(1), 159.

Rahmati, M., Mills, D. K., Urbanska, A. M., Saeb, M. R., Venugopal, J. R., Ramakrishna, S., Mozafari, M., 2021. "Electrospinning for tissue engineering applications". *Progress in Materials Science* 117, 100721.

Ramminger, I., Steinberg, T., Rolauffs, B., Selig, M., Tomakidi, P., 2026. "Form meets function: Fiber architecture directs proliferation and differentiation in gingival keratinocytes". *Cells* 15(3), 300.

Ratner, B. D., Hoffman, A. S., Schoen, F. J., Lemons, J. E., 2004. *Biomaterials Science: An Introduction to Materials in Medicine*. Ed. by Ratner, B. D. 4th ed. Netherlands: Elsevier Science.

Rediguieri, C. F., Sassonia, R. C., Dua, K., Kikuchi, I. S., Jesus Andreoli Pinto, T. de, 2016. "Impact of sterilization methods on electrospun scaffolds for tissue engineering". *European Polymer Journal* 82, 181–195.

Reichenbach, M., Reimann, K., Reuter, H., 2014. "Gene expression in response to cyclic mechanical stretch in primary human dermal fibroblasts". *Genomics Data* 2, 335–339.

Ren, Y.-J., Zhang, S., Mi, R., Liu, Q., Zeng, X., Rao, M., Hoke, A., Mao, H.-Q., 2013. "Enhanced differentiation of human neural crest stem cells towards the Schwann cell lineage by aligned electrospun fiber matrix". *Acta Biomaterialia* 9(8), 7727–7736.

Rens, E. G., Merks, R. M. H., 2017. "Cell contractility facilitates alignment of cells and tissues to static uniaxial stretch". *Biophysical Journal* 112(4), 755–766.

Ribeiro, C., Sencadas, V., Areias, A. C., Gama, F. M., Lanceros-Méndez, S., 2015. "Surface roughness dependent osteoblast and fibroblast response on poly(L-lactide) films and electrospun membranes". *Journal of Biomedical Materials Research Part A* 103(7), 2260–2268.

Riehl, B. D., Park, J.-H., Kwon, I. K., Lim, J. Y., 2012. "Mechanical stretching for tissue engineering: two-dimensional and three-dimensional constructs." *Tissue Engineering Part B: Reviews* 18(4), 288–300.

Roman, M. D., Fleaca, R. S., Boicean, A., Bratu, D., Birlutiu, V., Rus, L. L., Tantar, C., Mitariu, S. I. C., 2017. "Assesment of synovial fluid pH in osteoarthritis of the HIP and knee". *Revista de Chimie* 68(6), 1340–1342.

Rosato, A., Romano, A., Totaro, G., Celli, A., Fava, F., Zanaroli, G., Sisti, L., 2022. "Enzymatic degradation of the most common aliphatic bio-polyesters and evaluation of the mechanisms involved: An extended study". *Polymers* 14(9).

Rouwkema, J., Khademhosseini, A., 2016. "Vascularization and angiogenesis in tissue engineering: beyond creating static networks". *Trends in Biotechnology* 34(9), 733–745.

Rühs, P. A., Malollari, K. G., Binelli, M. R., Crockett, R., Balkenende, D. W. R., Studart, A. R., Messersmith, P. B., 2020. "Conformal bacterial cellulose coatings as lubricious surfaces". *ACS Nano* 14(4), 3885–3895.

Ruiz-Alonso, S., Lafuente-Merchan, M., Ciriza, J., Saenz-del-Burgo, L., Pedraz, J. L., 2021. "Tendon tissue engineering: Cells, growth factors, scaffolds and production techniques". *Journal of Controlled Release* 333, 448–486.

Ruskowitz, E. R., DeForest, C. A., 2018. "Photoresponsive biomaterials for targeted drug delivery and 4D cell culture". *Nature Reviews Materials* 3(2), 1–17.

Ryu, J. H., Lee, Y., Kong, W. H., Kim, T. G., Park, T. G., Lee, H., 2011. "Catechol-functionalized chitosan/pluronic hydrogels for tissue adhesives and hemostatic materials". *Biomacromolecules* 12(7), 2653–2659.

Ryu, J. H., Messersmith, P. B., Lee, H., 2018. "Polydopamine surface chemistry: a decade of discovery". *ACS Applied Materials & Interfaces* 10(9), 7523–7540.

Ryu, J., Ku, S. H., Lee, H., Park, C. B., 2010. "Mussel-inspired polydopamine coating as a universal route to hydroxyapatite crystallization". *Advanced Functional Materials* 20(13), 2132–2139.

Sadeghi-Avalshahr, A. R., Nokhasteh, S., Molavi, A. M., Mohammad-pour, N., Sadeghi, M., 2020. "Tailored PCL scaffolds as skin substitutes using sacrificial PVP fibers and collagen/chitosan blends". *International Journal of Molecular Sciences* 21(7), 2311.

Sadtler, K., Estrellas, K., Allen, B. W., Wolf, M. T., Fan, H., Tam, A. J., Patel, C. H., Luber, B. S., Wang, H., Wagner, K. R., 2016. "Developing a pro-regenerative biomaterial scaffold microenvironment requires T helper 2 cells". *Science* 352(6283), 366–370.

Sadtler, K., Sommerfeld, S. D., Wolf, M. T., Wang, X., Majumdar, S., Chung, L., Kelkar, D. S., Pandey, A., Elisseeff, J. H., 2017. "Proteomic composition and immunomodulatory properties of urinary bladder matrix scaffolds in homeostasis and injury". *Seminars in Immunology* 29, 14–23.

Sadtler, K., Wolf, M. T., Ganguly, S., Moad, C. A., Chung, L., Majumdar, S., Housseau, F., Pardoll, D. M., Elisseeff, J. H., 2019. "Divergent immune responses to synthetic and biological scaffolds". *Biomaterials* 192, 405–415.

Samadian, H., Mobasheri, H., Hasanpour, S., Faridi Majidi, R., 2017. "Electrospinning of polyacrylonitrile nanofibers and simulation of electric field via finite element method". *Nanomedicine Research Journal* 2, 87–92.

Sanz-Herrera, J. A., García-Aznar, J. M., Doblaré, M., 2009. "On scaffold designing for bone regeneration: A computational multiscale approach". *Acta Biomaterialia* 5(1), 219–229.

Selders, G. S., Fetz, A. E., Radic, M. Z., Bowlin, G. L., 2017. "An overview of the role of neutrophils in innate immunity, inflammation and host-biomaterial integration". *Regenerative Biomaterials* 4(1), 55–68.

Seok, J., Warren, H. S., Cuenca, A. G., Mindrinos, M. N., Baker, H. V., Xu, W., Richards, D. R., McDonald-Smith, G. P., Gao, H., Hennessy, L., 2013. "Genomic responses in mouse models poorly mimic human inflammatory diseases". *Proceedings of the National Academy of Sciences of the USA* 110(9), 3507–3512.

Shaban, M., Mosa, T. M., Abdel-Hamid, H., Abdalfarg, N., Hashim, G., 2026. "Advancements in electrospinning: a comprehensive review of historical development, key parameters, applications, and challenges". *Discover Chemistry* 3(1), 82.

Sharpe, J. R., Harris, K. L., Jubin, K., Bainbridge, N. J., Jordan, N. R., 2009. "The effect of pH in modulating skin cell behaviour". *British Journal of Dermatology* 161(3), 671–673.

Sheets, K., Wunsch, S., Ng, C., Nain, A. S., 2013. "Shape-dependent cell migration and focal adhesion organization on suspended and aligned nanofiber scaffolds". *Acta Biomaterialia* 9(7), 7169–7177.

Sheikh, Z., Brooks, P. J., Barzilay, O., Fine, N., Glogauer, M., 2015. "Macrophages, foreign body giant cells and their response to implantable biomaterials". *Materials* 8(9), 5671–5701.

Shi, S., Ou, X., Cheng, D., 2023. "How advancing is peripheral nerve regeneration using nanofiber scaffolds? A comprehensive review of the literature". *International Journal of Nanomedicine* 18, 6763–6779.

Shi, W., Cassmann, T. J., Bhagwate, A. V., Hitosugi, T., Ip, W. K. E., 2024. "Lactic acid induces transcriptional repression of macrophage inflammatory response via histone acetylation". *Cell Reports* 43(2), 113746.

Shields, K. J., Beckman, M. J., Bowlin, G. L., Wayne, J. S., 2004. "Mechanical properties and cellular proliferation of electrospun collagen type II". *Tissue Engineering* 10(9-10), 1510–1517.

Shin, H., Jo, S., Mikos, A. G., 2003. "Biomimetic materials for tissue engineering". *Biomaterials* 24(24), 4353–4364.

Shuai, C., Zan, J., Qi, F., Wang, G., Liu, Z., Yang, Y., Peng, S., 2019. "nMgO-incorporated PLLA bone scaffolds: Enhanced crystallinity and neutralized acidic products". *Materials & Design* 174, 107801.

Skinner, B. M., Johnson, E. E., 2017. "Nuclear morphologies: Their diversity and functional relevance". *Chromosoma* 126(2), 195–212.

Spagnuolo, M., Liu, L., 2012. "Fabrication and degradation of electrospun scaffolds from L-tyrosine-based polyurethane blends for tissue engineering applications". *ISRN Nanotechnology* 2012. Ed. by Obraztsov, A. N., Coasne, B., Zhang, Y., 627420.

Sperling, L. E., Reis, K. P., Pozzobon, L. G., Girardi, C. S., Pranke, P., 2017. "Influence of random and oriented electrospun fibrous poly(lactic-co-glycolic acid) scaffolds on neural differentiation of mouse embryonic stem cells." *Journal of Biomedical Materials Research Part A* 105(5), 1333–1345.

Stabler, C. L., Li, Y., Stewart, J. M., Keselowsky, B. G., 2019. "Engineering immunomodulatory biomaterials for type 1 diabetes". *Nature Reviews Materials* 4(6), 429–450.

Stachewicz, U., Bailey, R. J., Wang, W., Barber, A. H., 2012. "Size dependent mechanical properties of electrospun polymer fibers from a composite structure". *Polymer* 53(22), 5132–5137.

Stender, C. J., Rust, E., Martin, P. T., Neumann, E. E., Brown, R. J., Lujan, T. J., 2018. "Modeling the effect of collagen fibril alignment on ligament mechanical behavior." *Biomechanics and Modeling in Mechanobiology* 17(2), 543–557.

Sun, L., Qu, L., Zhu, R., Li, H., Xue, Y., Liu, X., Fan, J., Fan, H., 2016. "Effects of mechanical stretch on cell Proliferation and matrix formation of mesenchymal stem cell and anterior cruciate ligament fibroblast". *Stem Cells International* 2016, 9842075.

Sun, Z., Guo, S. S., Fässler, R., 2016. "Integrin-mediated mechanotransduction". *Journal of Cell Biology* 215(4), 445–456.

Sundararaghavan, H. G., Saunders, R. L., Hammer, D. A., Burdick, J. A., 2013. "Fiber alignment directs cell motility over chemotactic gradients". *Biotechnology and Bioengineering* 110(4), 1249–1254.

Sussman, E. M., Halpin, M. C., Muster, J., Moon, R. T., Ratner, B. D., 2014. "Porous implants modulate healing and induce shifts in local macrophage polarization in the foreign body reaction". *Annals of Biomedical Engineering* 42(7), 1508–1516.

Suuronen, R., Pohjonen, T., Hietanen, J., Lindqvist, C., 1998. "A 5-year in vitro and in vivo study of the biodegradation of polylactide plates". *Journal of Oral and Maxillofacial Surgery* 56(5), 604–614.

Tajima, S., Chu, J. S. F., Li, S., Komvopoulos, K., 2008. "Differential regulation of endothelial cell adhesion, spreading, and cytoskeleton on low-density polyethylene by nanotopography and surface chemistry modification induced by argon plasma treatment." *Journal of Biomedical Materials Research Part A* 84(3), 828–836.

Tang, Y., Tian, J., Li, L., Huang, L., Shen, Q., Guo, S., Jiang, Y., 2021. "Biomimetic biphasic electrospun scaffold for anterior cruciate ligament tissue engineering". *Tissue Engineering and Regenerative Medicine* 18(5), 819–830.

Tasdelen, M. A., 2011. "Diels–Alder "click" reactions: recent applications in polymer and material science". *Polymer Chemistry* 2(10), 2133–2145.

Thakar, R. G., Cheng, Q., Patel, S., Chu, J., Nasir, M., Liepmann, D., Komvopoulos, K., Li, S., 2009. "Cell-shape regulation of smooth muscle cell proliferation". *Biophysical Journal* 96(8), 3423–3432.

ThermoFisher Scientific, 2014. *General fix, perm, and block protocol. School of Fluorescence, Molecular Probes.*

Tijore, A., Cai, P., Nai, M. H., Zhuyun, L., Yu, W., Tay, C. Y., Lim, C. T., Chen, X., Tan, L. P., 2015. "Role of cytoskeletal tension in the induction of cardiomyogenic differentiation in micropatterned human mesenchymal stem cell". *Advanced Healthcare Materials* 4(9), 1399–1407.

Tondon, A., Kaunas, R., 2014. "The direction of stretch-induced cell and stress fiber orientation depends on collagen matrix stress". *PLOS ONE* 9(2), e89592.

Truong, V. X., Ablett, M. P., Richardson, S. M., Hoyland, J. A., Dove, A. P., 2015. "Simultaneous orthogonal dual-click approach to tough, in-situ-forming hydrogels for cell encapsulation". *Journal of the American Chemical Society* 137(4), 1618–1622.

Tsai, W.-B., Chen, W.-T., Chien, H.-W., Kuo, W.-H., Wang, M.-J., 2014. "Poly (dopamine) coating to biodegradable polymers for bone tissue engineering". *Journal of Biomaterials Applications* 28(6), 837–848.

Tyler, B., Gullotti, D., Mangraviti, A., Utsuki, T., Brem, H., 2016. "Polylactic acid (PLA) controlled delivery carriers for biomedical applications". *Advanced Drug Delivery Reviews* 107, 163–175.

Ulrich, T. A., Jain, A., Tanner, K., MacKay, J. L., Kumar, S., 2010. "Probing cellular mechanobiology in three-dimensional culture with collagen–agarose matrices". *Biomaterials* 31(7), 1875–1884.

Uzer, G., Rubin, C. T., Rubin, J., 2016. "Cell mechanosensitivity is enabled by the LINC nuclear complex". *Current Molecular Biology Reports* 2(1), 36–47.

Valentin, J. E., Stewart-Akers, A. M., Gilbert, T. W., Badylak, S. F., 2009. "Macrophage participation in the degradation and remodeling of extracellular matrix scaffolds". *Tissue Engineering Part A* 15(7), 1687–1694.

Vatankhah, E., Prabhakaran, M. P., Semnani, D., Razavi, S., Zamani, M., Ramakrishna, S., 2014. "Phenotypic modulation of smooth muscle cells by chemical and mechanical cues of electrospun tecophilic/gelatin nanofibers". *ACS Applied Materials & Interfaces* 6(6), 4089–4101.

Veiseh, O., Doloff, J. C., Ma, M., Vegas, A. J., Tam, H. H., Bader, A. R., Li, J., Langan, E., Wyckoff, J., Loo, W. S., 2015. "Size-and shape-dependent foreign body immune response to materials implanted in rodents and non-human primates". *Nature Materials* 14(6), 643–651.

Vimal, S. K., Ahamad, N., Katti, D. S., 2016. "A simple method for fabrication of electrospun fibers with controlled degree of alignment having potential for nerve regeneration applications". *Materials Science and Engineering: C* 63, 616–627.

Vogel, V., Sheetz, M., 2006. "Local force and geometry sensing regulate cell functions". *Nature Reviews Molecular Cell Biology* 7(4), 265–275.

Voleti, P. B., Buckley, M. R., Soslowsky, L. J., 2012. "Tendon healing: Repair and regeneration". *Annual Review of Biomedical Engineering* 14, 47–71.

Waldrop, K., Wycisk, R., Pintauro, P. N., 2020. "Application of electrospinning for the fabrication of proton-exchange membrane fuel cell electrodes". *Current Opinion in Electrochemistry* 21, 257–264.

Walker, J. L., Santoro, M., 2017. "Processing and production of bioresorbable polymer scaffolds for tissue engineering". In: *Bioresorbable Polymers for Biomedical Applications From Fundamentals to Translational Medicine*. Ed. by Perale, G., Hilborn, J. B. T. .-. B. P. f. B. A. Woodhead Publishing, 181–203.

Walters, B., Uynuk-Ool, T., Rothdiener, M., Palm, J., Hart, M. L., Stegemann, J. P., Rolauffs, B., 2017. "Engineering the geometrical shape of mesenchymal stromal cells through defined cyclic stretch regimens". *Scientific Reports* 7(1), 6640.

Wan, Y., Wu, H., Cao, X., Dalai, S., 2008. "Compressive mechanical properties and biodegradability of porous poly (caprolactone)/ chitosan scaffolds". *Polymer Degradation and Stability* 93(10), 1736–1741.

Wang, H. B., Mullins, M. E., Cregg, J. M., McCarthy, C. W., Gilbert, R. J., 2010. "Varying the diameter of aligned electrospun fibers alters neurite outgrowth and Schwann cell migration". *Acta Biomaterialia* 6(8), 2970–2978.

Wang, J. H.-C., Thampatty, B. P., 2006. "An introductory review of cell mechanobiology". *Biomechanics and Modeling in Mechanobiology* 5(1), 1–16.

Wang, J. H.-C., Grood, E. S., 2000. "The strain magnitude and contact guidance determine orientation response of fibroblasts to cyclic substrate strains". *Connective Tissue Research* 41(1), 29–36.

Wang, J. H.-C., 2006. "Mechanobiology of tendon". *Journal of Biomechanics* 39(9), 1563–1582.

Wang, J., Ye, R., Wei, Y., Wang, H., Xu, X., Zhang, F., Qu, J., Zuo, B., Zhang, H., 2012. "The effects of electrospun TSF nanofiber diameter and alignment on neuronal differentiation of human embryonic stem cells". *Journal of Biomedical Materials Research Part A* 100 A(3), 632–645.

Wang, N., Tytell, J. D., Ingber, D. E., 2009. "Mechanotransduction at a distance: mechanically coupling the extracellular matrix with the nucleus". *Nature Reviews Molecular Cell Biology* 10(1), 75–82.

Wang, Q., Ji, P., Bu, T., Mao, Y., He, H., Ge, N., 2025. "Recent progress in the application of electrospinning technology in the biomedical field". *Journal of Functional Biomaterials* 16(7), 266.

Wang, Y., Wu, T., Zhang, J., Feng, Z., Yin, M., Mo, X., 2021. "A bilayer vascular scaffold with spatially controlled release of growth factors to enhance in situ rapid endothelialization and smooth muscle regeneration". *Materials & Design* 204, 109649.

Watari, S., Hayashi, K., Wood, J. A., Russell, P., Nealey, P. F., Murphy, C. J., Genetos, D. C., 2012. "Modulation of osteogenic differentiation in hMSCs cells by submicron topographically-patterned ridges and grooves". *Biomaterials* 33(1), 128–136.

Weir, N. A., Buchanan, F. J., Orr, J. F., Farrar, D. F., Dickson, G. R., 2004. "Degradation of poly-L-lactide. Part 2: increased temperature accelerated degradation". *Proceedings of the Institution of Mechanical Engineers, Part H: Journal of Engineering in Medicine* 218(5), 321–330.

Wen, J. H., Vincent, L. G., Fuhrmann, A., Choi, Y. S., Hribar, K. C., Taylor-Weiner, H., Chen, S., Engler, A. J., 2014. "Interplay of matrix stiffness and protein tethering in stem cell differentiation". *Nature Materials* 13(10), 979–987.

Wingate, K., Bonani, W., Tan, Y., Bryant, S. J., Tan, W., 2012. "Compressive elasticity of three-dimensional nanofiber matrix directs mesenchymal stem cell differentiation to vascular cells with endothelial or smooth muscle cell markers". *Acta Biomaterialia* 8(4), 1440–1449.

Wong, S.-C., Baji, A., Leng, S., 2008. "Effect of fiber diameter on tensile properties of electrospun poly (ε-caprolactone)". *Polymer* 49(21), 4713–4722.

World Health Organization, 2018. *The top 10 causes of death.*

Wu, M.-H., Urban, J. P. G., Cui, Z. F., Cui, Z., Xu, X., 2007. "Effect of extracellular pH on matrix synthesis by chondrocytes in 3D agarose gel". *Biotechnology Progress* 23(2), 430–434.

Wu, Q., Liu, J., Wang, X., Feng, L., Wu, J., Zhu, X., Wen, W., Gong, X., 2020. "Organ-on-a-chip: recent breakthroughs and future prospects". *BioMedical Engineering OnLine* 19(1), 9.

Wu, X., Zhao, F., Wang, H., Schirhagl, R., Włodarczyk-Biegun, M. K., 2025. "Integrating melt electrowriting (MEW) PCL scaffolds with fibroblast-laden hydrogel toward vascularized skin tissue engineering". *Materials Today Bio* 31, 101593.

Wylie, R. G., Ahsan, S., Aizawa, Y., Maxwell, K. L., Morshead, C. M., Shoichet, M. S., 2011. "Spatially controlled simultaneous patterning of multiple growth factors in three-dimensional hydrogels". *Nature Materials* 10(10), 799–806.

Xi, W., Scott, T. F., Kloxin, C. J., Bowman, C. N., 2014. "Click chemistry in materials science". *Advanced Functional Materials* 24(18), 2572–2590.

Xie, S., Zeng, Y., 2012. "Effects of electric field on multineedle electrospinning: Experiment and simulation study". *Industrial & Engineering Chemistry Research* 51, 5336–5345.

Xu, Y., Guan, J., 2016. "Interaction of cells with polyurethane scaffolds". In: *Advances in Polyurethane Biomaterials*. Ed. by Cooper, S. L., Guan, J. Woodhead Publishing. Chap. 18, 523–542.

Yamamoto, N., Ohno, K., Hayashi, K., Kuriyama, H., Yasuda, K., Kaneda, K., 1993. "Effects of stress shielding on the mechanical properties of rabbit patellar tendon". *Journal of Biomechanical Engineering* 115(1), 23–28.

Yan, J., Qiang, L., Gao, Y., Cui, X., Zhou, H., Zhong, S., Wang, Q., Wang, H., 2012. "Effect of fiber alignment in electrospun scaffolds on keratocytes and corneal epithelial cells behavior." *Journal of Biomedical Materials Research Part A* 100(2), 527–535.

Yang, C.-W., Zhang, Y.-Q., Chang, H., Gao, R., Chen, D., Yao, H., 2025. "Aligned nanofiber scaffolds combined with cyclic stretch facilitate mesenchymal stem cell differentiation for ligament engineering". *World Journal of Stem Cells* 17(8), 107124.

Yang, H., Zhang, Q., Lin, B., Fu, G., Zhang, X., Guo, L., 2012. "Thermo-sensitive electrospun fibers prepared by a sequential thiol-ene click chemistry approach". *Journal of Polymer Science Part A: Polymer Chemistry* 50(20), 4182–4190.

Yang, J., Stuart, M. A. C., Kamperman, M., 2014. "Jack of all trades: versatile catechol crosslinking mechanisms". *Chemical Society Reviews* 43(24), 8271–8298.

Yang, Q., Li, J., Su, W., Yu, L., Li, T., Wang, Y., Zhang, K., Wu, Y., Wang, L., 2022. "Electrospun aligned poly(ϵ-caprolactone) nanofiber yarns guiding 3D organization of tendon stem/progenitor cells in tenogenic differentiation and tendon repair." *Frontiers in Bioengineering and Biotechnology* 10, 960694.

Yang, Y., Tang, G., Zhao, Y., Yuan, X., Fan, Y., 2010. "Effect of cyclic loading on in vitro degradation of poly(l-lactide-co- glycolide) scaffolds". *Journal of Biomaterials Science, Polymer Edition* 21(1), 53–66.

Yang, Z., Yin, G., Sun, S., Xu, P., 2024. "Medical applications and prospects of polylactic acid materials". *iScience* 27(12), 111512.

Yao, X., Peng, R., Ding, J., 2013. "Effects of aspect ratios of stem cells on lineage commitments with and without induction media." *Biomaterials* 34(4), 930–939.

Ye, K., Wang, X., Cao, L., Li, S., Li, Z., Yu, L., Ding, J., 2015. "Matrix stiffness and nanoscale spatial organization of cell-adhesive ligands direct stem cell fate". *Nano Letters* 15(7), 4720–4729.

Ye, Q., Harmsen, M. C., Luyn, M. J. A. van, Bank, R. A., 2010. "The relationship between collagen scaffold cross-linking agents and neutrophils in the foreign body reaction". *Biomaterials* 31(35), 9192–9201.

Yevick, H. G., Duclos, G., Bonnet, I., Silberzan, P., 2015. "Architecture and migration of an epithelium on a cylindrical wire". *Proceedings of the National Academy of Sciences of the USA* 112(19), 5944–5949.

Yixiang, D., Yong, T., Liao, S., Chan, C. K., Ramakrishna, S., 2008. "Degradation of electrospun nanofiber scaffold by short wave length ultraviolet radiation treatment and its potential applications in tissue engineering". *Tissue Engineering Part A* 14(8), 1321–1329.

You, Y., Min, B.-M., Lee, S. J., Lee, T. S., Park, W. H., 2005. "In vitro degradation behavior of electrospun polyglycolide, polylactide, and poly(lactide-co-glycolide)". *Journal of Applied Polymer Science* 95(2), 193–200.

Yuan, X., Mak, A. F., Yao, K., 2002. "Comparative observation of accelerated degradation of poly(l-lactic acid) fibres in phosphate buffered saline and a dilute alkaline solution". *Polymer Degradation and Stability* 75(1), 45–53.

Zhang, B., Korolj, A., Lai, B. F. L., Radisic, M., 2018. "Advances in organ-on-a-chip engineering". *Nature Reviews Materials* 3(8), 257–278.

Zhang, H., Zhou, L., Zhang, W., 2014. "Control of scaffold degradation in tissue engineering: A review". *Tissue Engineering Part B: Reviews* 20(5), 492–502.

Zhang, Q., Lu, H., Kawazoe, N., Chen, G., 2014. "Pore size effect of collagen scaffolds on cartilage regeneration". *Acta Biomaterialia* 10(5), 2005–2013.

Zhang, Y., Fan, W., Ma, Z., Wu, C., Fang, W., Liu, G., Xiao, Y., 2010. "The effects of pore architecture in silk fibroin scaffolds on the growth and differentiation of mesenchymal stem cells expressing BMP7". *Acta Biomaterialia* 6(8), 3021–3028.

Zhao, P., Gu, H., Mi, H., Rao, C., Fu, J., Turng, L.-s., 2018. "Fabrication of scaffolds in tissue engineering: A review". *Frontiers of Mechanical Engineering* 13(1), 107–119.

Zheng, J., Liu, K., Reneker, D. H., Becker, M. L., 2012. "Post-assembly derivatization of electrospun nanofibers via strain-promoted azide alkyne cycloaddition". *Journal of the American Chemical Society* 134(41), 17274–17277.

Zheng, Q., Chu, Z., Li, X., Kang, H., Yang, X., Fan, Y., 2017. "The effect of fluid shear stress on the in vitro release kinetics of sirolimus from PLGA films". *Polymers* 9(11), 1–12.

Zhou, G., Jiang, H., Yin, Z., Liu, Y., Zhang, Q., Zhang, C., Pan, B., Zhou, J., Zhou, X., Sun, H., Li, D., He, A., Zhang, Z., Zhang, W., Liu, W., Cao, Y., 2018. "In vitro regeneration of patient-specific ear-shaped cartilage and its first clinical application for auricular reconstruction". *EBioMedicine* 28, 287–302.

Zhu, X., Cui, W., Li, X., Jin, Y., 2008. "Electrospun fibrous mats with high porosity as potential scaffolds for skin tissue engineering". *Biomacromolecules* 9(7), 1795–1801.

Zou, Y., Zhang, L., Yang, L., Zhu, F., Ding, M., Lin, F., Wang, Z., Li, Y., 2018. ""Click" chemistry in polymeric scaffolds: Bioactive materials for tissue engineering". *Journal of Controlled Release* 273, 160–179.

Zouani, O. F., Chanseau, C., Brouillaud, B., Bareille, R., Deliane, F., Foulc, M. P., Mehdi, A., Durrieu, M. C., 2012. "Altered nanofeature size dictates stem cell differentiation". *Journal of Cell Science* 125(5), 1217–1224.